Elettra Sincrotrone Trieste

Elettra
Sincrotrone
Trieste

X-ray imaging and spectromicroscopy using XAS and XRF

Alessandra Gianoncelli

alessandra.gianoncelli@elettra.eu

Elettra
Sincrotrone
Trieste

Outline

- X-ray microscopes:
  Full-field, STXM, projection
- Standard imaging technique and new advanced ones (CDI, Ptychography)
- Special attention to the TwinMic beamline (Elettra, Trieste)
- Multidisciplinary applications: life sciences, food science, environmental science, materials science, cultural heritage…

X-ray microscopy types

Elettra
Sincrotrone
Trieste

X-ray microscopy:
bridge between **visible light** microscopy and **electron** microscopies

Spatial resolution:

visible light microscopy < X-ray microscopy < **electron** microscopy

Air	Vacuum (or air)	Vacuum

X-ray Microscopy vs Electron Microscopy:

- Easier sample preparation (no metalisation)
- Higher penetration depth of X-rays compared to electrons

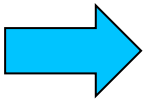

thicker samples can be analysed

Projection microscopy

Scheme of a projection microscope with the source to specimen plane distance R_1 and specimen to detector distance R_2

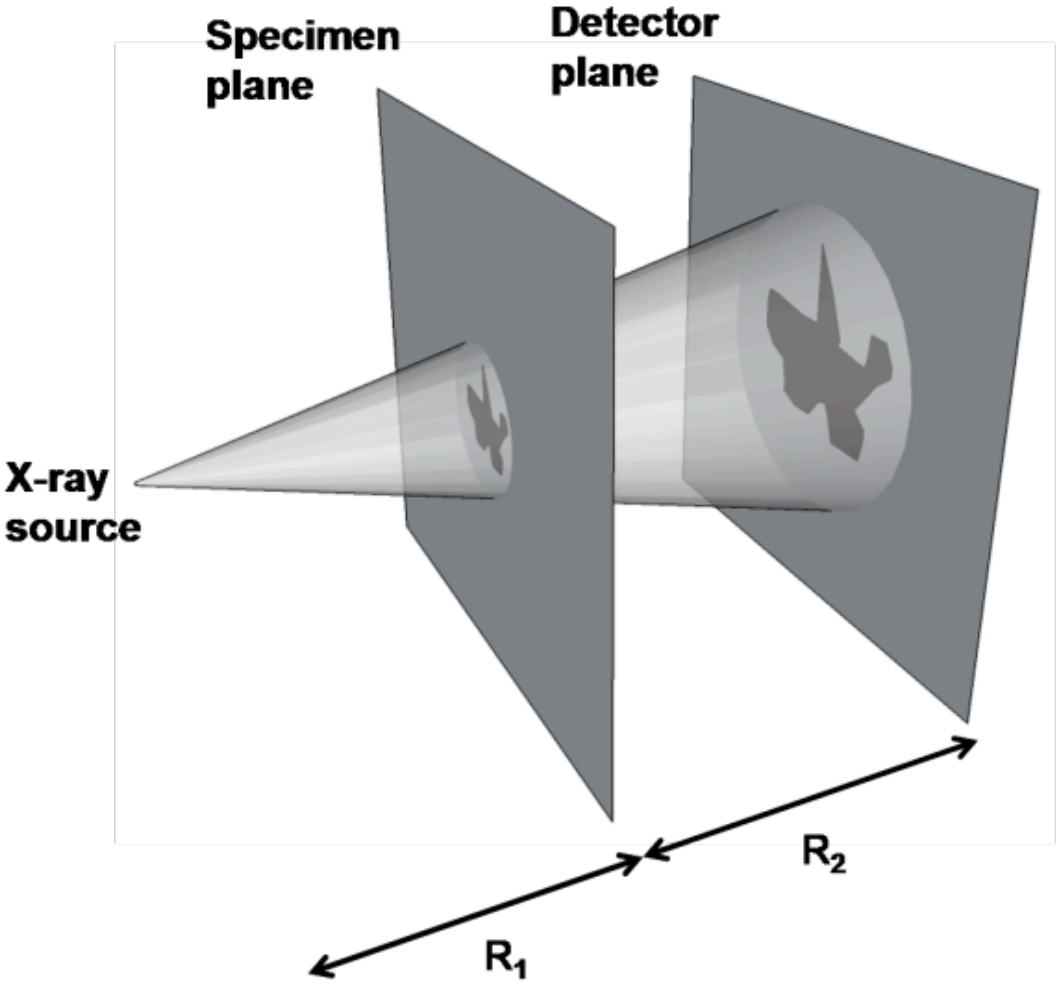

Kaulich B., Thibault P., Gianoncelli A., Kiskinova M. "Transmission and emission x-ray microscopy: operation modes, contrast mechanisms and applications" *Journal of Physics: Condensed Matter*, Vol. 23 - 8, pp. 083002 (2011)

Elettra
Sincrotrone
Trieste

Projection microscopy

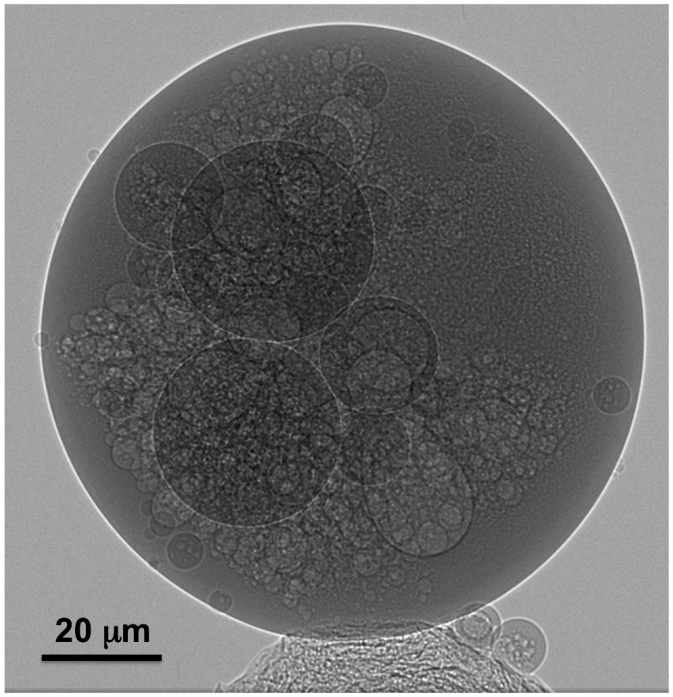

3D phase contrast dataset view, reconstructed cross section of part of a ceramisphere (projection X-ray microscope at the CSIRO, Australia).

The total collection time of the microtomogram was 10 h.
The diameter of the sphere is 110 μ m

A state-of-the art instrument for projection microscopy, including phase-sensitive imaging and microtomography based on a converted scanning electron microscope, is reported for example by Mayo et al. (Mayo et al 2002; Mayo et al 2003).

Mayo S C, Miller P R, Wilkins S W, Davis T J, Gao D, Gureyev T E, Paganin D, Parry D J, Pogany A and Stevenson A W 2003 *Journal De Physique IV* 104 543-546

Elettra Sincrotrone Trieste

Full field Imaging mode

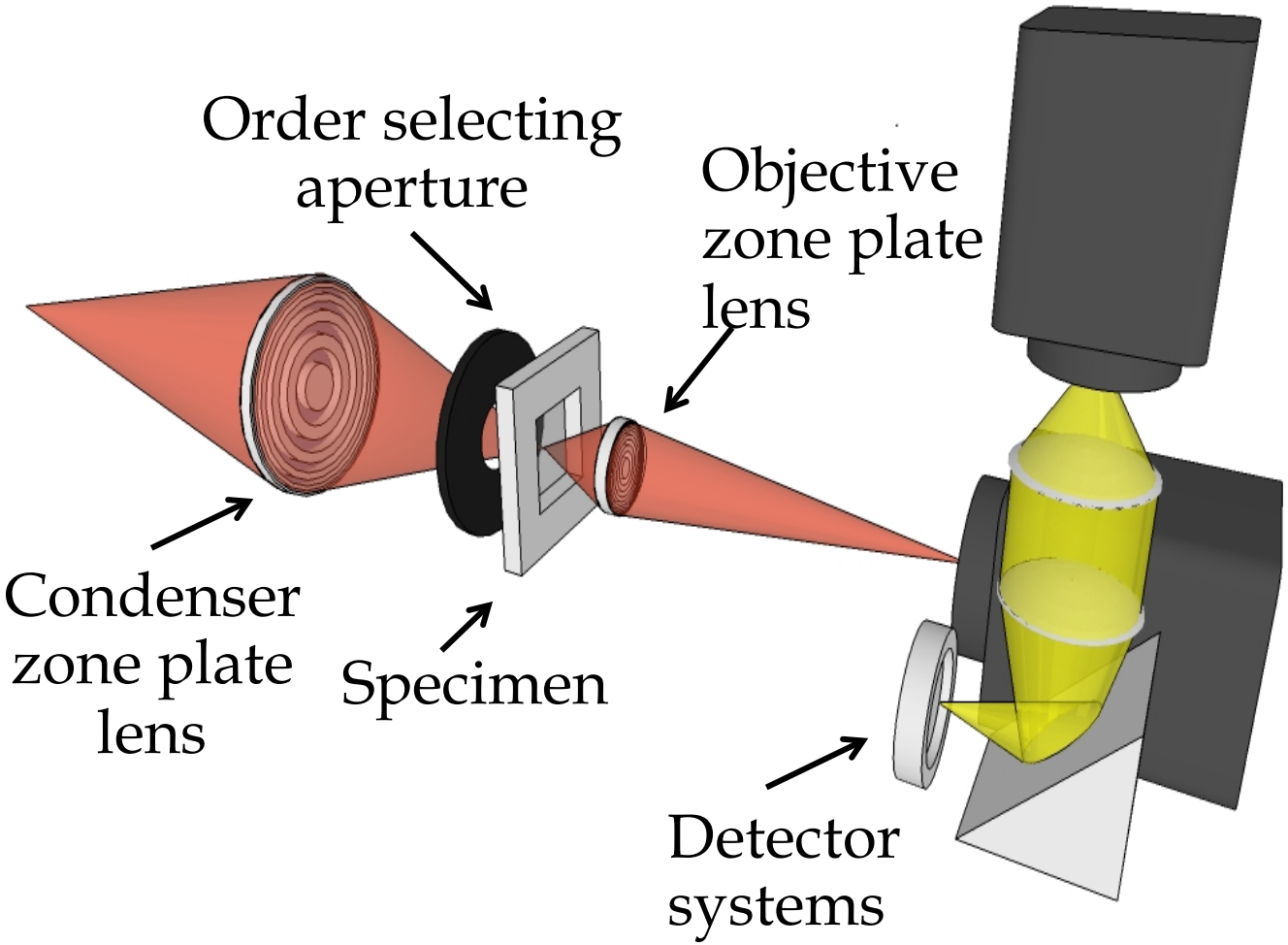

- Similar to conventional visible light microscope
- Analysis of morphology in transmission
- Fast imaging, dynamics, microtomography

Elettra
Sincrotrone
Trieste

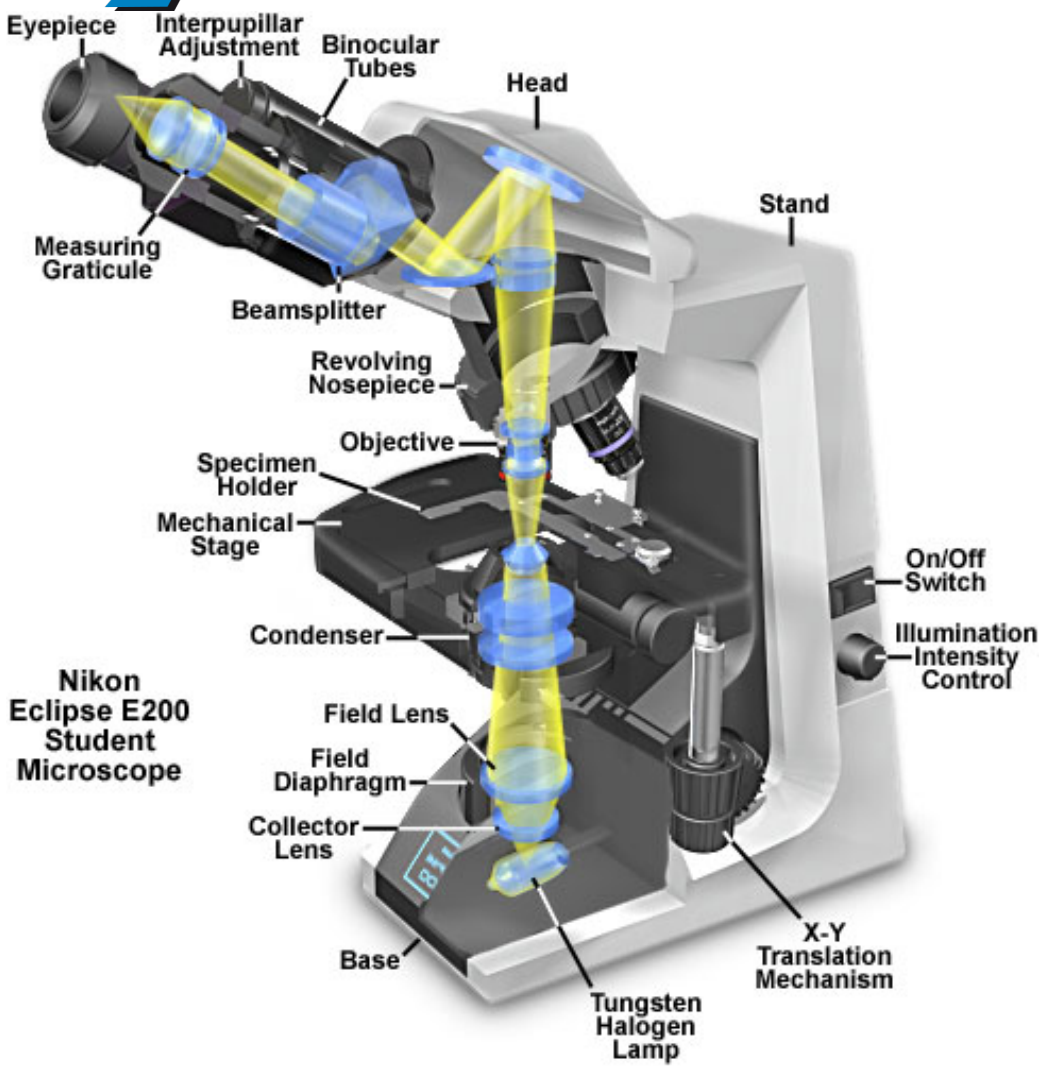

Cutaway diagram of a visible light microscope

Full-field X-ray imaging or "one shot" X-ray image acquisition can be considered as the optical analogon to a visible light transmission microscope

BUT

Refractive index n is very close to unity and smaller than unity!!!

$$n = 1 - \delta(\lambda) - i\beta(\lambda) \lesssim 1$$

Background info: X-ray microscopy types

Elettra
Sincrotrone
Trieste

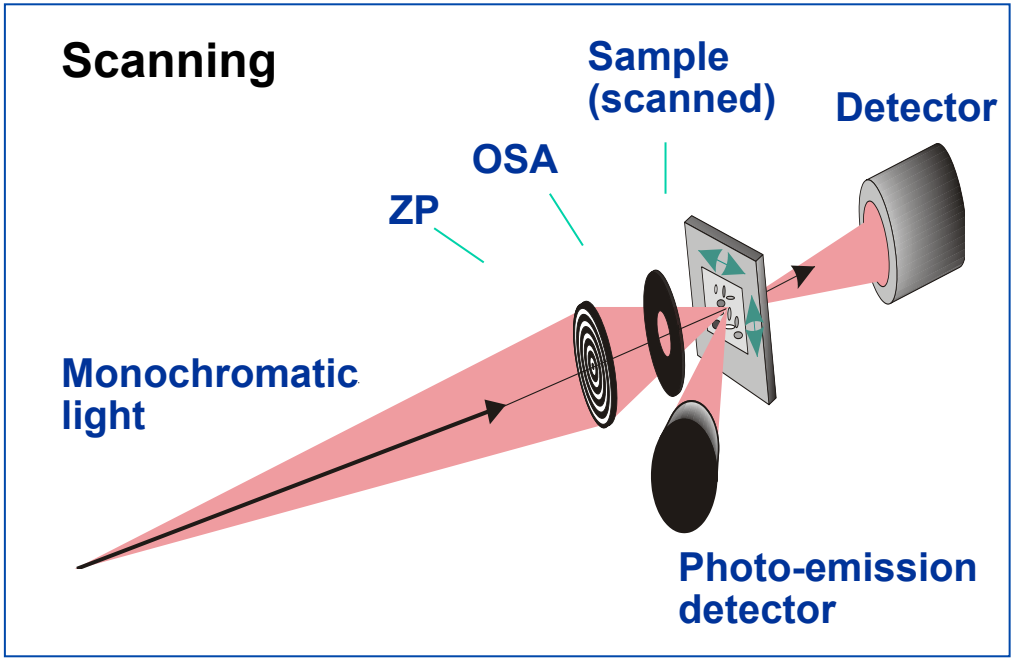

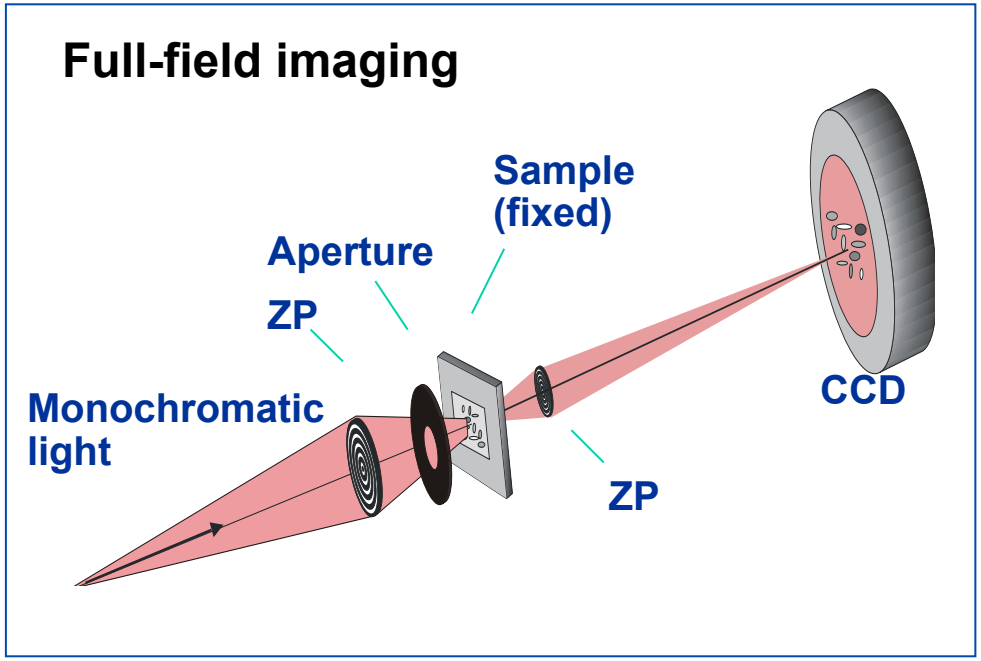

+ versatile detectors can run simultaneously;
+ easier optics set-up;
- long exposure time;
- complex electronics.

Ideal for spectromicroscopy

+ short exposure time;
+ higher resolution
- static system;
- complex optical alignment.

Ideal for dynamic studies and tomography

Elettra
Sincrotrone
Trieste

Background info: Diffraction by a grating

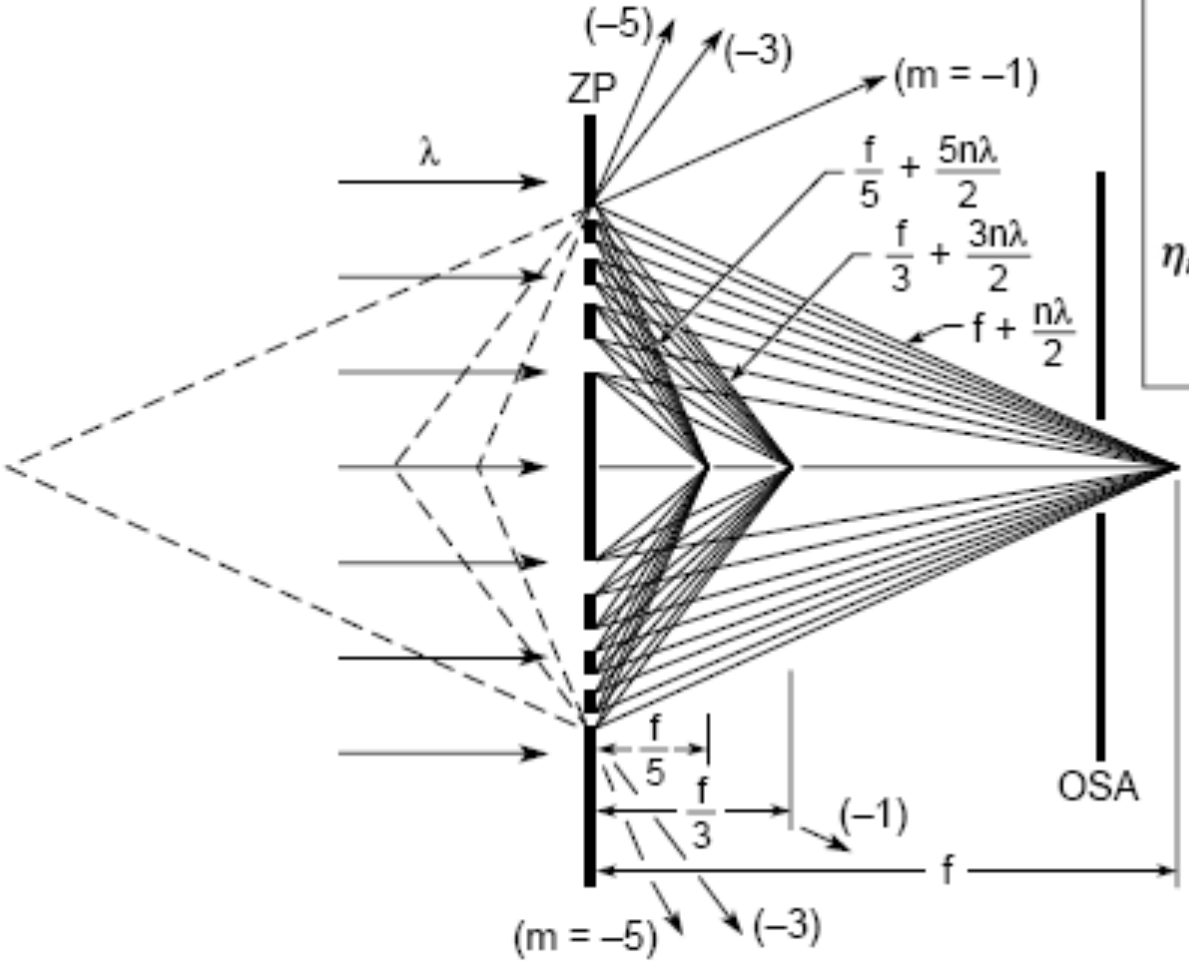

$$r_n^2 \simeq mn\lambda f_m \qquad (9.19)$$

$$\eta_m = \begin{cases} \frac{1}{4} & m = 0 \\ 1/m^2\pi^2 & m \text{ odd} \\ 0 & m \text{ even} \end{cases} \qquad (9.24)$$

$$f_m = \frac{1}{m}\,\frac{r_N^2}{N\lambda}$$

$$f_m = \frac{1}{m}\,f_1$$

Elettra
Sincrotrone
Trieste

The complex refractive index

$$n = 1 - \frac{n_a r_e \lambda^2}{\pi}\left(f_1 + i f_2\right) \equiv 1 - \delta - i\beta \leq 1$$

"Conventional refractive index" describing phase change:

$$\varphi(z) = \frac{2\pi}{\lambda}\delta z$$

Exploitation of phase contrasts possible using X-rays ?
Lower radiation damage ?

Describing photoelectric absorption with coefficient:

$$\mu = \frac{4\pi}{\lambda}\beta$$

Consequence:
Emission of Auger, photo-electrons and fluorescence photons, but also causes radiation damage (energetic secondary electrons!)

Elettra
Sincrotrone
Trieste

Delta versus beta

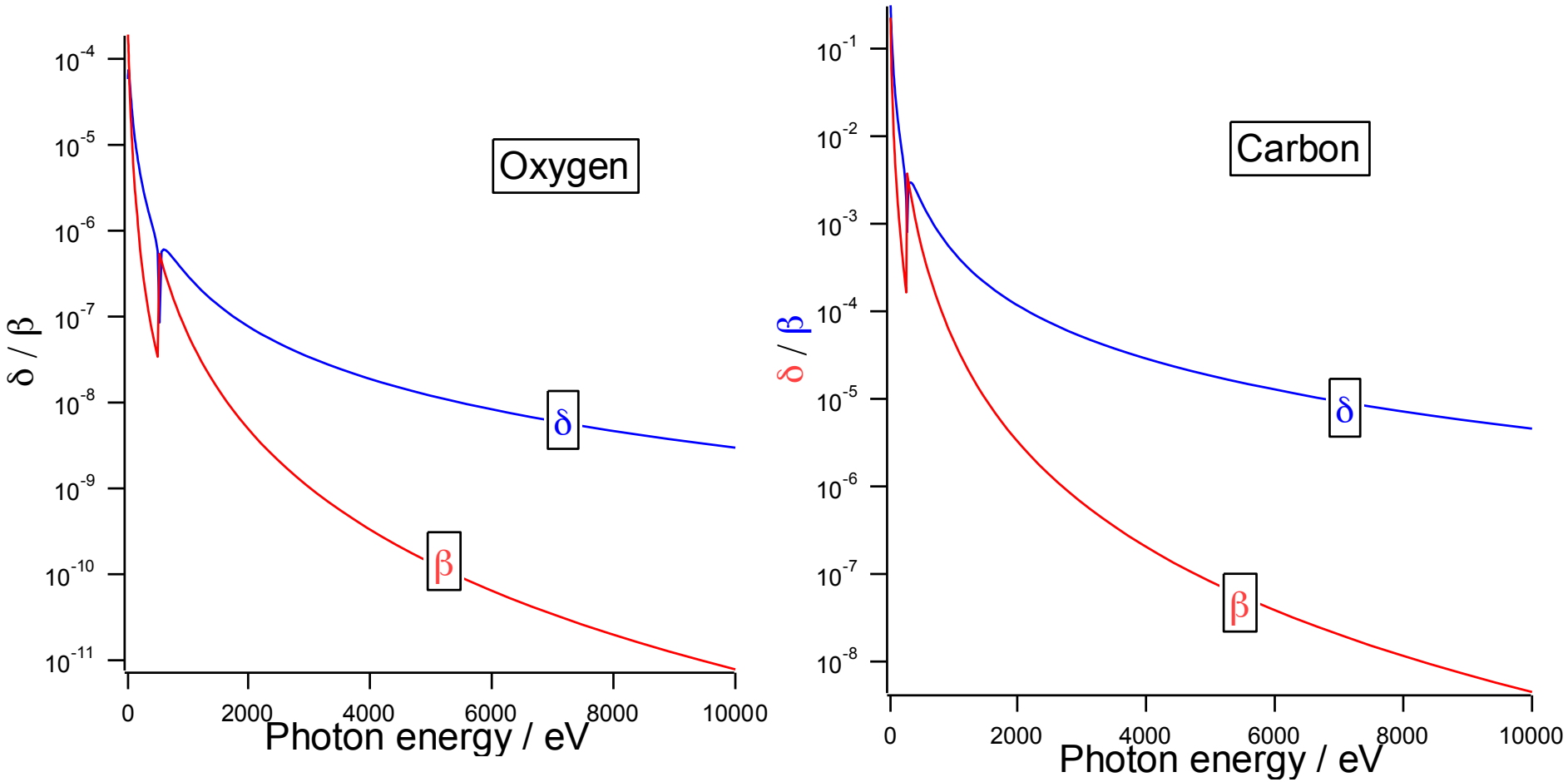

Delta is orders of magnitude larger !!!

Elettra
Sincrotrone
Trieste

Absorption mode

X-ray photons are selectively absorbed by the material according to its density and thickness
(ex. radiography)

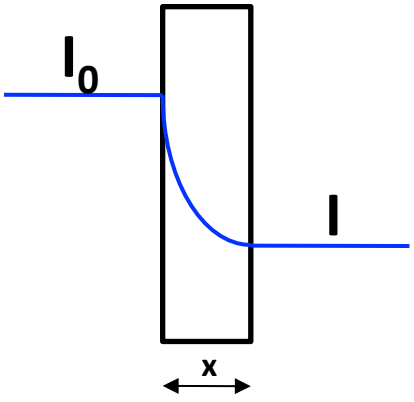

Beer - Lambert's law:
$I = I_0 e^{-mx}$

Phase contrast mode

Absorption can produce little contrast for light (transparent) materials or for materials with similar atomic number (similar attenuation factors).

Moreover as the energy increases the contrast diminishes (absorption coefficient $\propto 1/E^3$)

Phase contrast is more sensitive to edges and borders in the sample

Contrast techniques using the real, phase-shifting part of the complex refractive index are in many cases superior to absorption contrast because:
(i) the x-ray dose can be reduced dramatically
(ii) the throughput is higher (the phase shift dominates the absorption in the x-ray regime)

B. Kaulich et al. J. Phys.: Condens. Matter 23 (2011) 083002

Elettra
Sincrotrone
Trieste

Full field Imaging mode

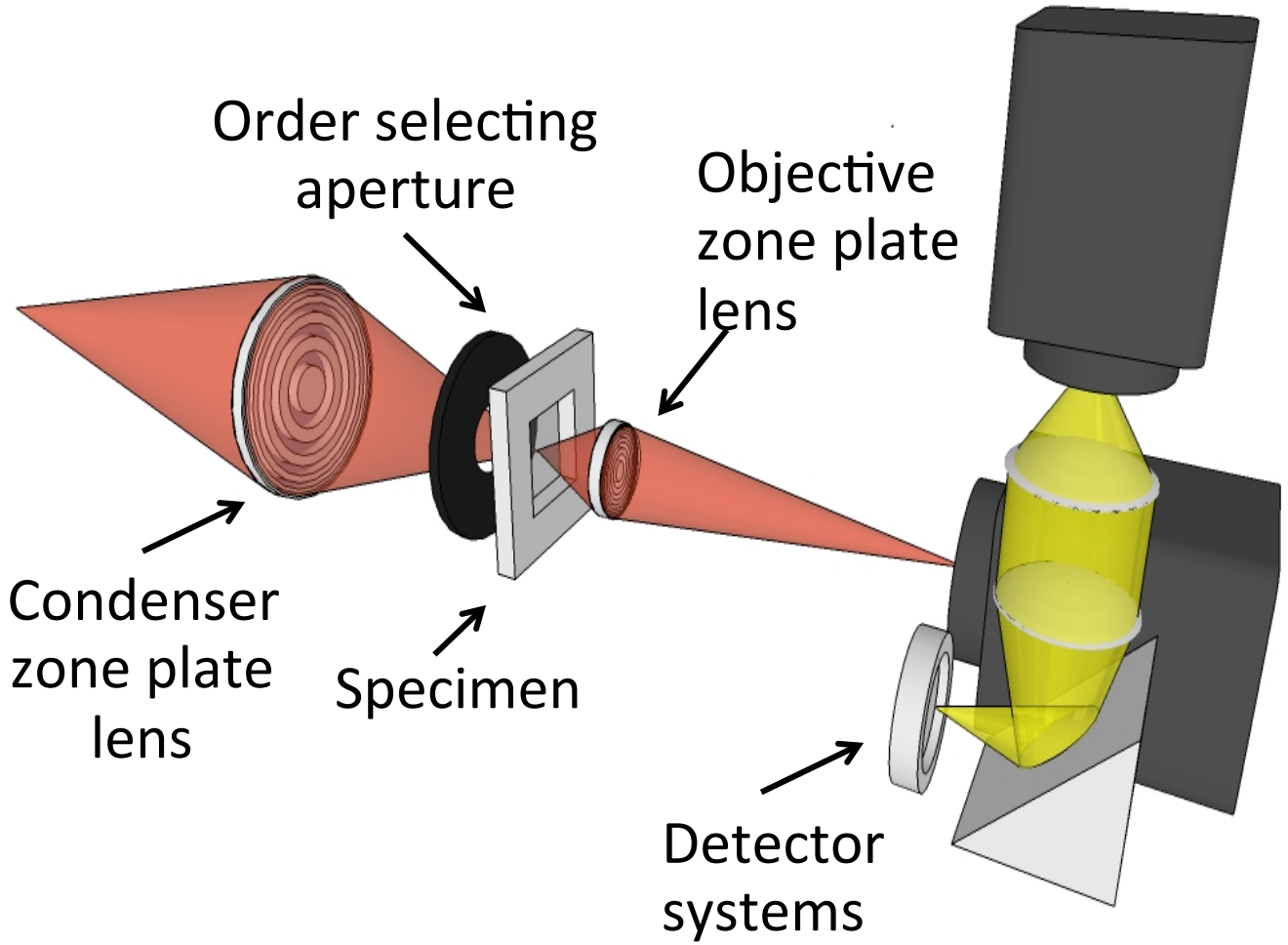

- Similar to conventional visible light microscope
- Analysis of morphology in transmission
- Fast imaging, dynamics, microtomography

Elettra Sincrotrone Trieste

Resolution tests in full-field imaging

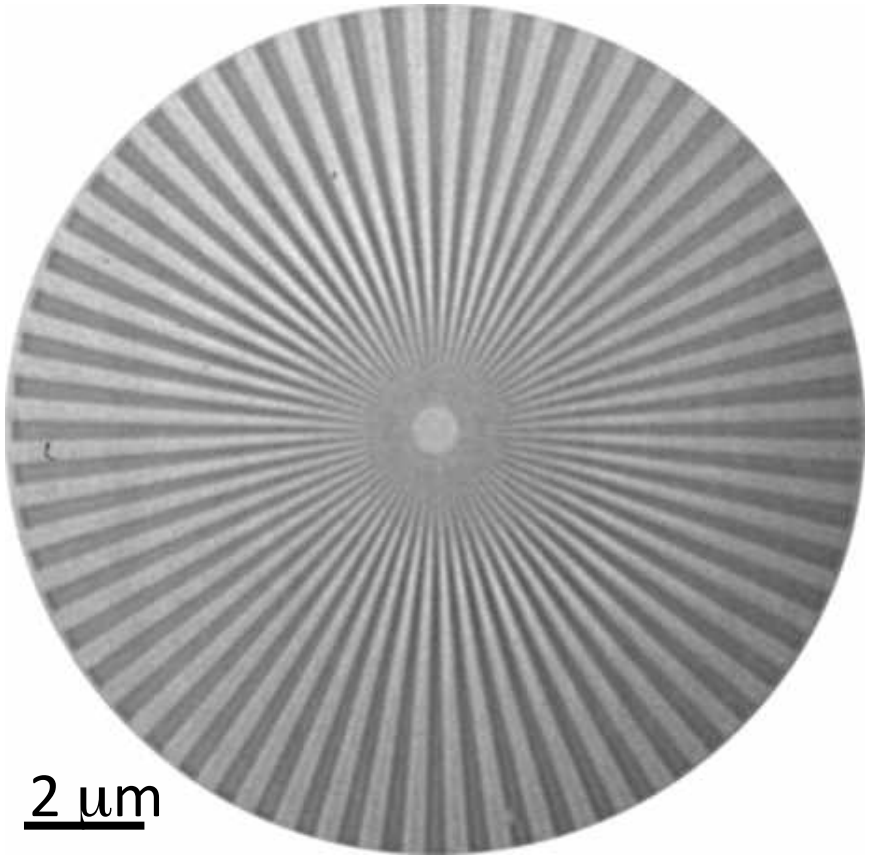

2 μm

ZP parameters:
110 μm diameter
50 nm outer zones
f=3.2 mm @ 720 eV
fabricated by TASC/ INFM

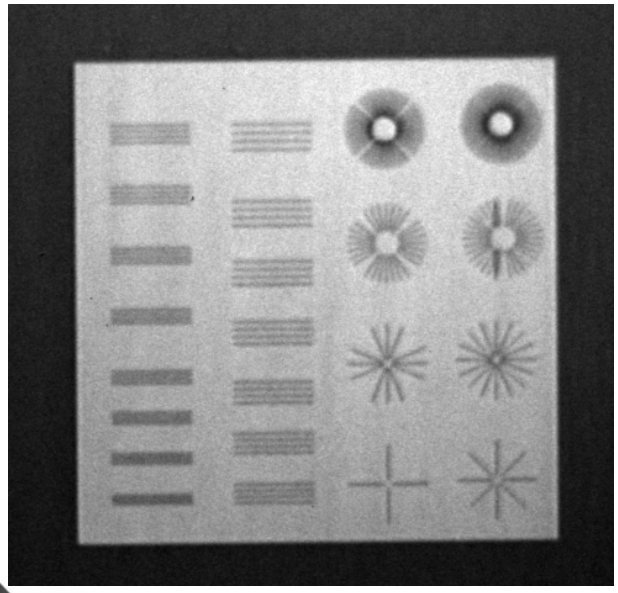

2 μm

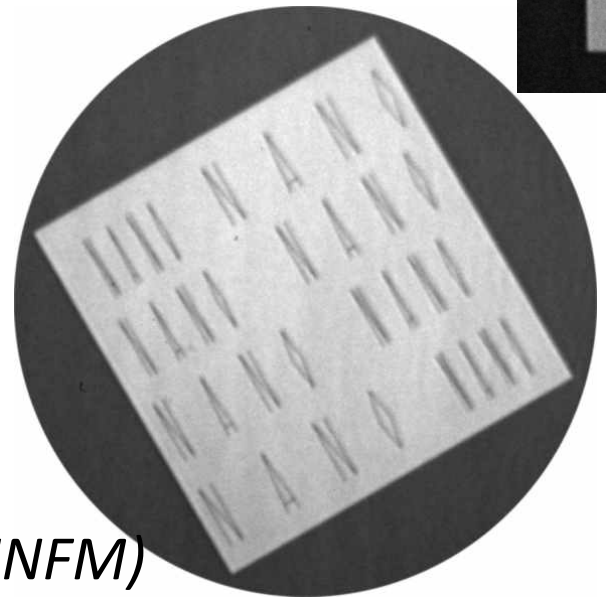

Test pattern with 30 nm features (fabricated by TASC/ INFM)

Experiment performed by M. Prasciolu and D. Cojoc, TASC/ INFM)

Natural amplitude contrast between water and organic matter

Elettra
Sincrotrone
Trieste

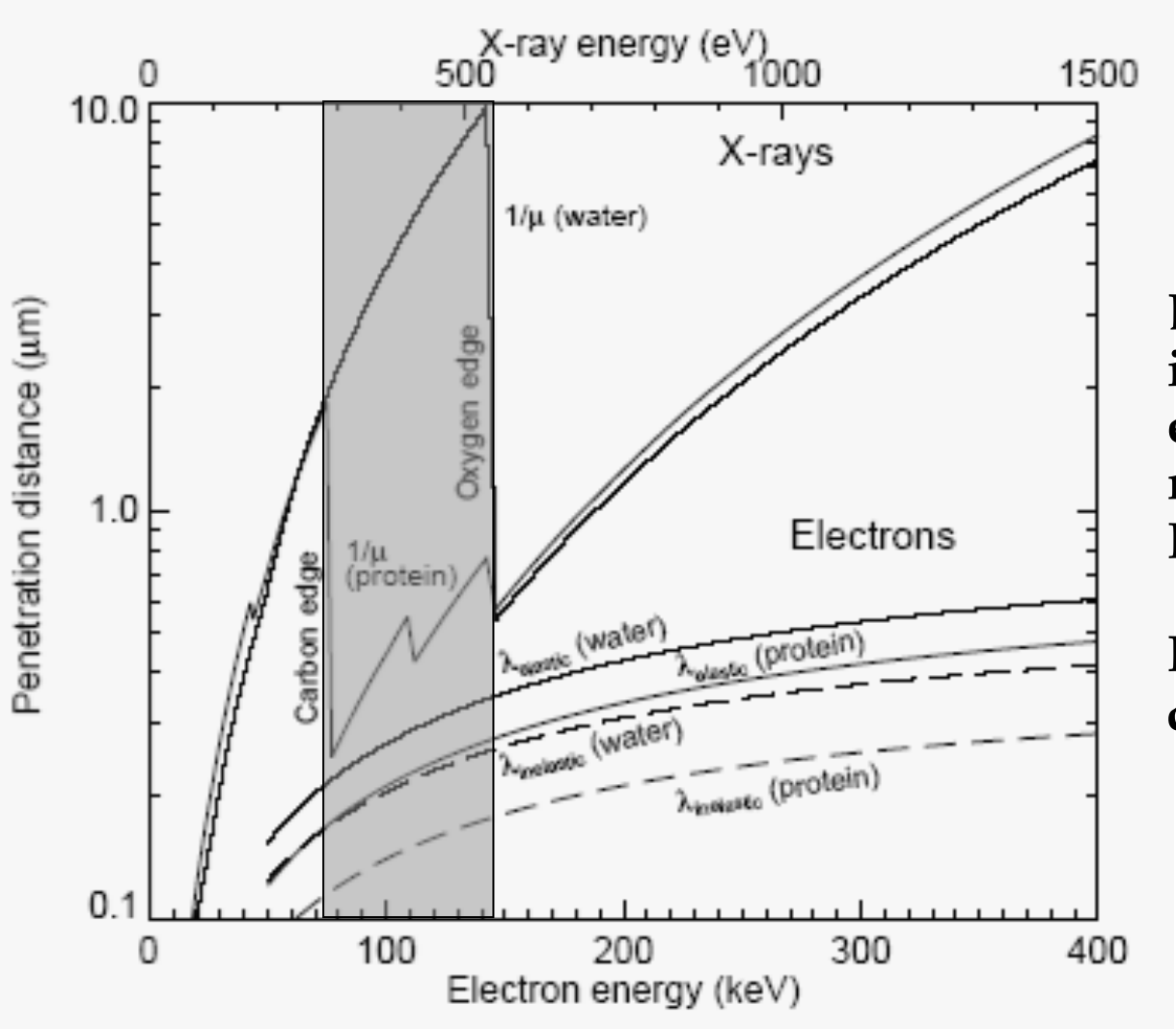

The "Water Window":

Due to dramatic difference in the f2 values of two materials, especially water and organic matter between the C and O K-absorption edges.

Note the penetration distance compared to electrons !!!

H. Wolter: *Spiegelsysteme streifenden Einfalls als abbildende Optiken fuer Roentgenstrahlen*, Ann. Phys. 10, 94-114, 286 (1952)

Elettra Sincrotrone Trieste

Environmental science: Imaging in liquids

Bacteria and clay dispersion: Destruction of associations of clay particles by soil microbes

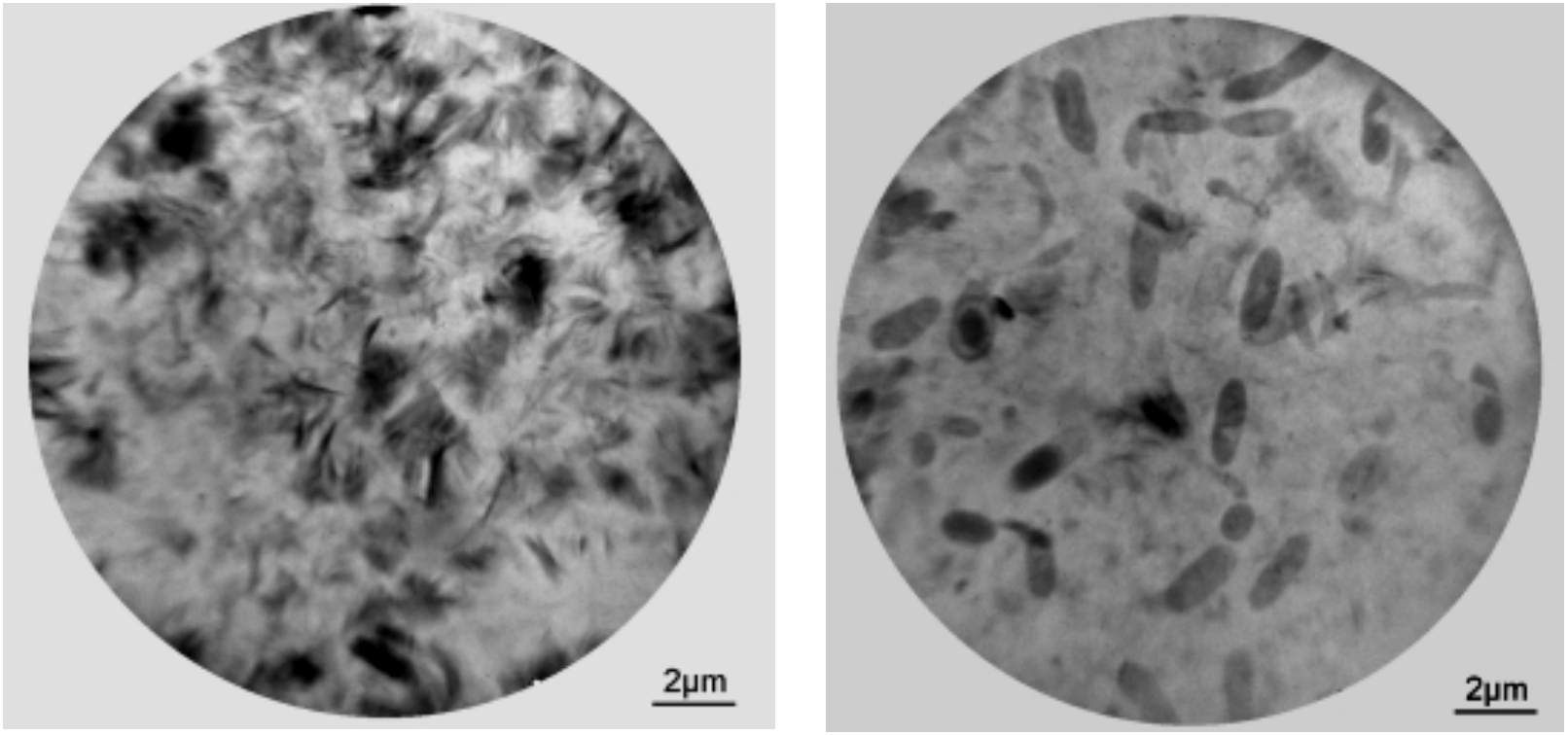

X-ray images acquired with the full-field imaging microscope at BESSY I @ 520 eV

Samples analysed in the natural hydrated state:
→ no alteration of the environment of the sample

J. Thieme et al., IRP, Uni Goettingen / G. Machulla, Uni Halle, D

Elettra
Sincrotrone
Trieste

Across edge imaging

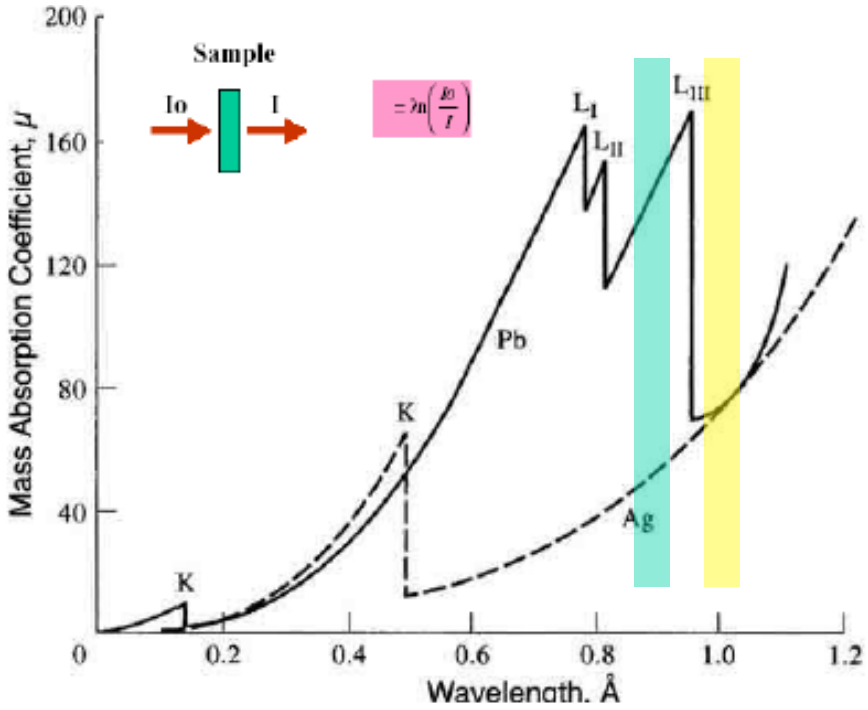

Discontinuities due to absorption

The absorption occures when the incoming X-rays are matching the electron binding energies

Absorption edges are fingerprints ⇒ they can be used to identify the chemical elements

By taking two images, one above and one below a specific absorption edge, the correspondent chemical element will give a high contrast difference in the two images

Brightfield imaging at higher photon energies

Elettra
Sincrotrone
Trieste

Characterization of morphology and defects in modern semiconductors with a full-field imaging microscope (@ 1.8 keV, XM1/ ALS)

Sample preparation:
Back side thinning of Si wafer

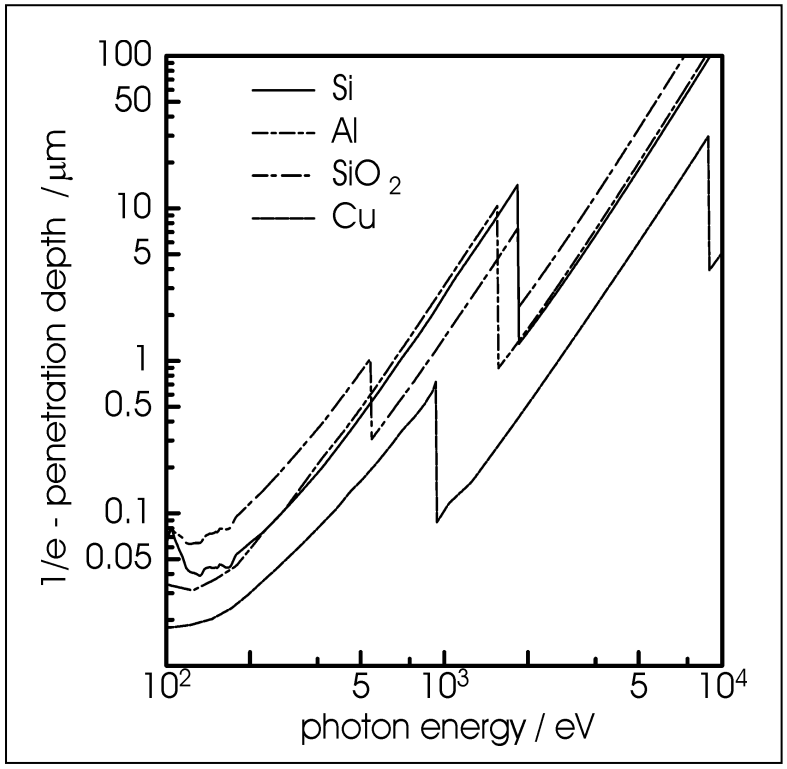

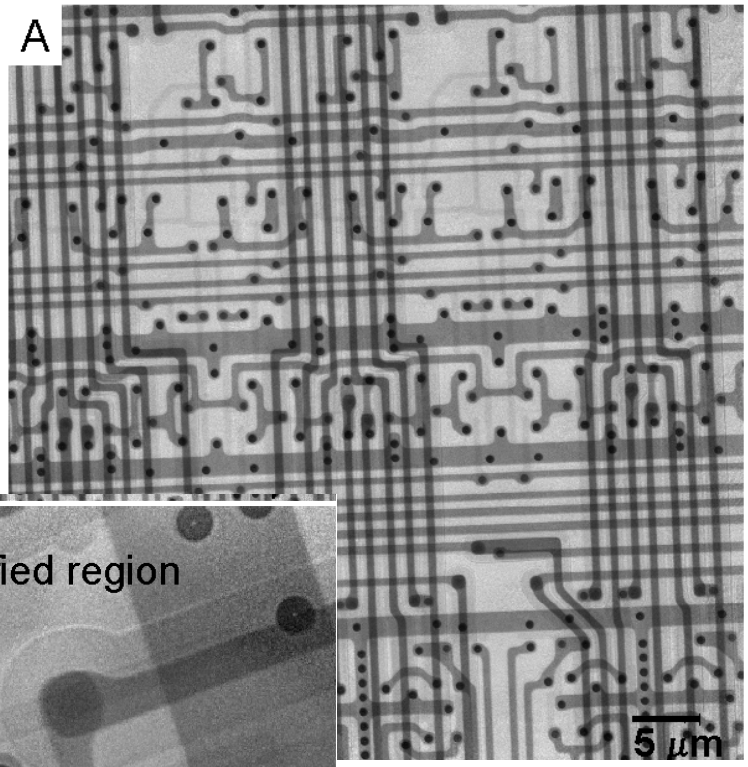

G. Schneider et al., BESSY II

Environmental science: Analysis of air particulate matter

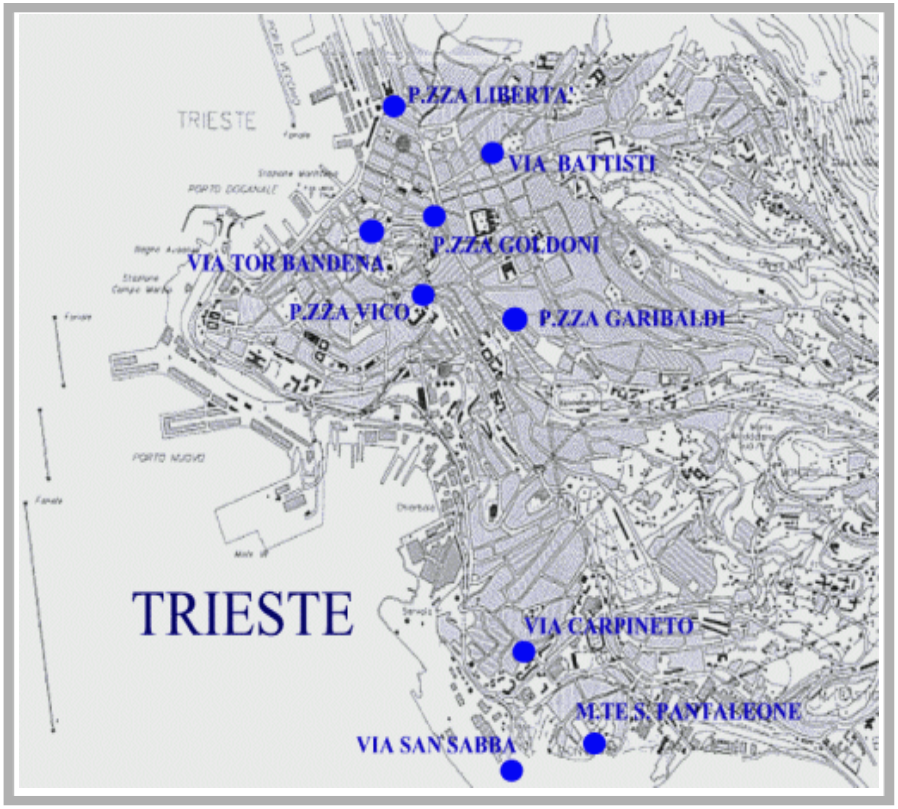

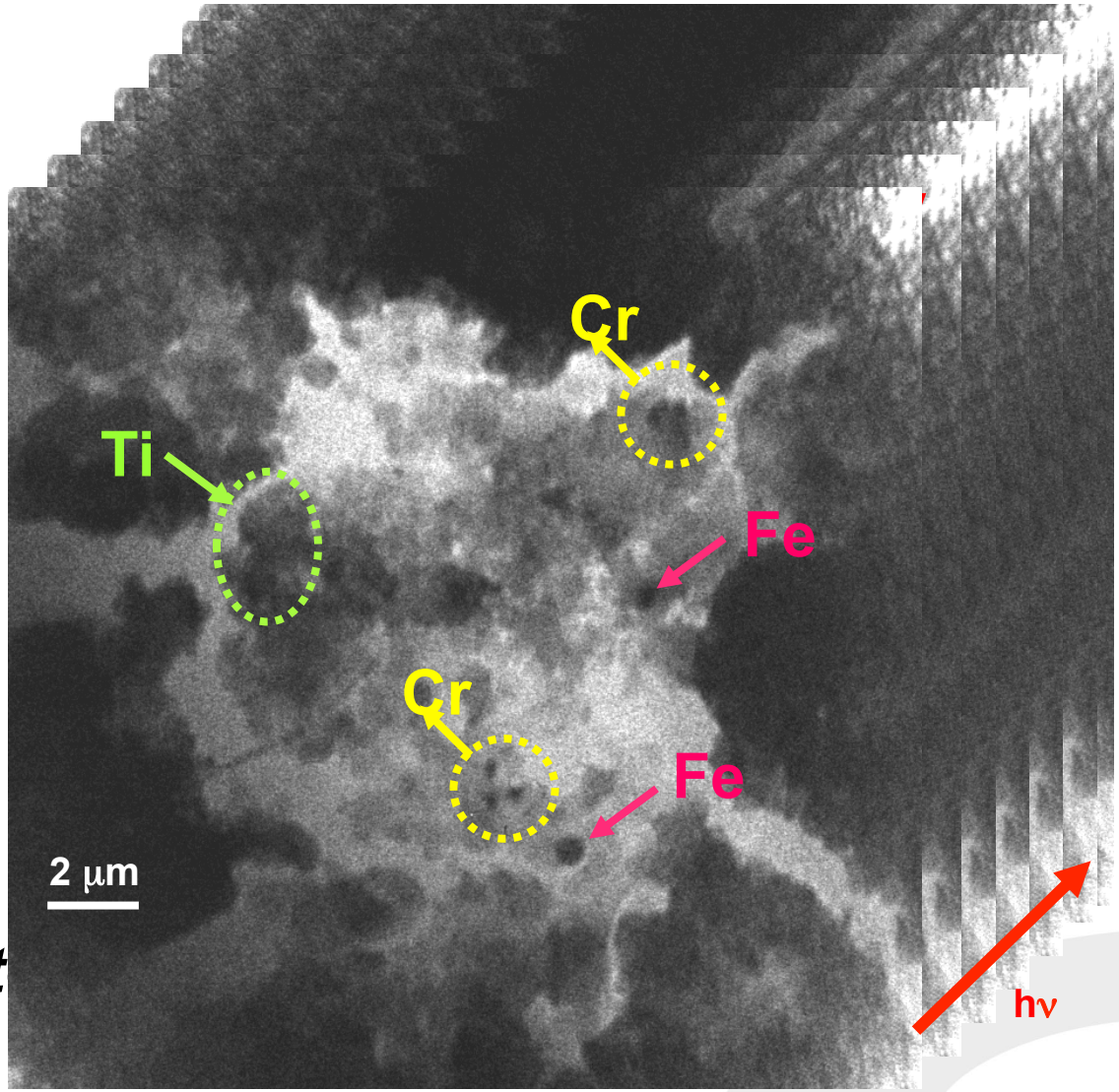

P. Barbieri et al.,
Dept. of Chem., Univ. Triest

Darkfield or darkground imaging

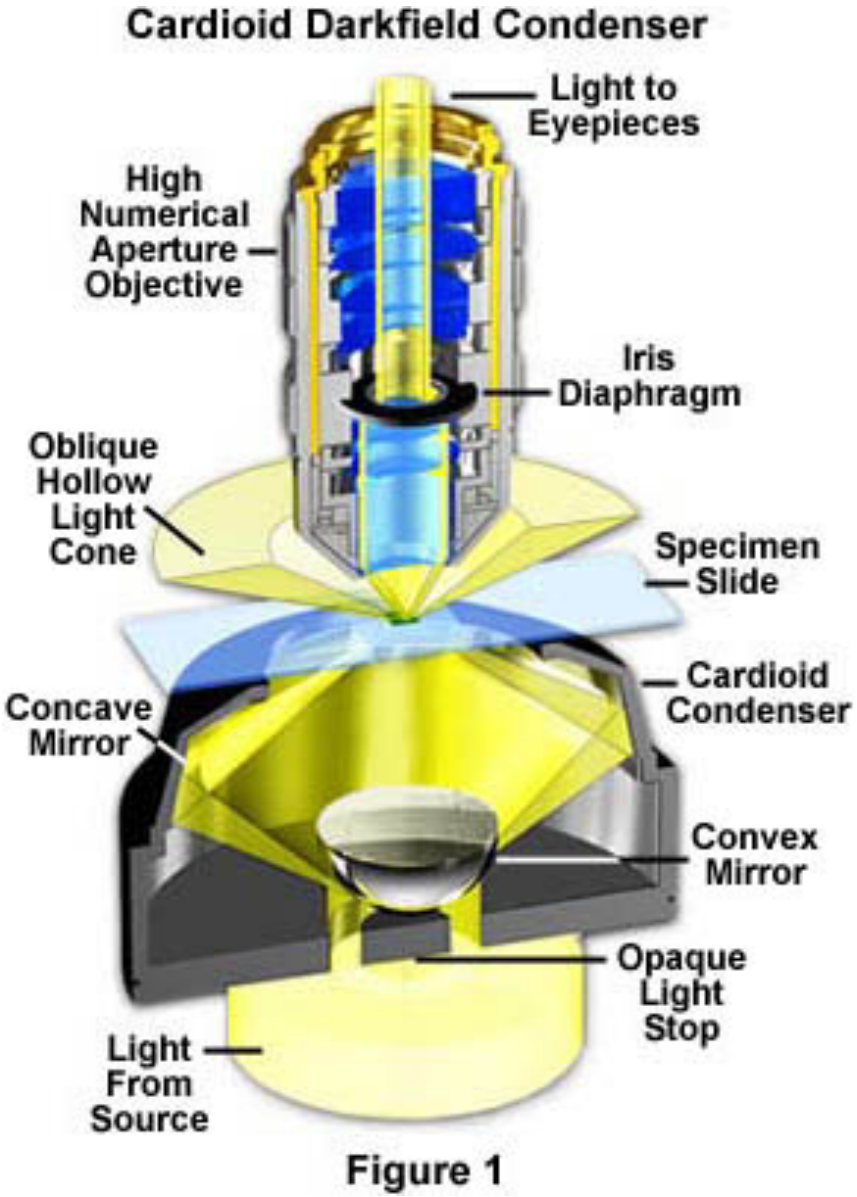

Figure 1

Darkfield illumination requires blocking out of the central light which ordinarily passes through and around (surrounding) the specimen, allowing only oblique rays from every azimuth to "strike" the specimen.

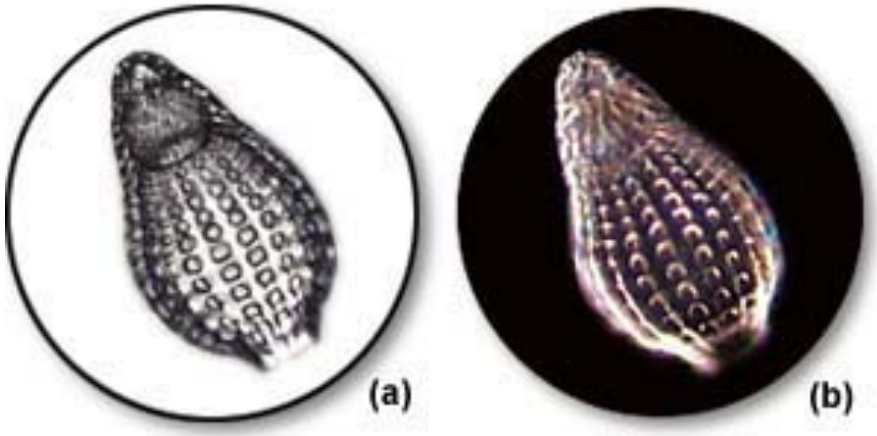

Visible light micrographs of silica skeletons from a small marine protozoan (radiolarian)

Darkfield imaging in scanning X-ray microscopy

Elettra
Sincrotrone
Trieste

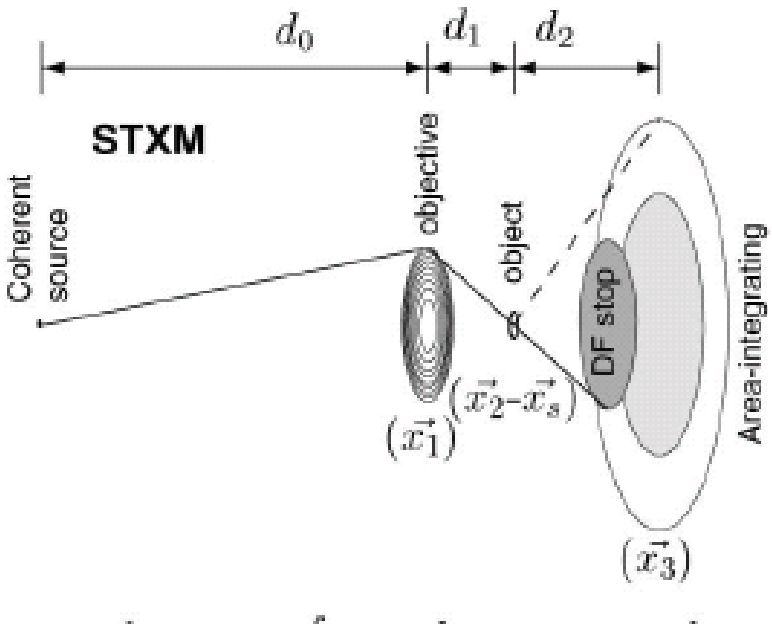

Technique is especially suited for small, strongly scattering particles as for example a few 10nm diameter labelling spheres

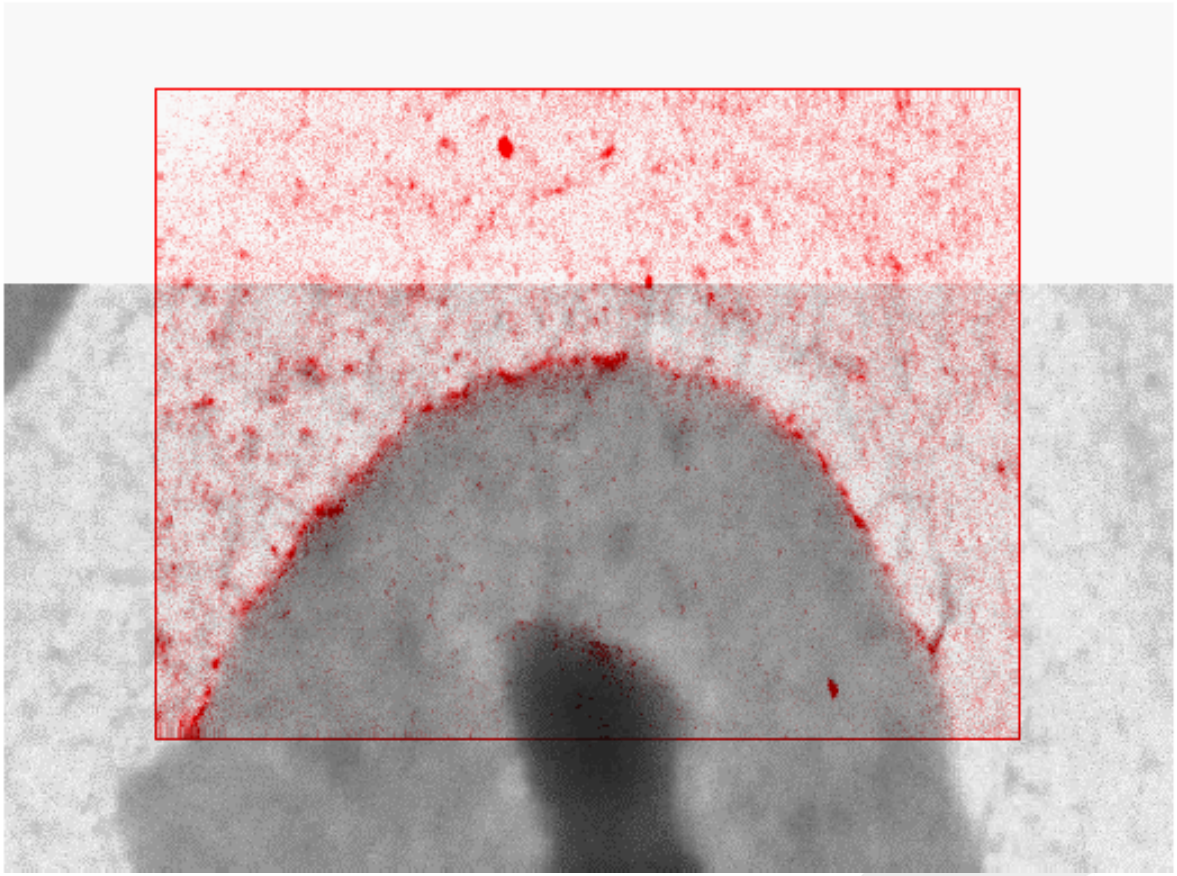

Brightfield image of a cell with Au labelling spheres overlayed with a darkfield image

Images acquired with STXM at the NSLS

S. Vogt, M.A. thesis, SUNY Stony Brook (1997).

Elettra
Sincrotrone
Trieste

Detector based contrast technologies in scanning X-ray microscopy:

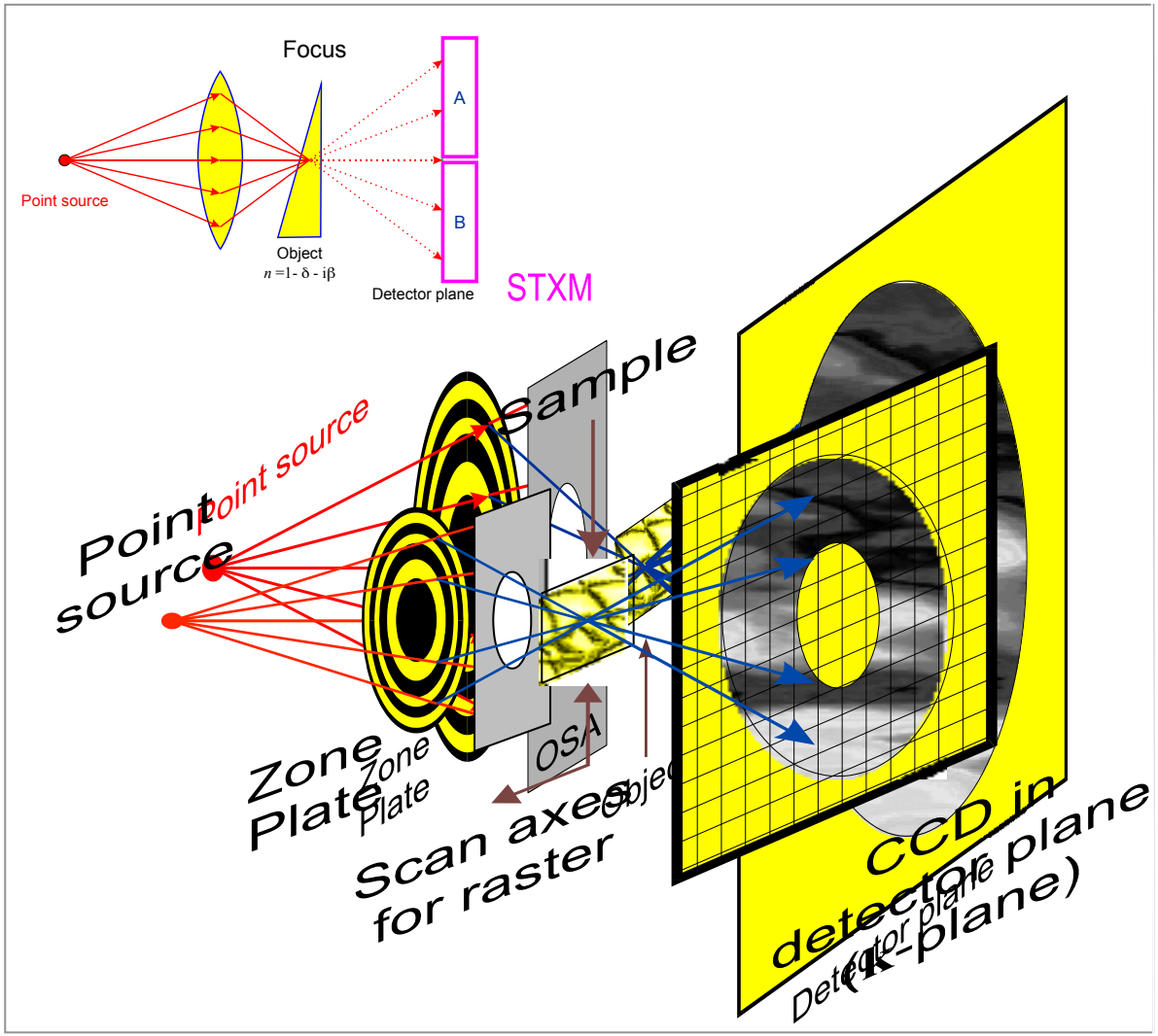

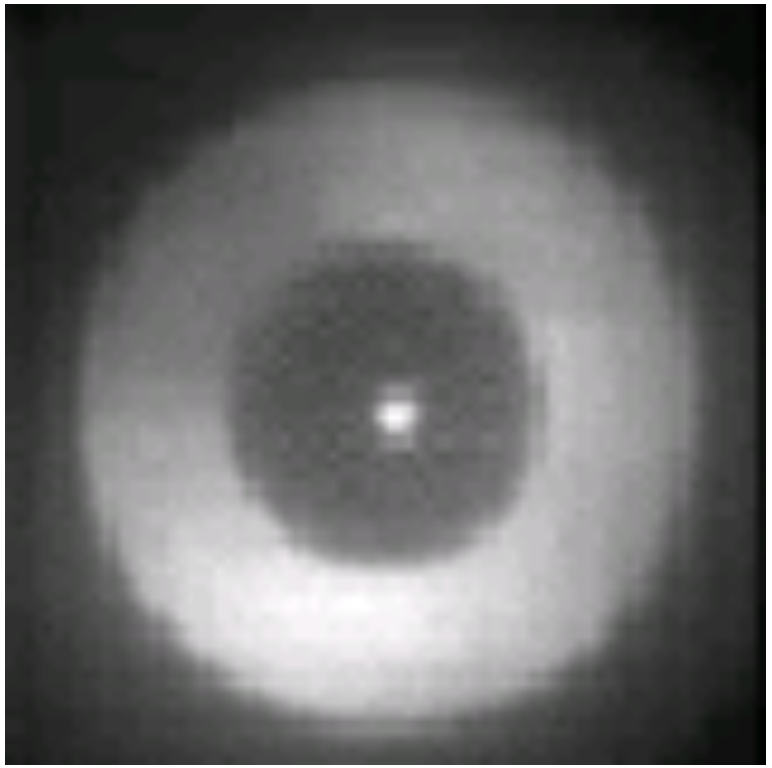

Frame transfer back-illuminated Electron Multiplying CCD with shutter and light converting system (128x128px, 5 Mhz, 110f/s)

Elettra
Sincrotrone
Trieste

Computational extraction of contrasts by masking:

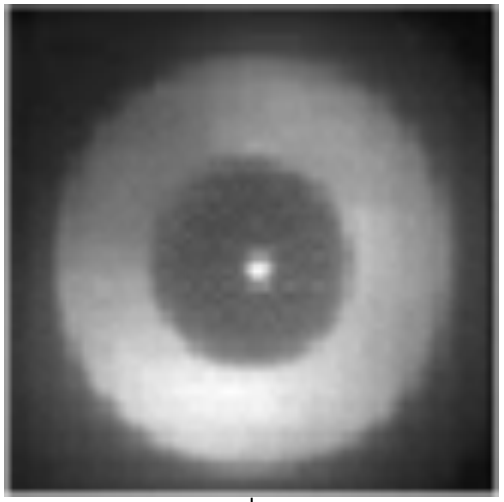

Raw data acquisition of first diffraction order image for each pixel of the raster scan

Applying different masks

Bright field

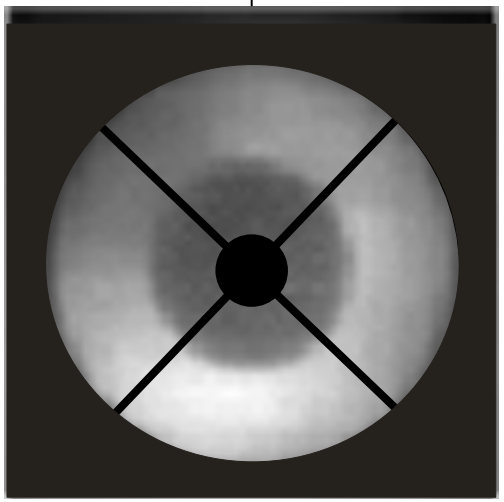

Differential phase and absorption

Darkfield

A. Gianoncelli et al., Appl. Phys. Lett.

Principle: Differential phase contrast

Elettra
Sincrotrone
Trieste

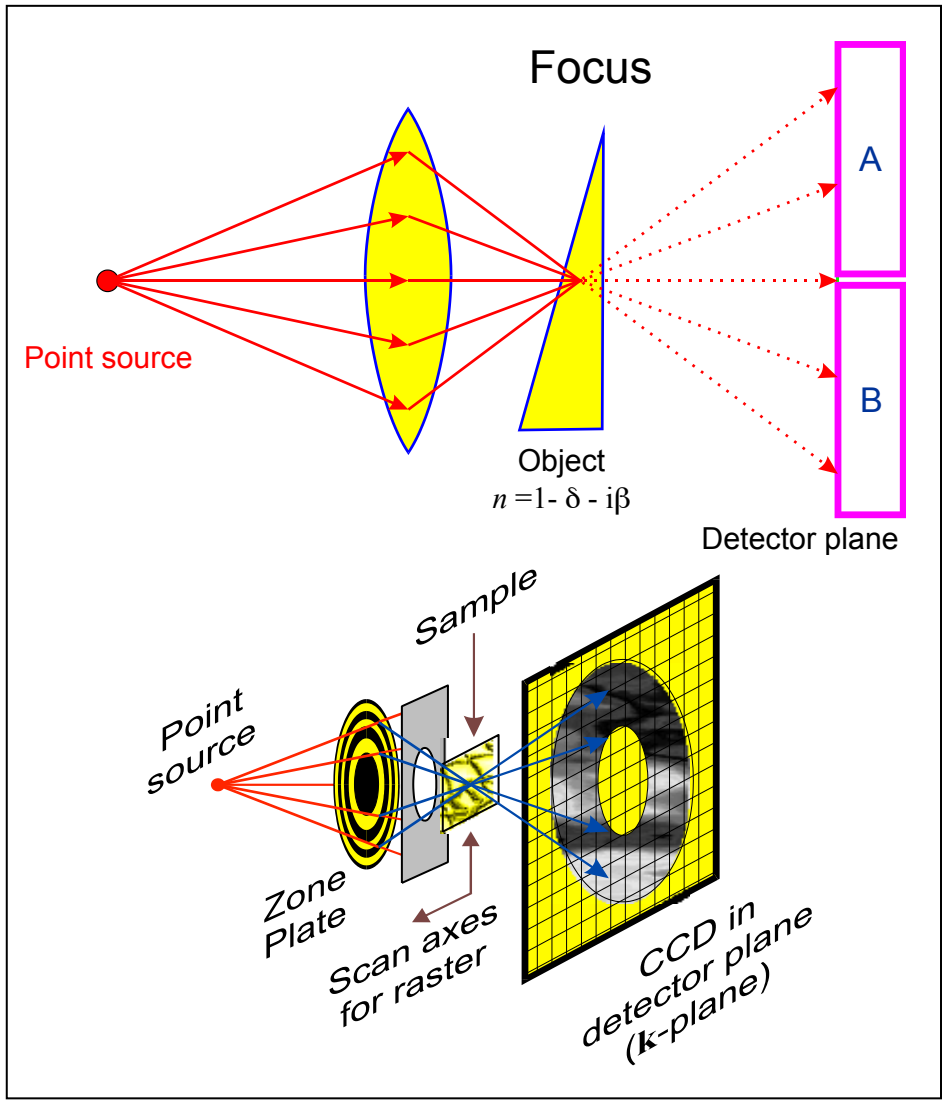

- The detector can be split into several elements
- The sum signal gives the incoherent bright-field signal
- Anti-symmetric signal combinations relate to the *phase gradient* of the object transmittance.

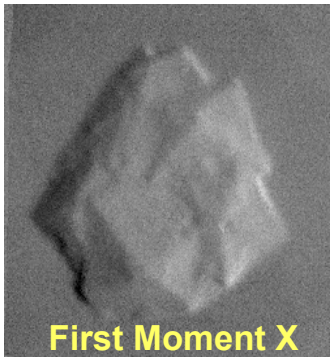

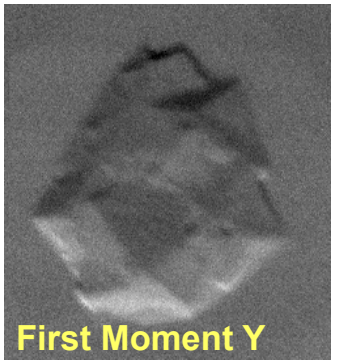

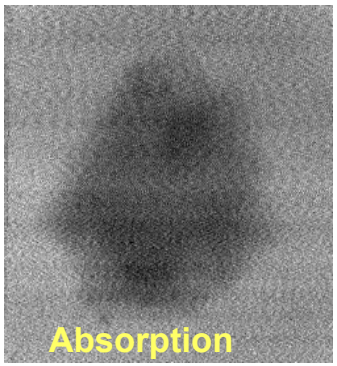

10 µm

3.3 keV

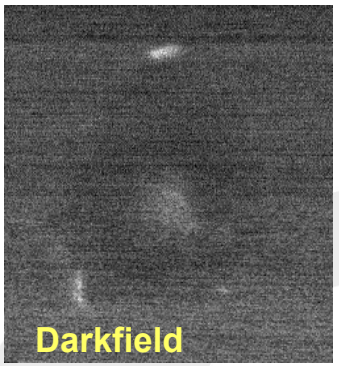

Elettra
Sincrotrone
Trieste

Marine biology: Imaging of giant diatoms

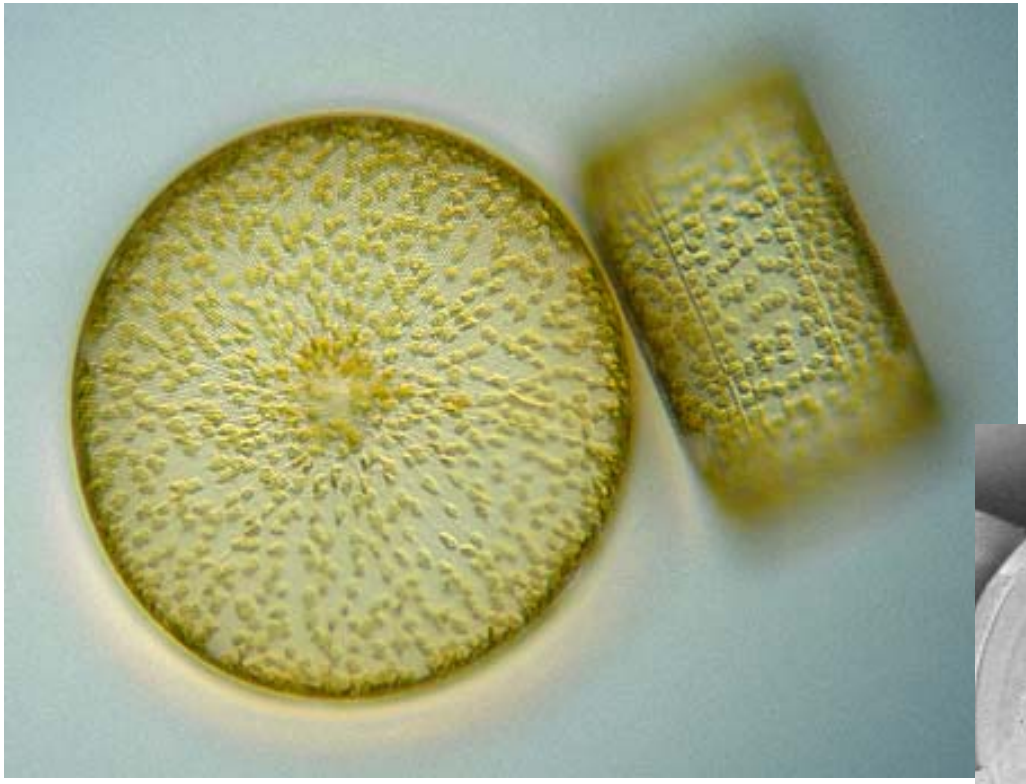

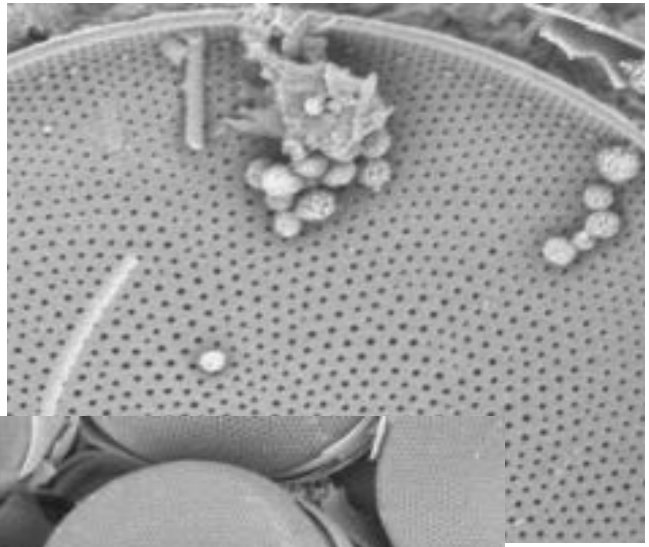

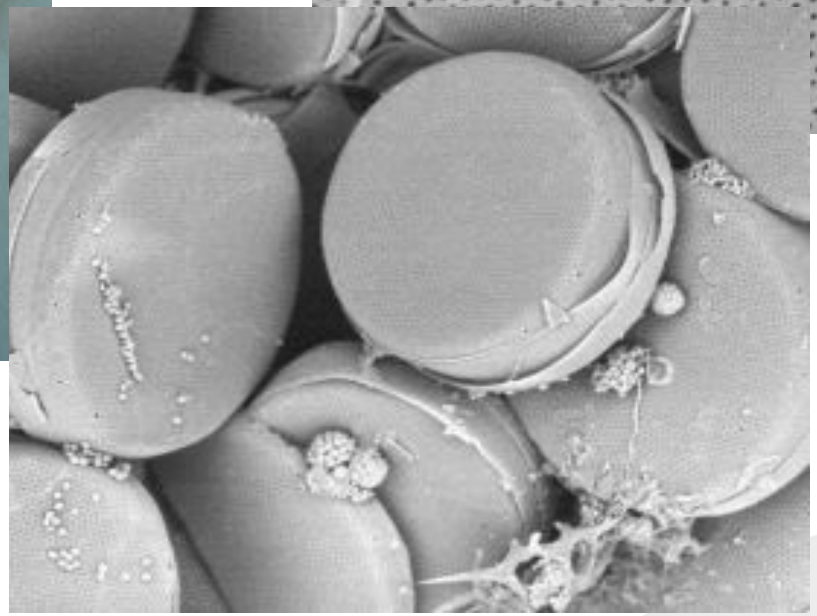

Planktonic diatom Coscinodiscus sp. (A. Beran, Laboratory for Marine Biology, Trieste, I)

Simultaneous absorption and phase contrast imaging

Elettra Sincrotrone Trieste

Planktonic diatom "Casciodiscus sp." (provided by LBM, Trieste, I)

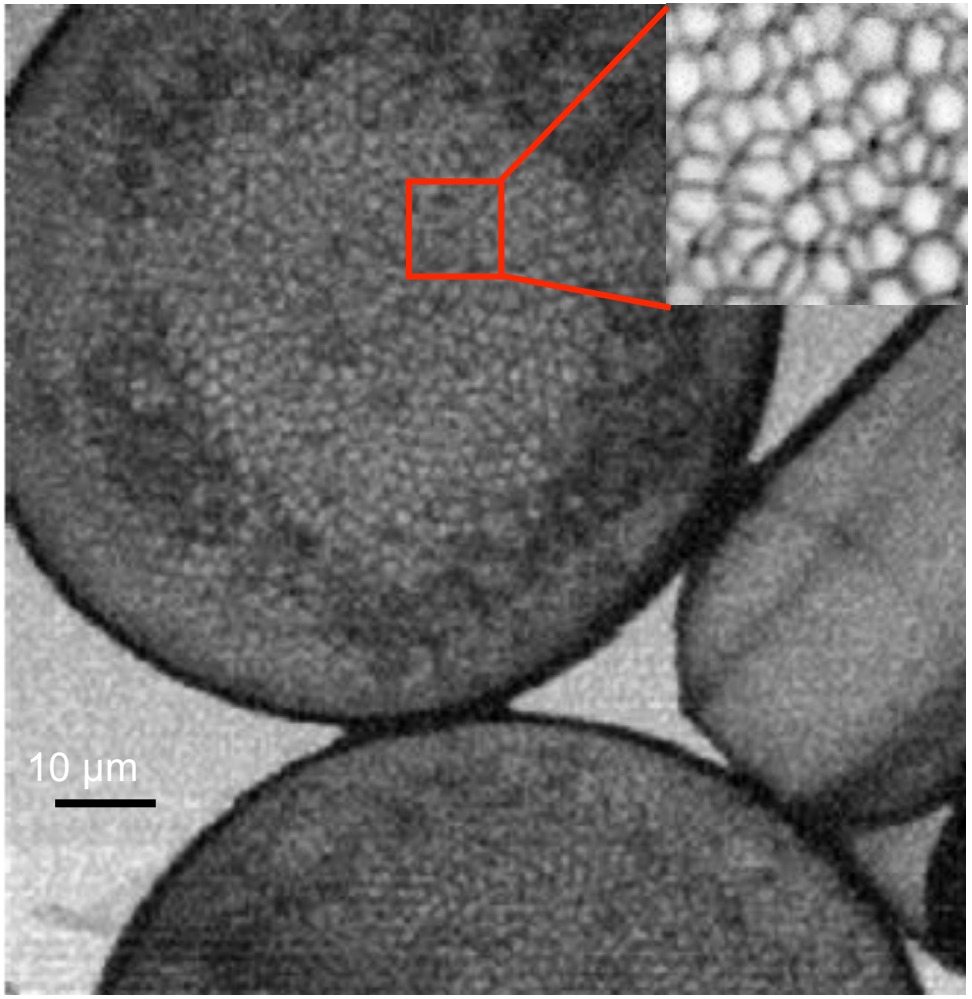

Bright field image

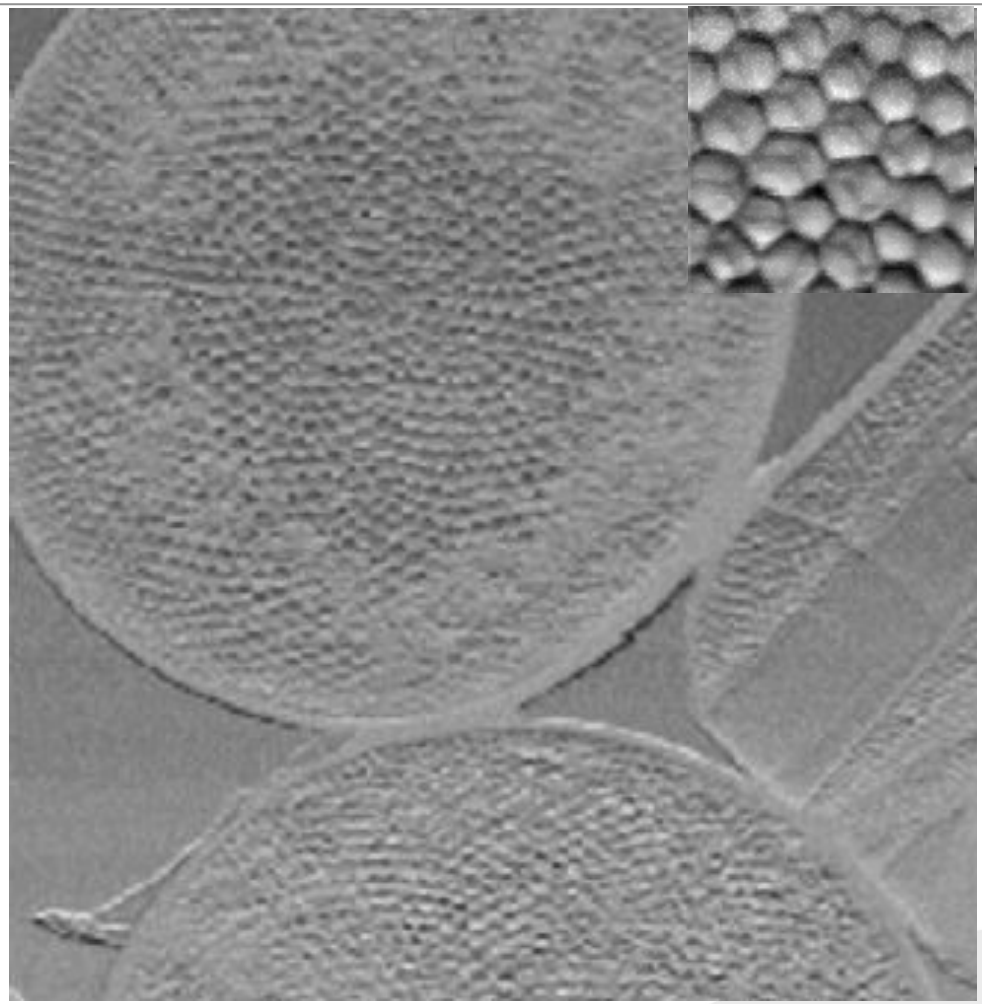

DPC mode – X-moment

Images acquired in STXM mode with FRCCD camera; E=1320 eV, 200x190 px, 50ms dwell/px

*B. Kaulich et al., JOSA A **19** (4), 797-806 (2002)*

Brightfield and differential phase contrast images acquired simultaneously with configured detector

Elettra
Sincrotrone
Trieste

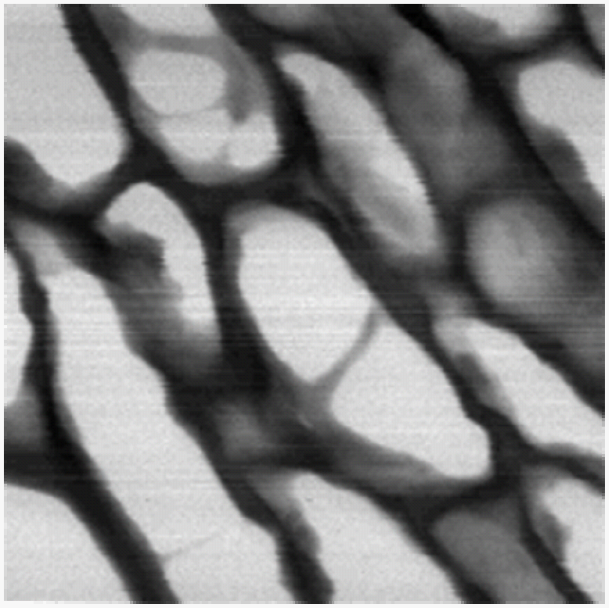

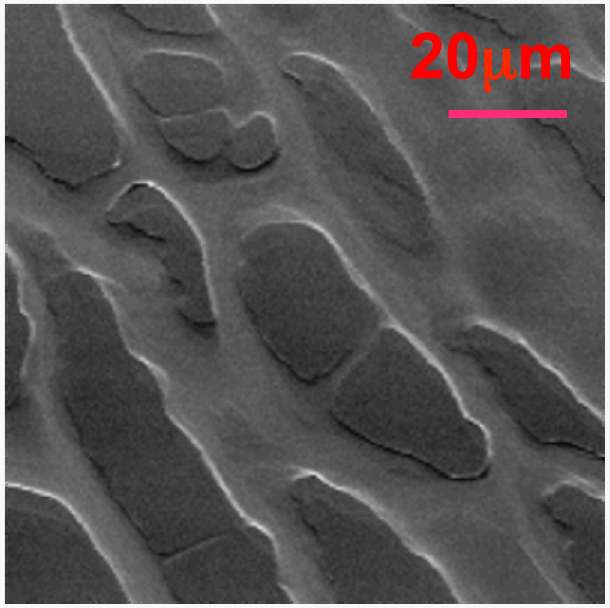

ffee bean cell membranes

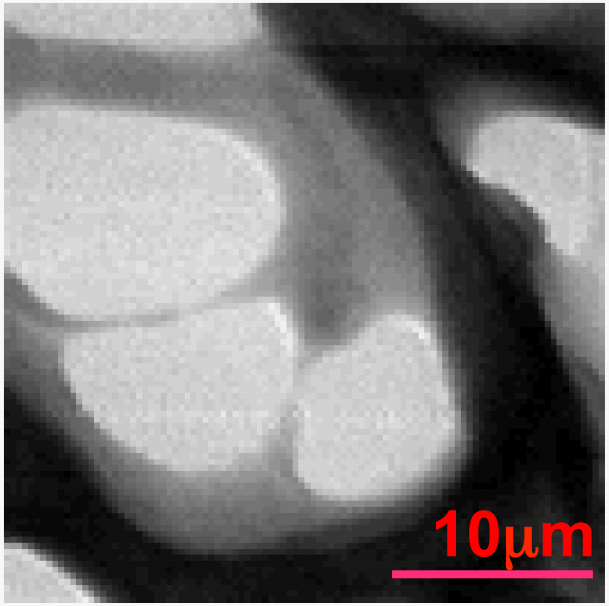

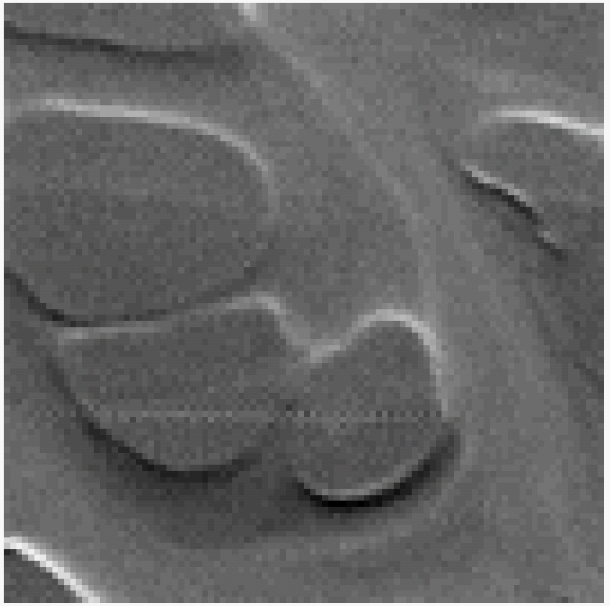

B. Bonnlaender, F. Sicilia, Illy AromaLab, et al.

Elettra
Sincrotrone
Trieste

Ptychography (CDI)

- Ptychography is rapidly developing into an important imaging tool in X-ray microscopy.
- It doesn't require X-ray Optics
- The technique involves successively illuminating overlapping regions of a specimen with a coherent probe and recording the resulting diffraction patterns.
- It is important that the illuminated areas overlap significantly since those common regions provide duplicate information that allows computer algorithms to reconstruct reliably both the sample transmission function and the illuminating probe from the measured diffraction patterns.

Elettra
Sincrotrone
Trieste

Ptychography (CDI)

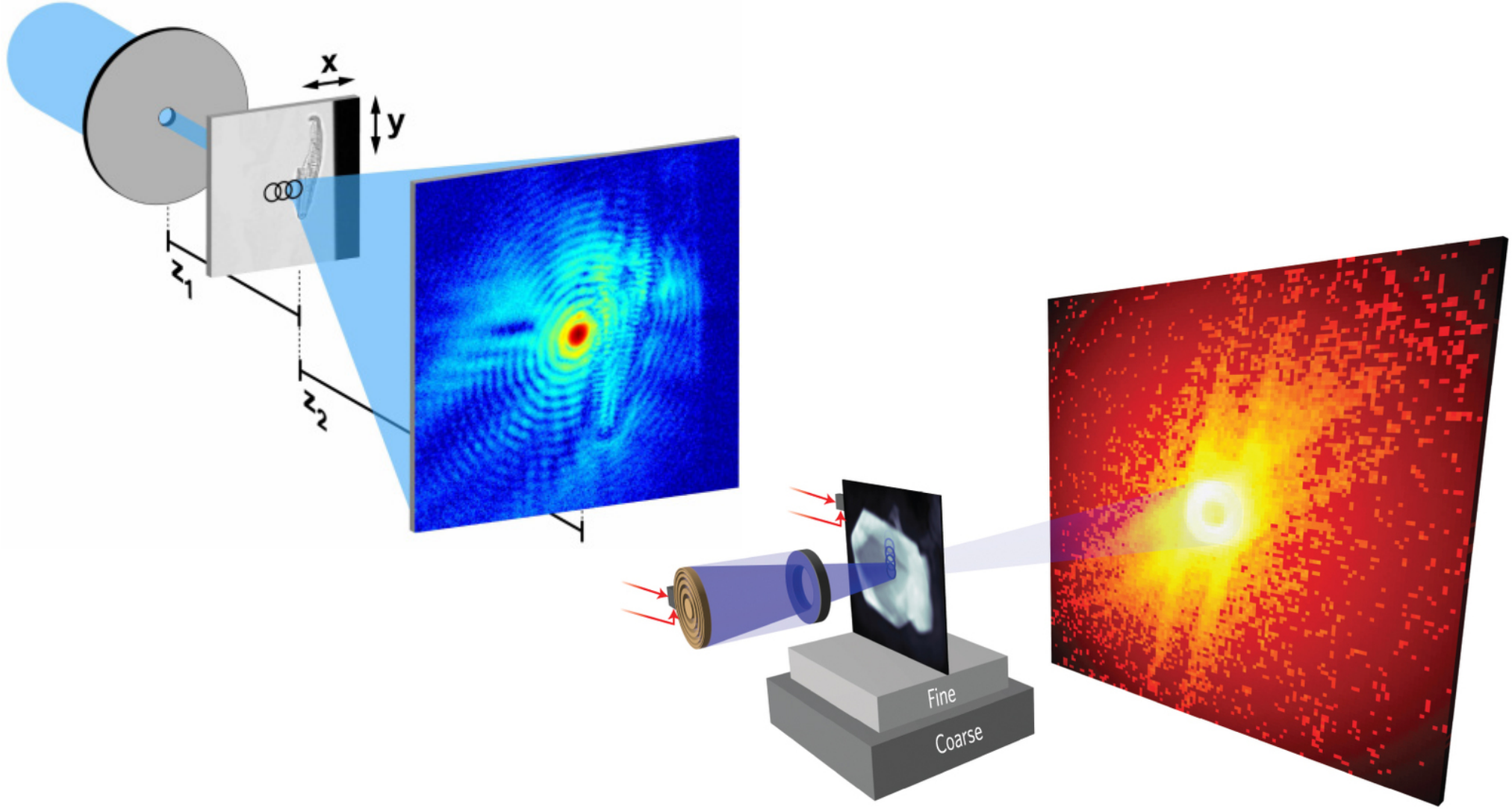

- K. Giewekemeyer, M. Beckers, T. Gorniak, M. Grunze, T. Salditt, and A. Rosenhahn Optics Express Vol. 19, Issue 2, pp. 1037-1050 (2011)
- D. A. Shapiro, Y.-S. Yu, T. Tyliszczak, J. Cabana, R. Celestre, W. Chao, K. Kaznatcheev, A. L. D. Kilcoyne, F. Maia, S. Marchesini, Y. Shirley Meng, T. Warwick, L. Lisheng Yang, H. A. Padmore Nature Photonics 8, 765–769 (2014)

Elettra
Sincrotrone
Trieste

Ptychography Algorithms

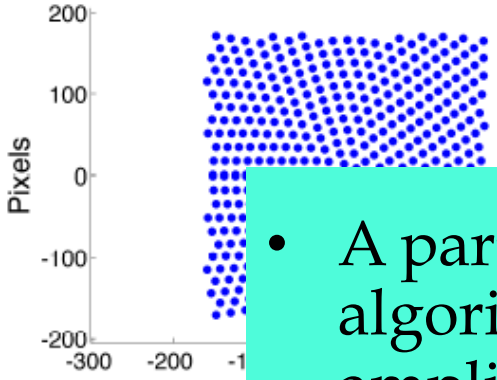

Start Guess Object

Scan

- A particularly useful feature of these algorithms is that they can recover the amplitude and phase of both these signals.
- The lateral resolution of the reconstructed image is not limited by the probe size, overcoming the limitation of X-ray microscopy imposed by the focusing optics

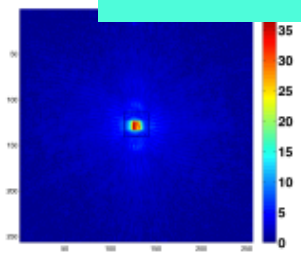

Processed Data

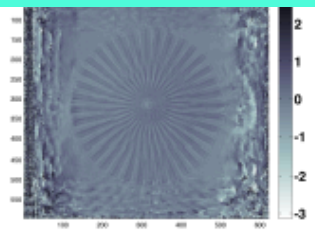

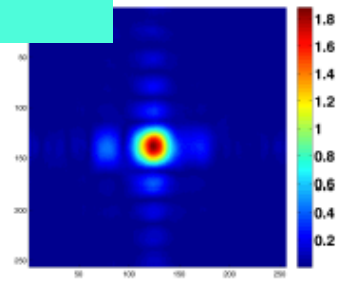

Probe from test object

Elettra
Sincrotrone
Trieste

Soft X-ray spectromicroscopy using ptychography with randomly phased illumination

- Illuminated area defined by a 5 μm pinhole
- Sample was scanned with raster steps ~1 μm

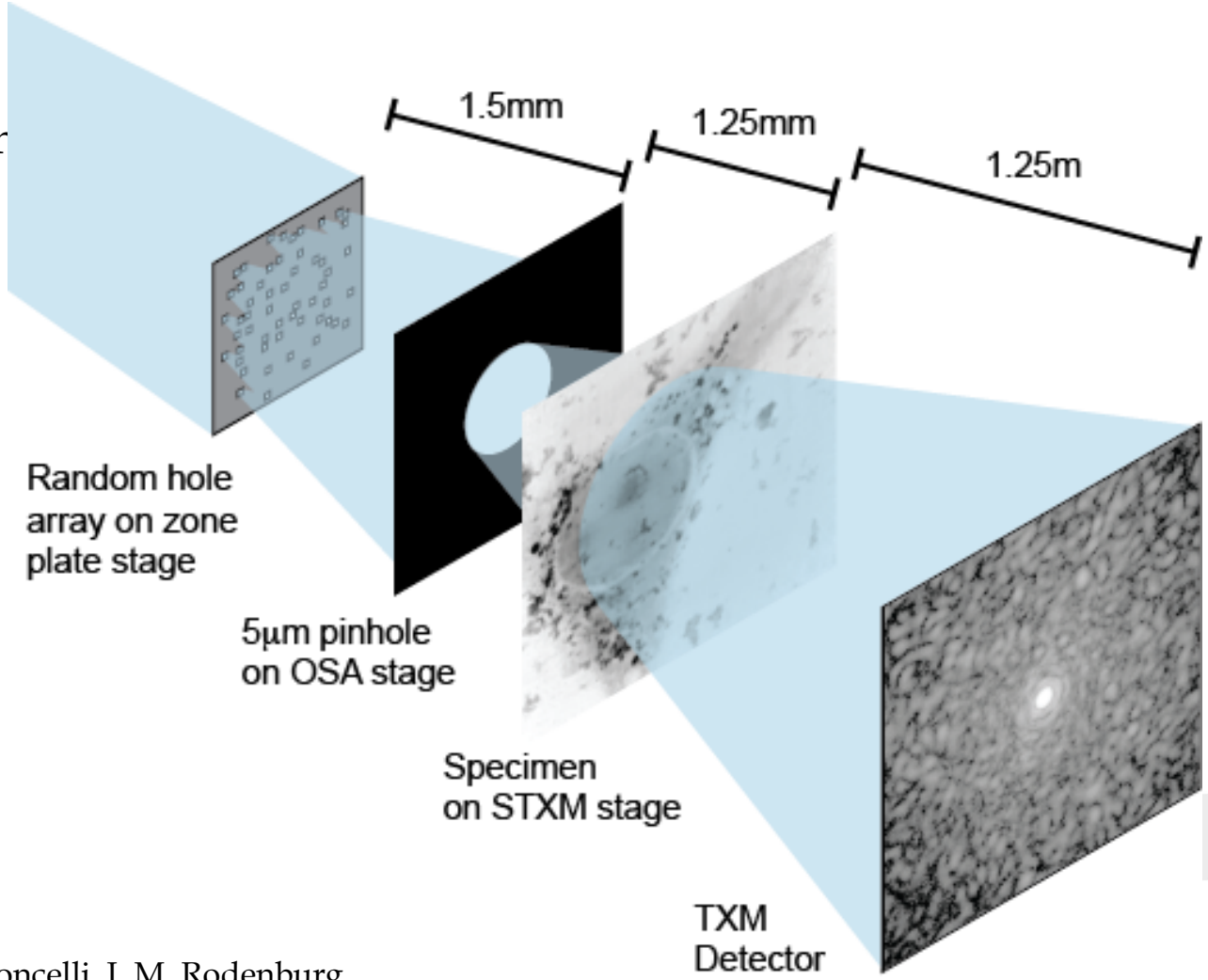

To spread the illumination across the detector

A. M. Maiden, G. R. Morrison, B. Kaulich, A. Gianoncelli, J. M. Rodenburg, *"Soft X-ray spectromicroscopy using ptychography with randomly phased illumination"*, Nature Communications 4, 1669, (2013)

Elettra
Sincrotrone
Trieste

Soft X-ray spectromicroscopy using ptychography with randomly phased illumination

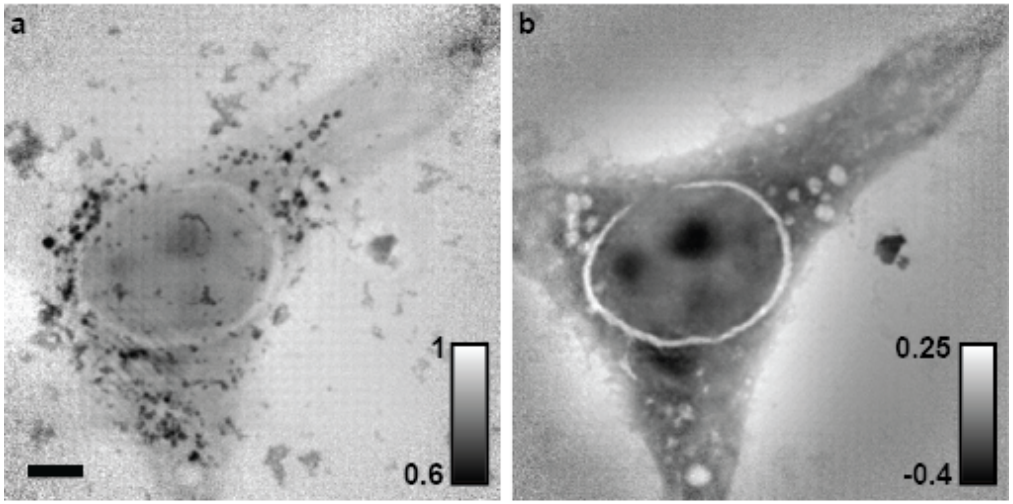

Balb/3T3 mouse fibroblast cells that had been exposed to cobalt ferrite ($CoFe_2O_4$) nanoparticles

Ptychography reconstruction
using the ePIE algorithm (Uni of Sheffiled)

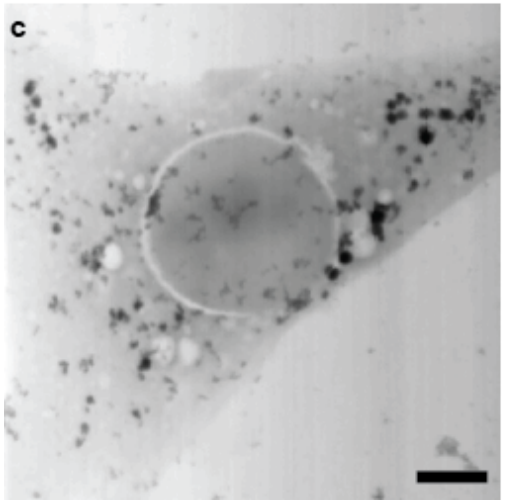

STXM absorption image

A. M. Maiden, G. R. Morrison, B. Kaulich, A. Gianoncelli, J. M. Rodenburg, *"Soft X-ray spectromicroscopy using ptychography with randomly phased illumination"*, Nature Communications 4, 1669, (2013)

Elettra
Sincrotrone
Trieste

Soft X-ray spectromicroscopy using ptychography

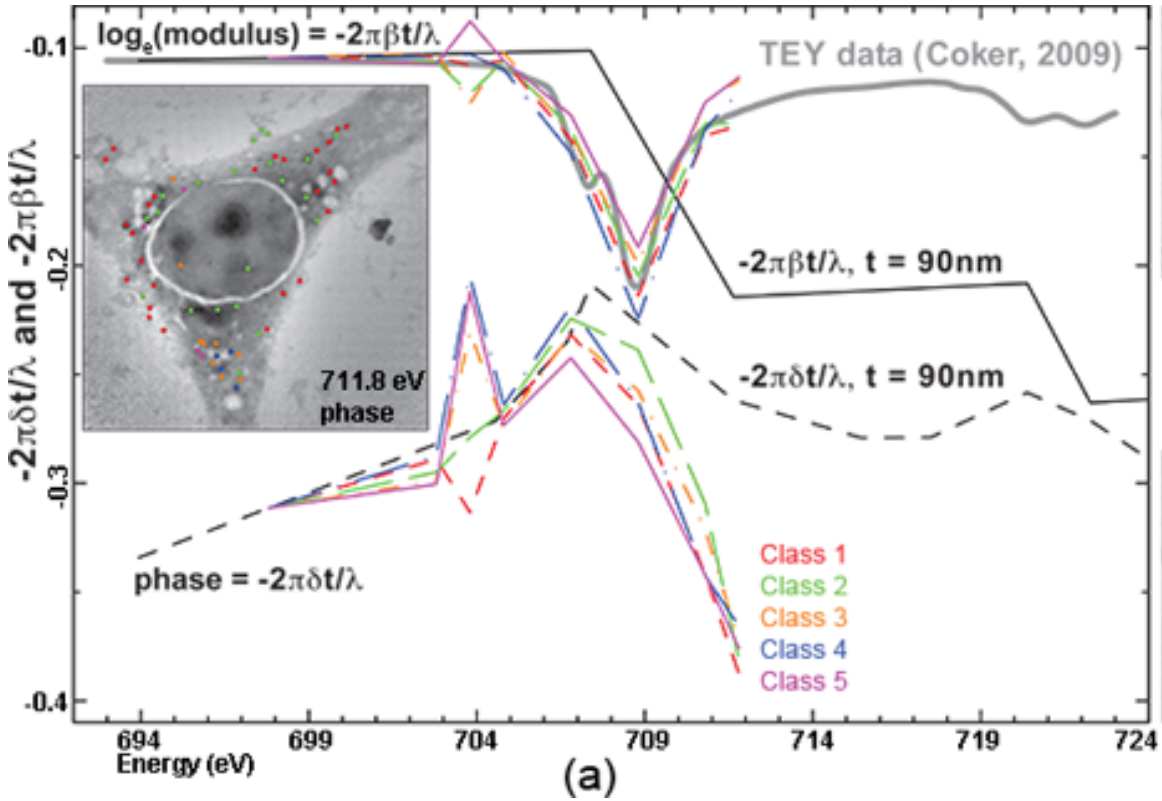

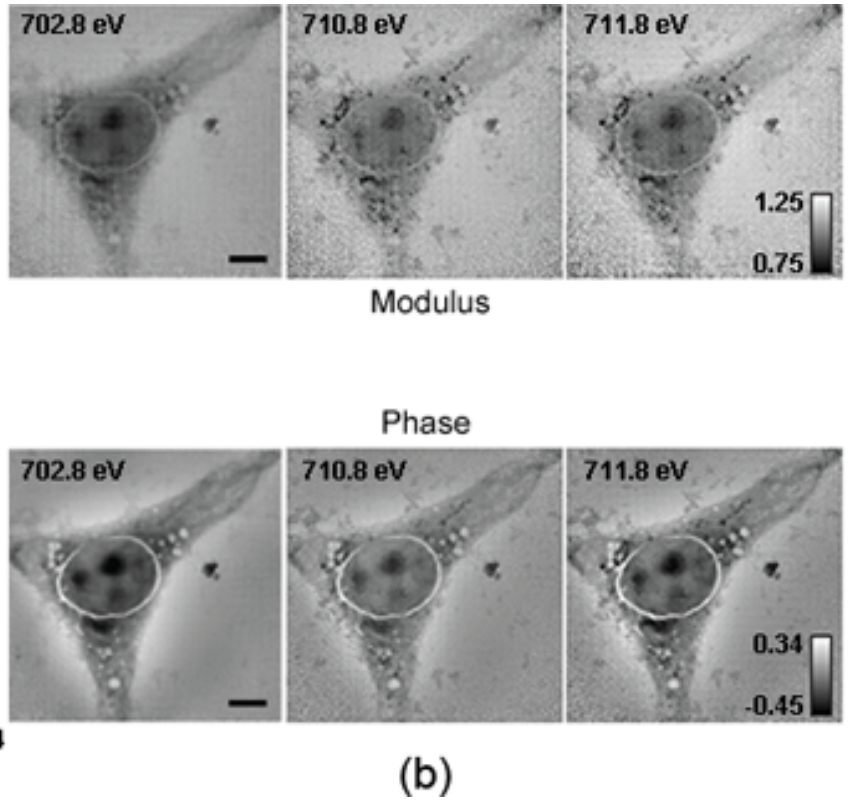

First direct measurements from cobalt ferrite nanoparticles of the phase variations across the iron L_3 edge, with the phase variations showing stronger and clearer features than the modulus data provided

The observed variations in modulus contrast across Fe L_3 edge are consistent with estimates based on total electron yield (TEY) measurements by Coker (Manchester University, UK)

A. M. Maiden, G. R. Morrison, B. Kaulich, A. Gianoncelli, J. M. Rodenburg,
"Soft X-ray spectromicroscopy using ptychography with randomly phased illumination",
Nature Communications 4, 1669, (2013)

Elettra
Sincrotrone
Trieste

SXRI Beamline

Australian Synchrotron

LA TROBE UNIVERSITY

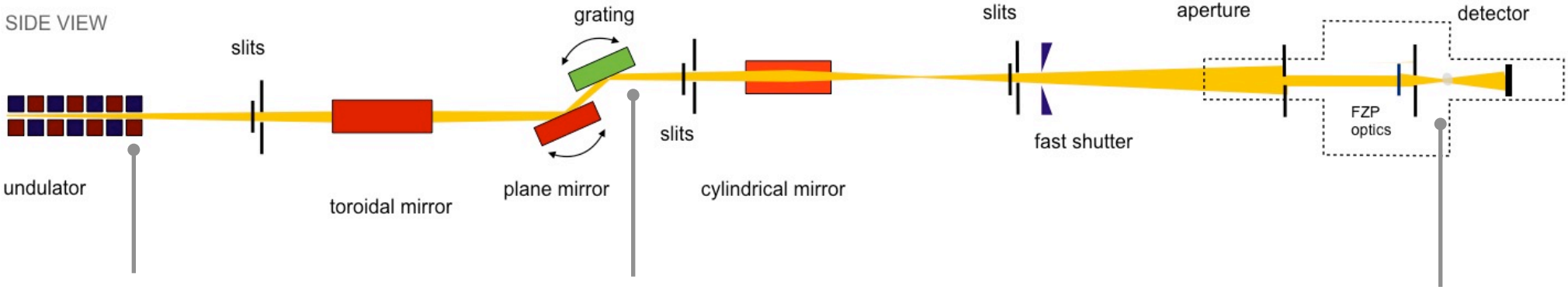

Active position stabilitisation: ~17 nm
RMS stability - no thermal drift

Elettra
Sincrotrone
Trieste

fCDI

CDI/FCDI

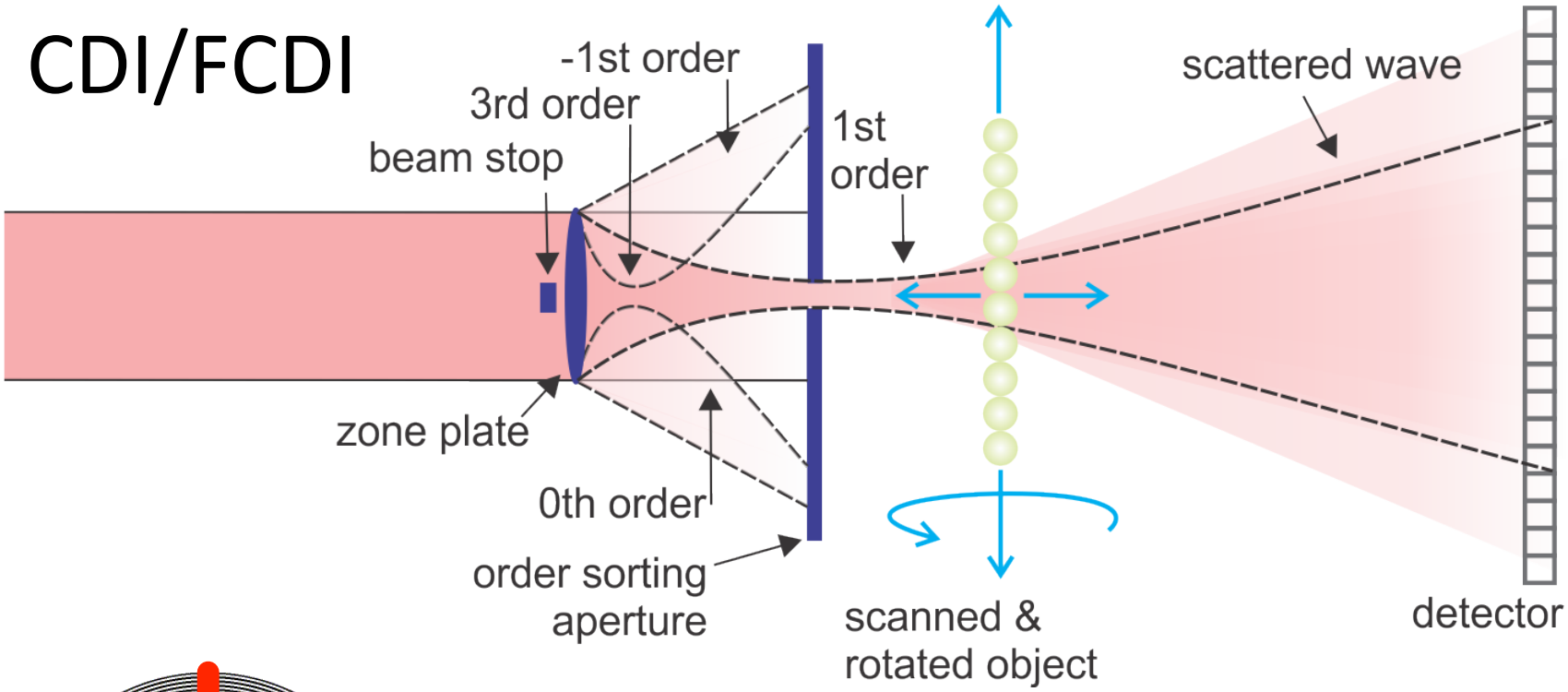

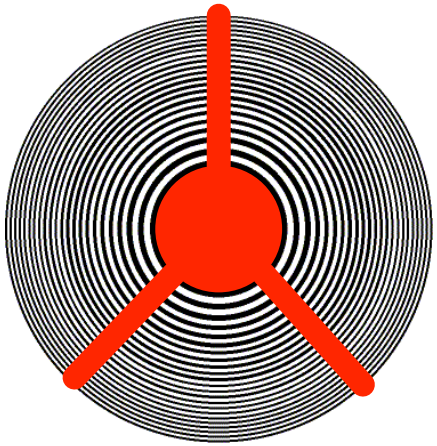

ZP: Diameter 160μm, Central stop 30μm, Outermost zone 30nm

Elettra
Sincrotrone
Trieste

Preliminary tests

Diffraction pattern (through unfocused ZP)

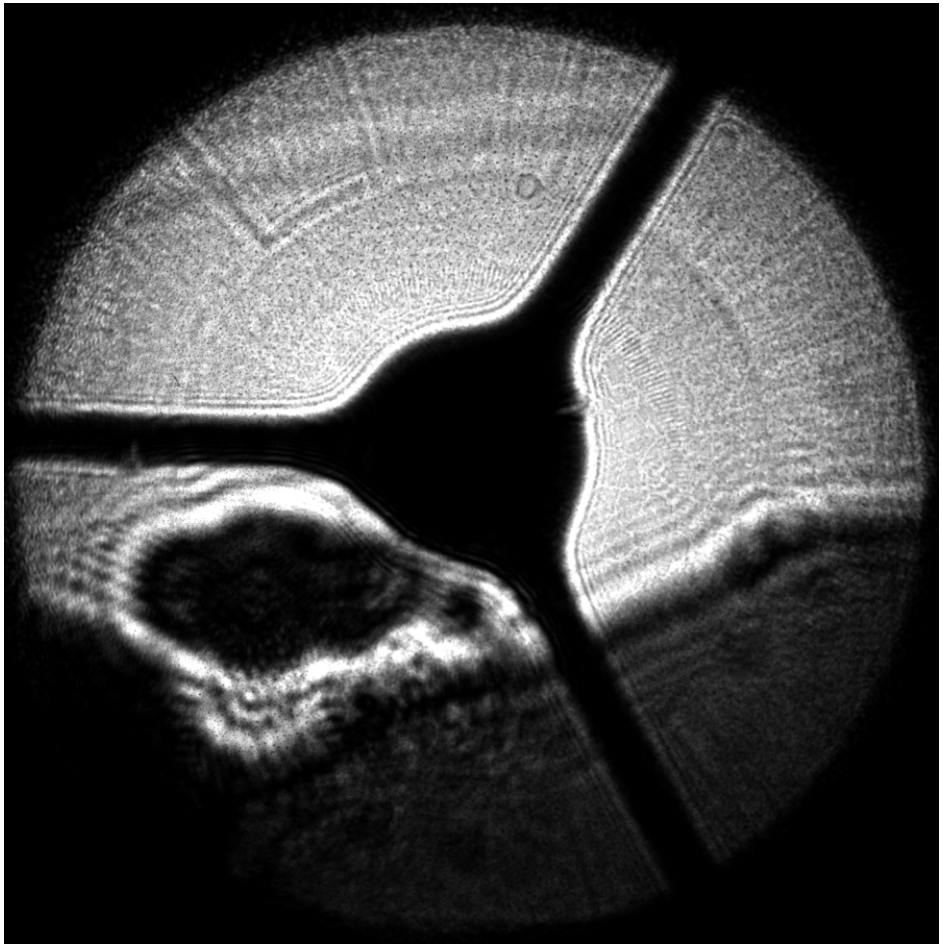

Reconstruction

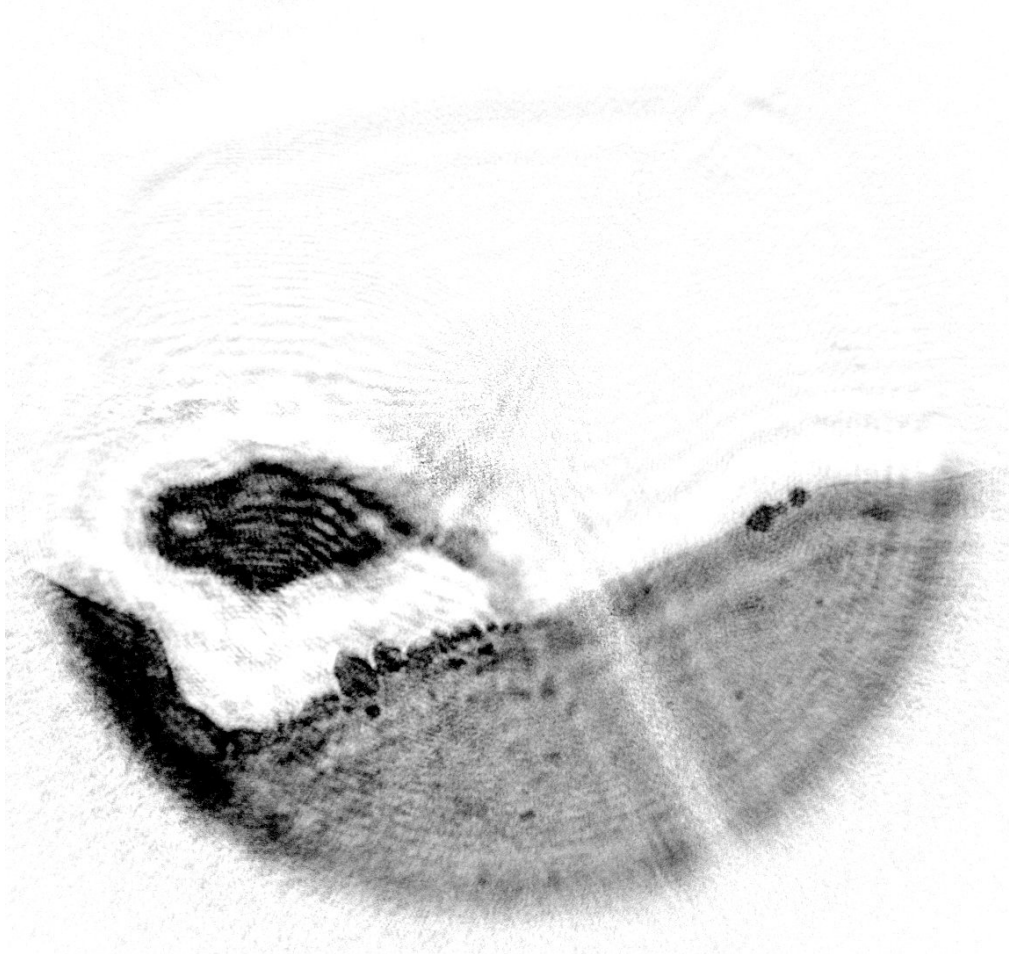

G. Kourousias, B. Bozzini, A. Gianoncelli, M. W. M. Jones, M. Junker, G. van Riessen, M. Kiskinova "Shedding light on electrodeposition dynamics tracked in situ via soft X-ray coherent diffraction imaging" **Nano Research**, 9 – 7, 2046-2056 (2016)

Scanning and oversampling

Elettra
Sincrotrone
Trieste

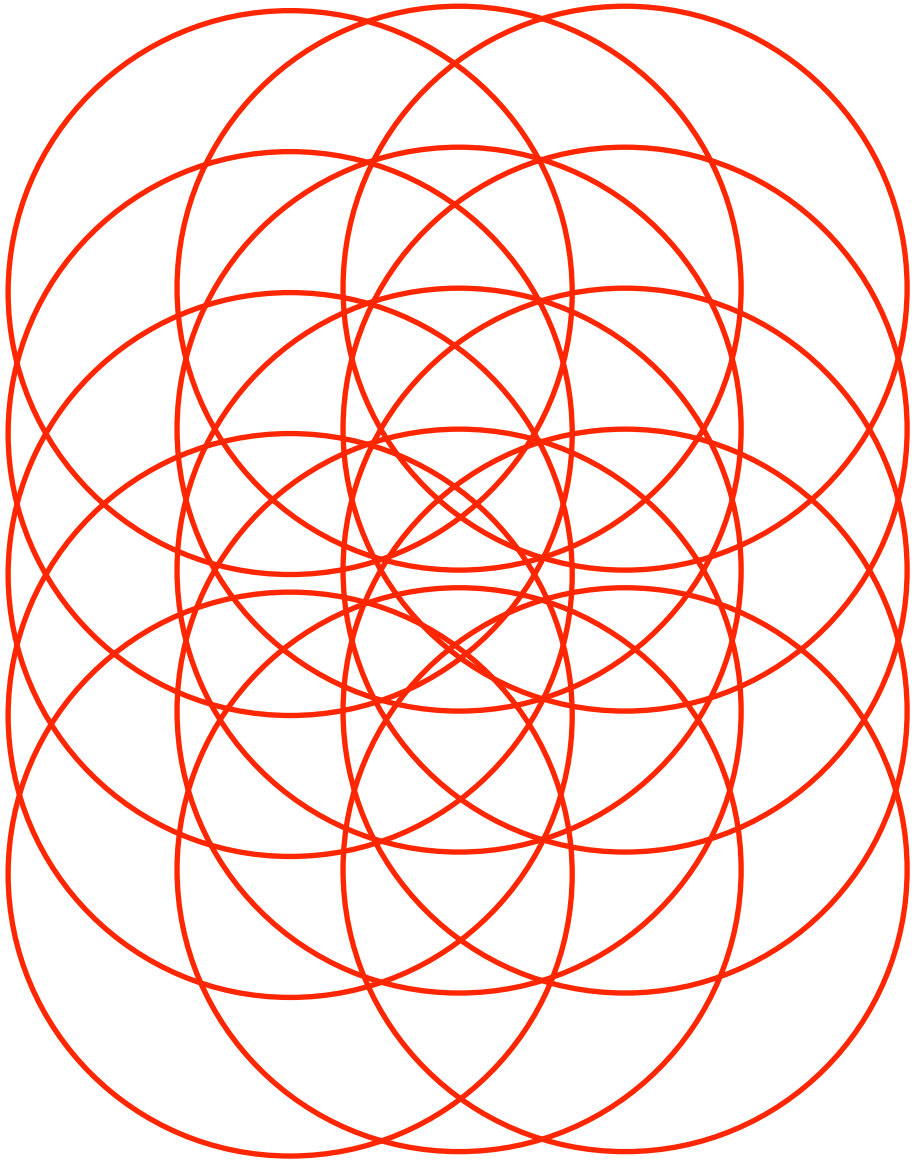

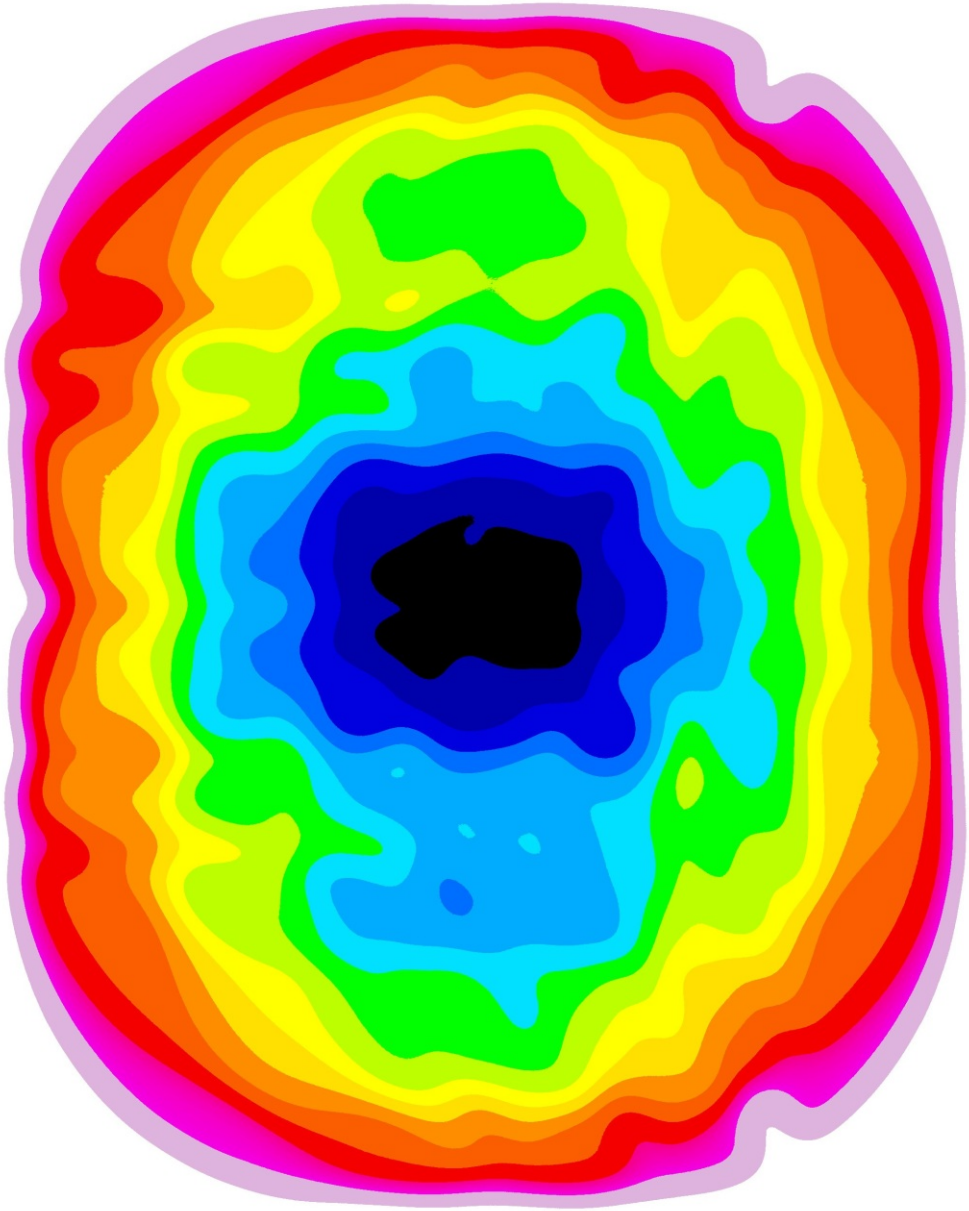

G. Kourousias, B. Bozzini, A. Gianoncelli, M. W. M. Jones, M. Junker, G. van Riessen, M. Kiskinova "Shedding light on electrodeposition dynamics tracked in situ via soft X-ray coherent diffraction imaging" **Nano Research**, 9 – 7, 2046-2056 (2016)

Elettra
Sincrotrone
Trieste

Electrochemical processes at local nanoscales by *in situ* soft FCDI imaging

TwinMic @ Elettra – SXRI @ Australian Synchrotron

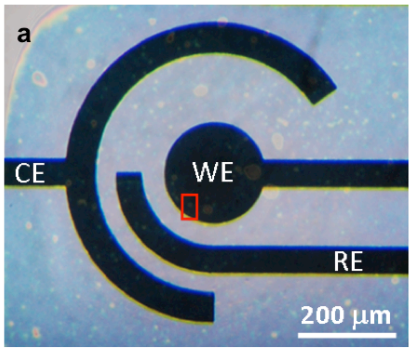

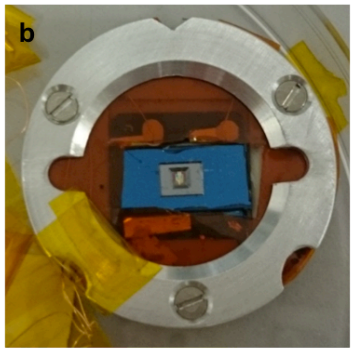

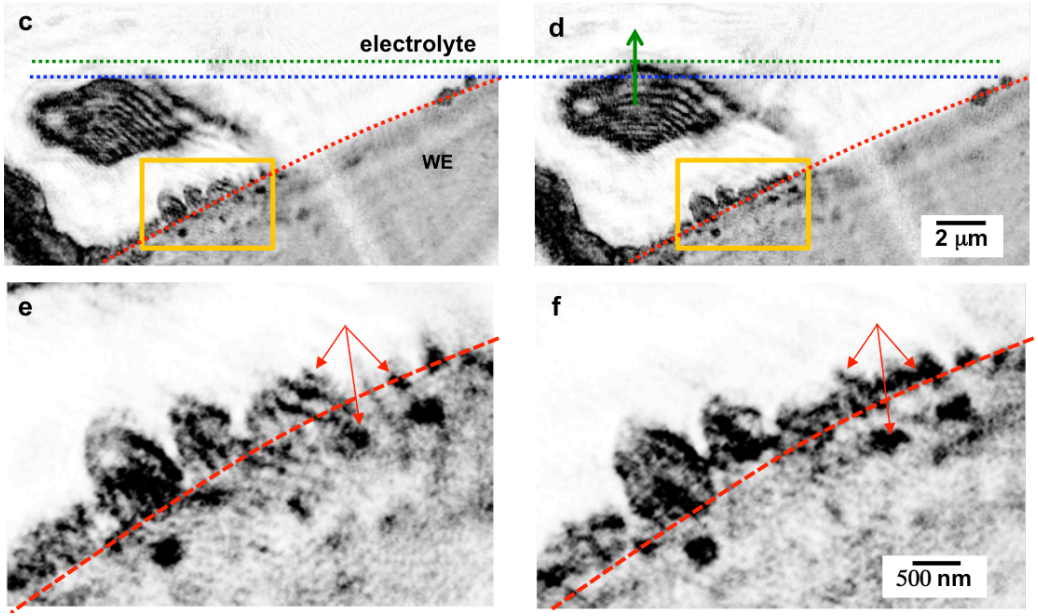

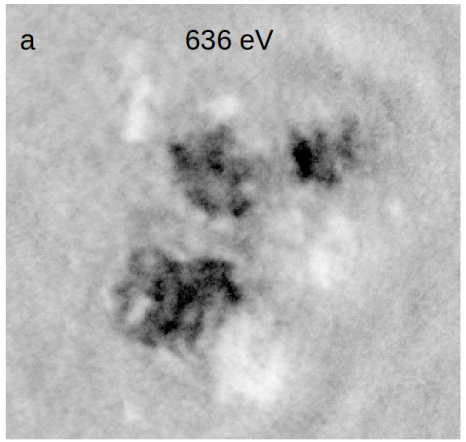

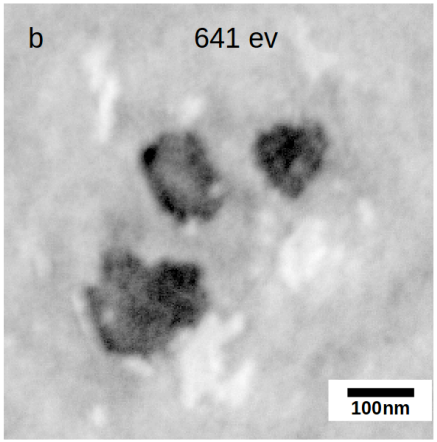

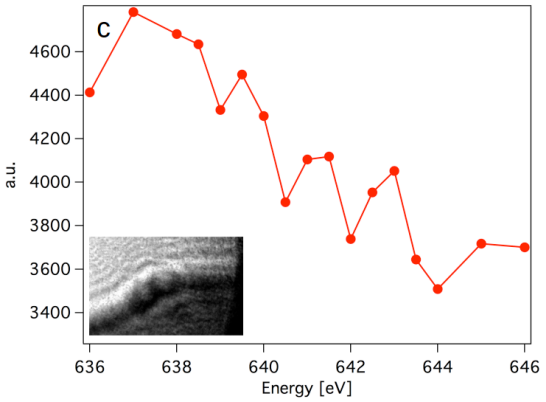

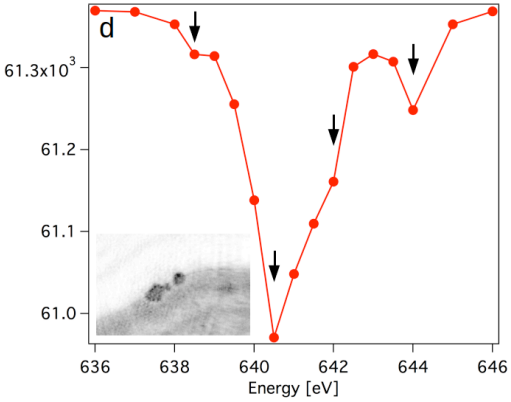

G. Kourousias, B. Bozzini, A. Gianoncelli, M. W. M. Jones, M. Junker, G. van Riessen, M. Kiskinova "Shedding light on electrodeposition dynamics tracked in situ via soft X-ray coherent diffraction imaging" **Nano Research**, 9 – 7, 2046-2056 (2016)

Elettra
Sincrotrone
Trieste

Spectroscopy across Mn edge through Ptycography

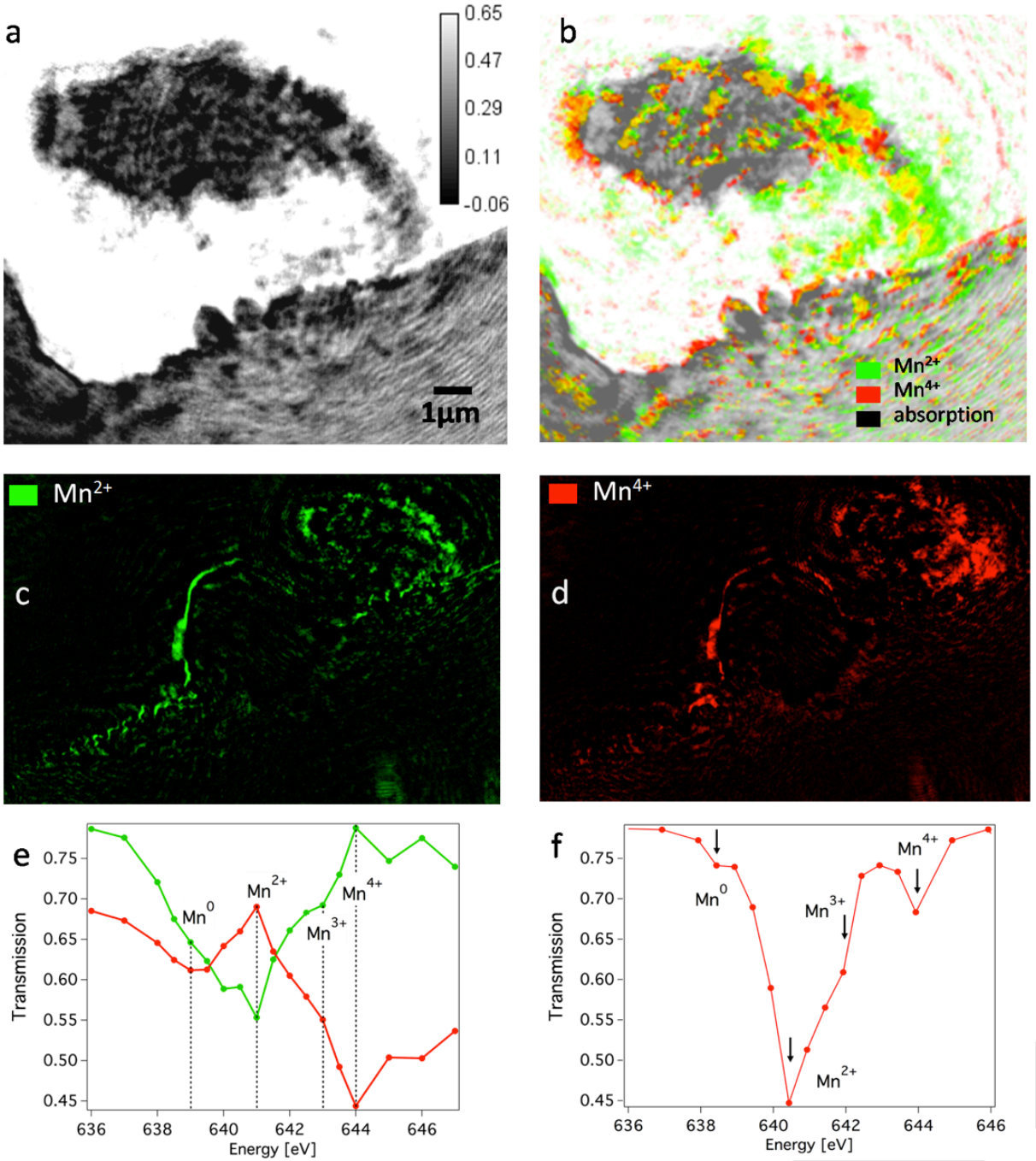

G. Kourousias, B. Bozzini, A. Gianoncelli, M. W. M. Jones, M. Junker, G. van Riessen, M. Kiskinova "Shedding light on electrodeposition dynamics tracked in situ via soft X-ray coherent diffraction imaging" **Nano Research**, 9 – 7, 2046-2056 (2016)

Elettra
Sincrotrone
Trieste

TwinMic: Integration of both imaging modes into a single instrument

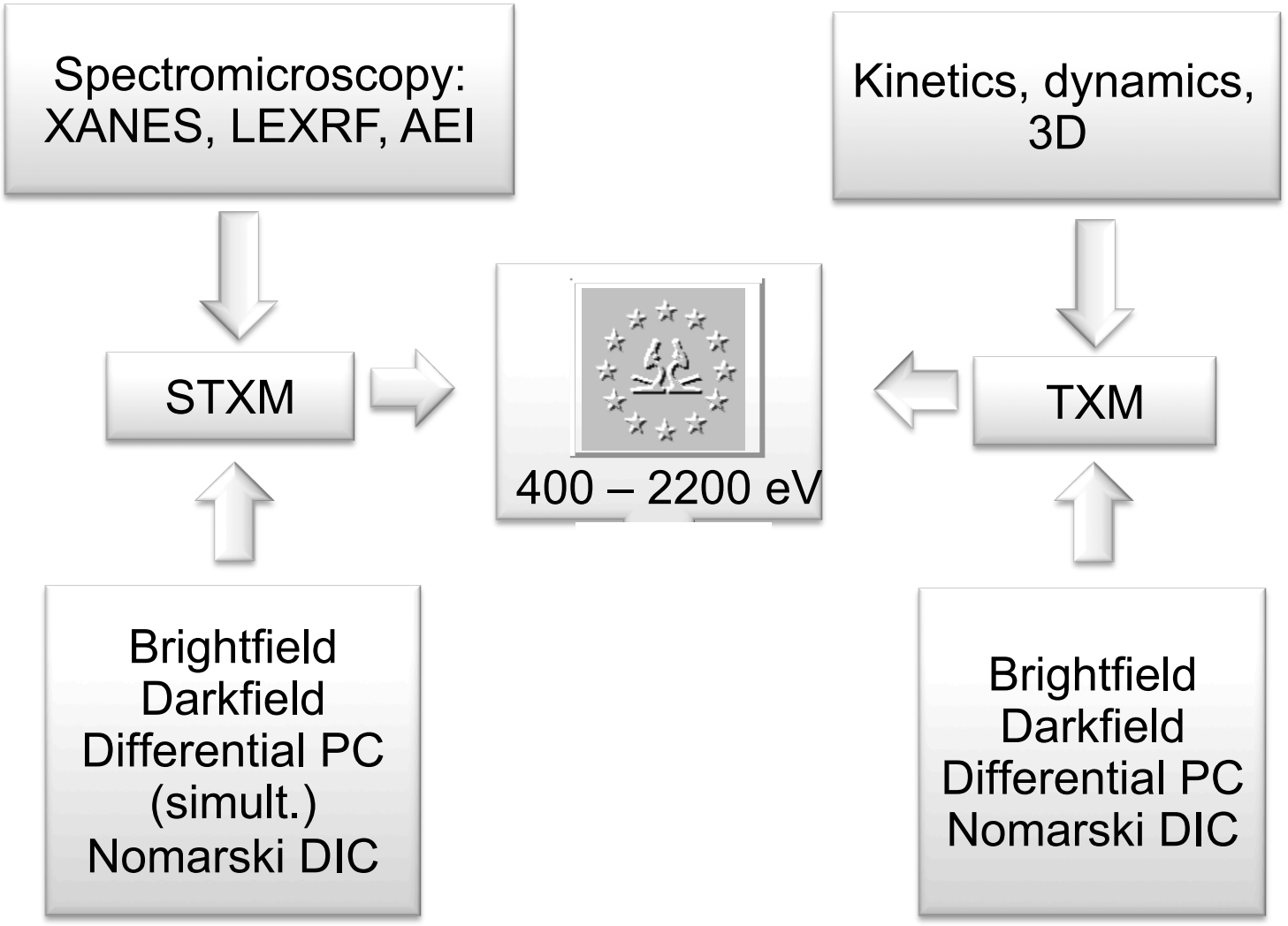

The European team that initiated the project

- Morphological analysis, XANES and AAEI
- Different contrasts incl. brightfield, differential phase and interference contrast, darkfield, etc
- Versatile specimen environment

Elettra
Sincrotrone
Trieste

TwinMic microscope

400 – 2200 eV

TwinMic – Combination of scanning and full-field imaging in a single instrument

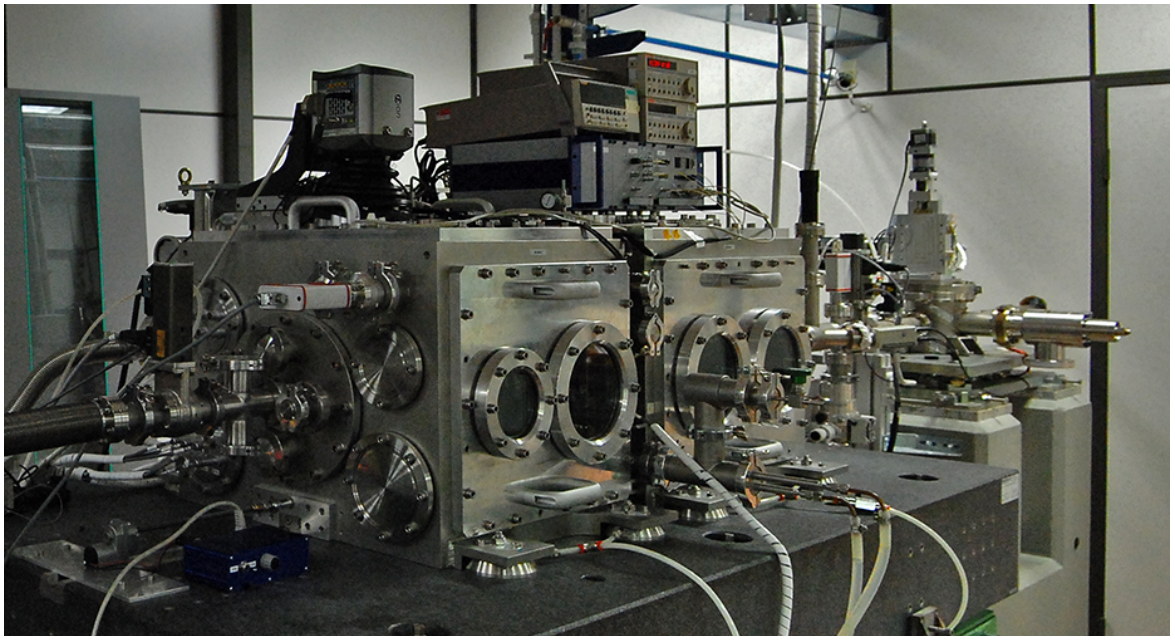

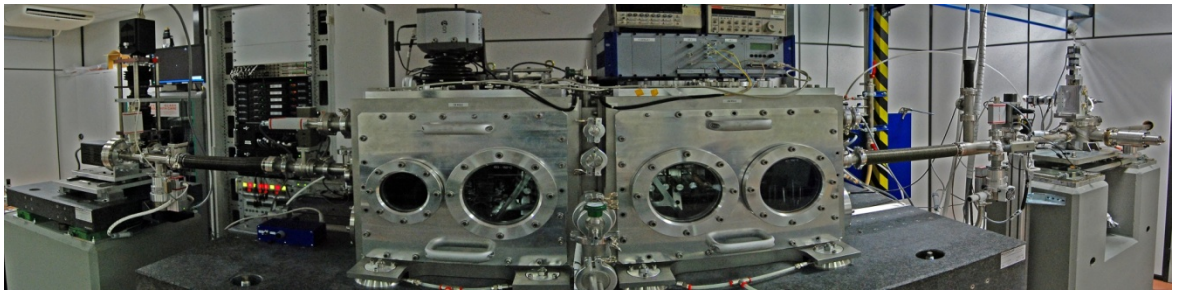

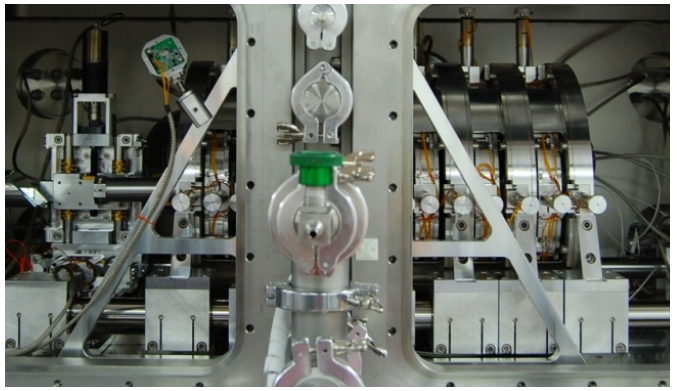

- Biotechnology
- Nanotechnology
- Environment
- Geochemistry
- Food Science
- Medicine
- Pharmacology
- Cultural Heritage
- New Materials

Elettra
Sincrotrone
Trieste

Scanning X-ray microscope (STXM)

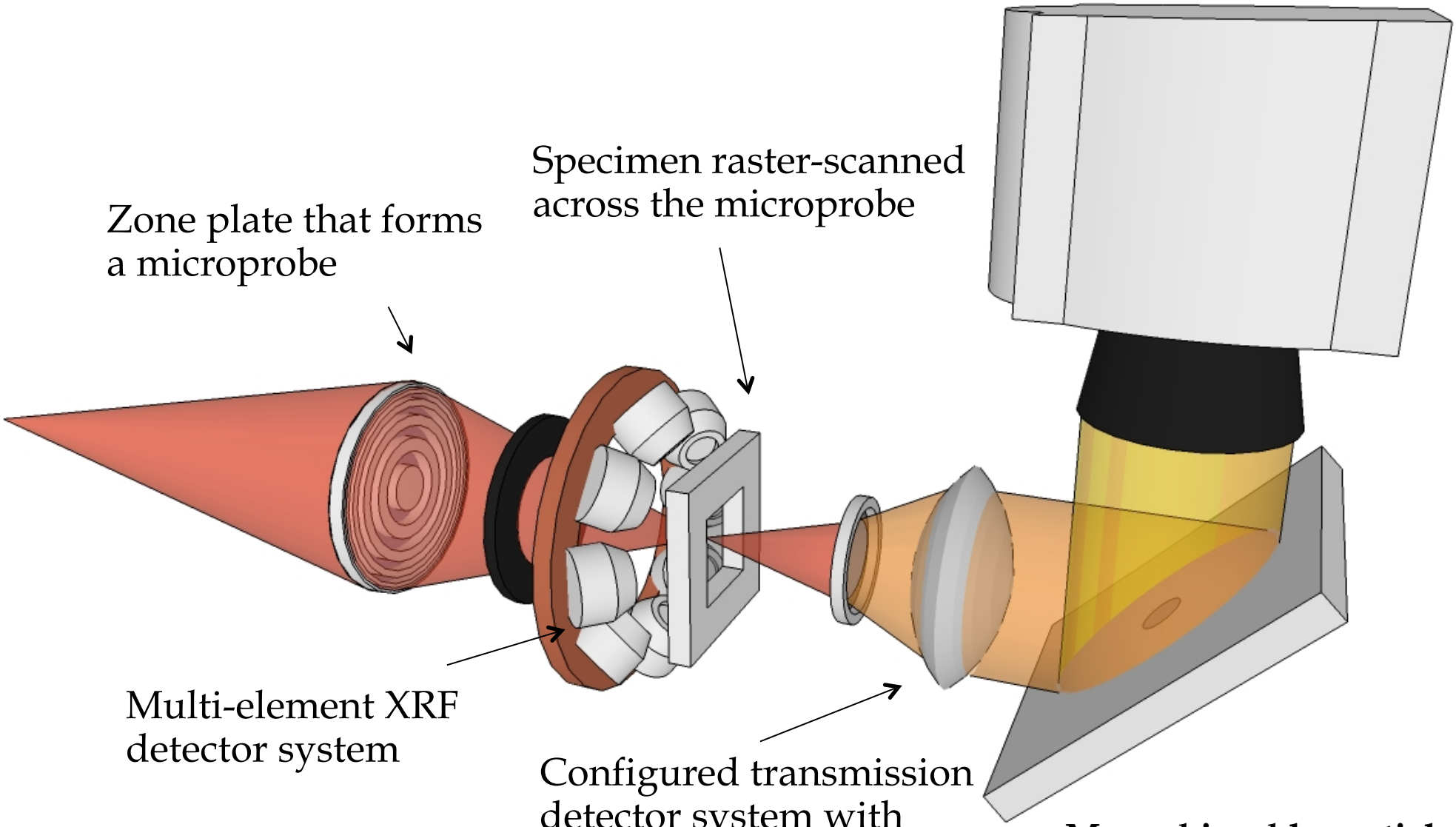

Max achievable spatial resolution: 50nm

Elettra
Sincrotrone
Trieste

STXM mode

Differential phase contrast with a fast read-out CCD camera

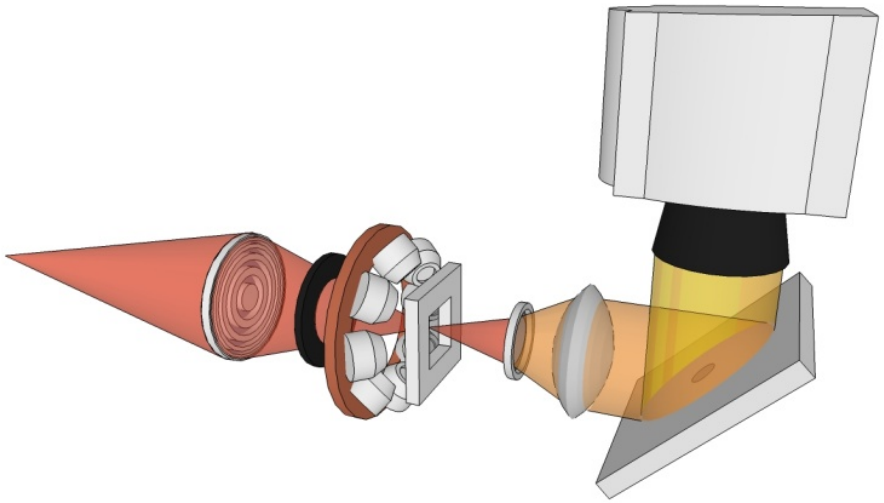

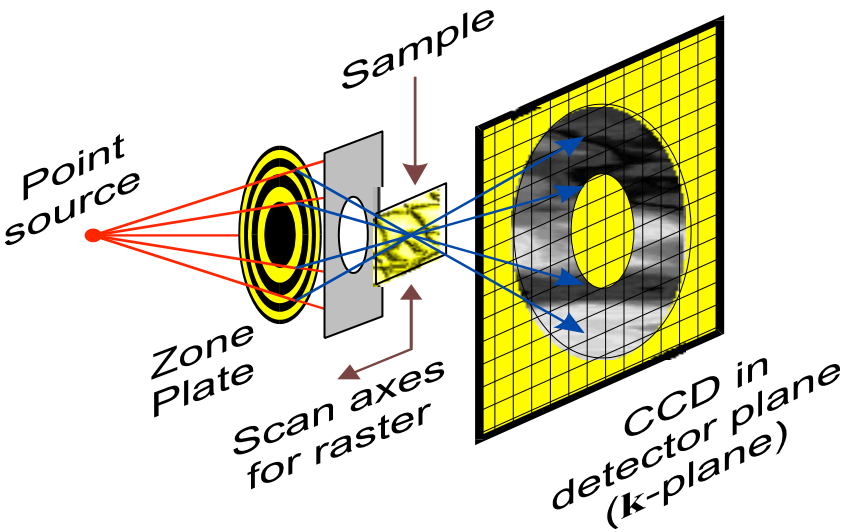

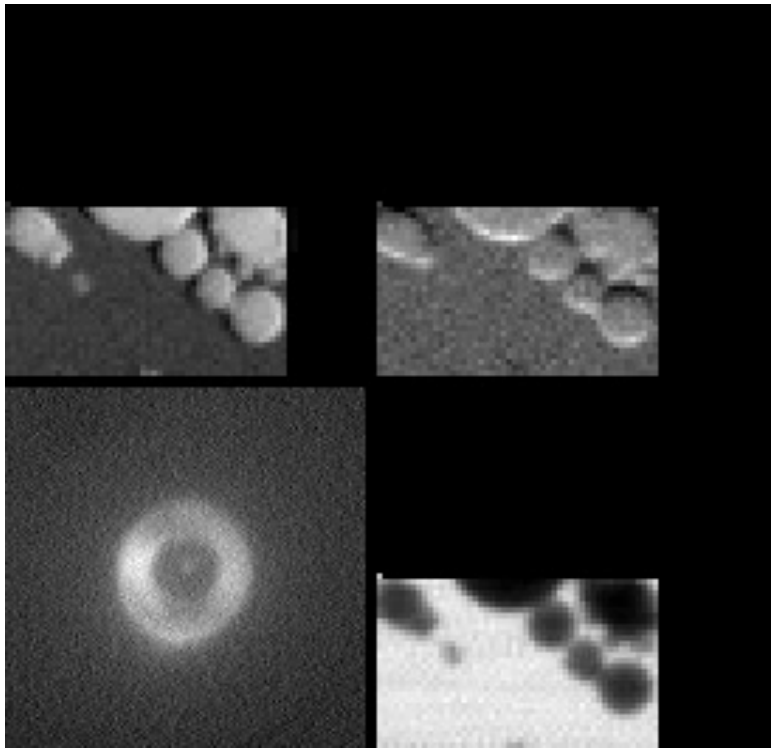

Simultaneous acquisition of:

- Absorption or transmission
- Differential phase contrast
- Darkfield images

Morrison, G. et al., IPAP Conf. Series 7, 377-379 (2006)
Gianoncelli A. et al., Appl Phys Lett 89, 251117 (2006)

Elettra
Sincrotrone
Trieste

Photoionization

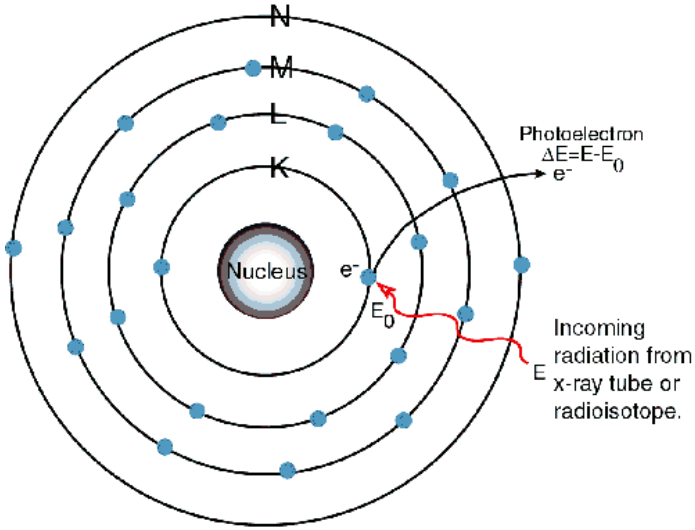

X-ray absorption
(through photoelectric effect)

The primary X-ray photon causes the ejection of electrons from the inner shells, creating vacancies

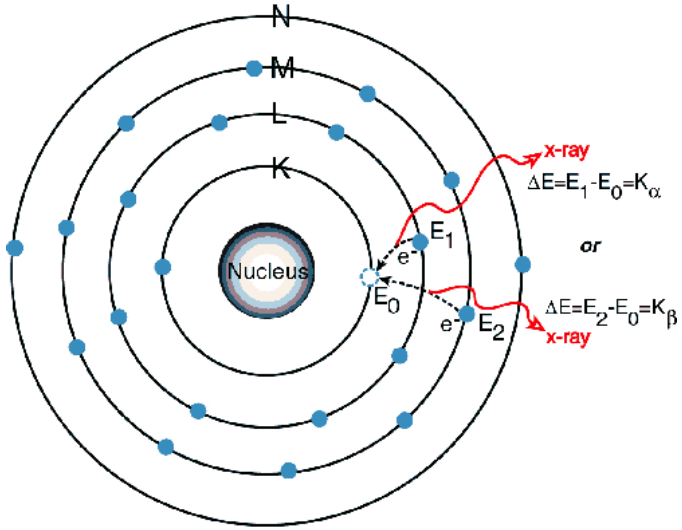

X-ray Fluorescence

The vacancy created by the primary X-ray photon is filled by an electron coming from an outer shell causing the emission of a characteristic X-ray photon whose energy is the difference between the two binding energies of the corresponding shells

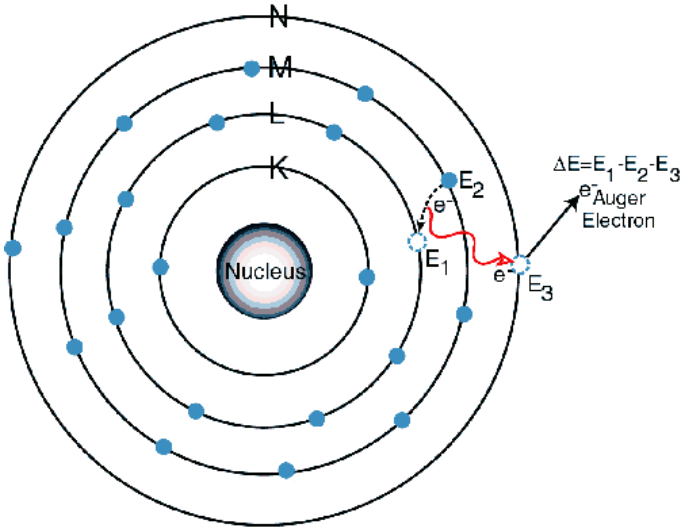

Auger effect

The vacancy created by the primary X-ray photon is filled by an electron coming from an outer shell and the energy is transferred directly to one of the outer electrons, causing it to be ejected from the atom.

http://www.amptek.com/xrf.htm

Low-energy X-ray fluorescence for elemental analysis:

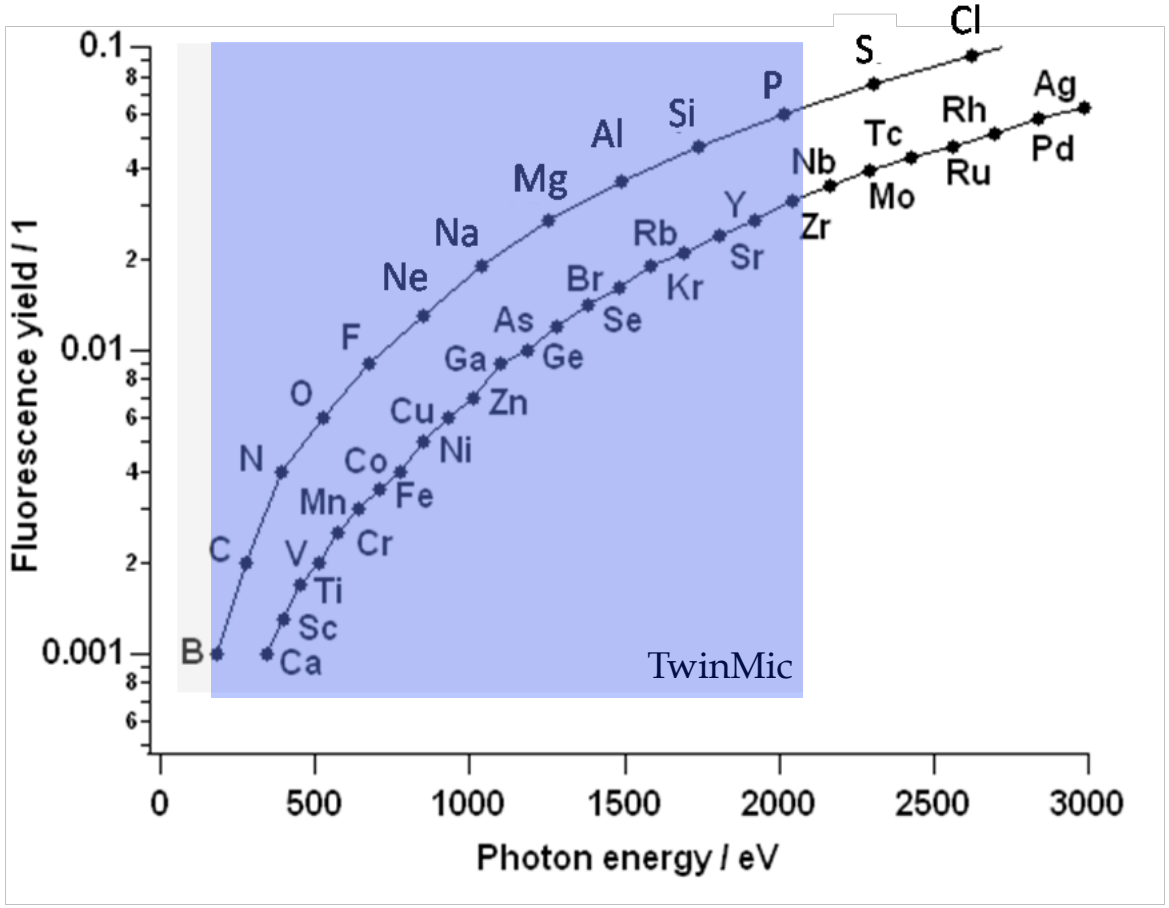

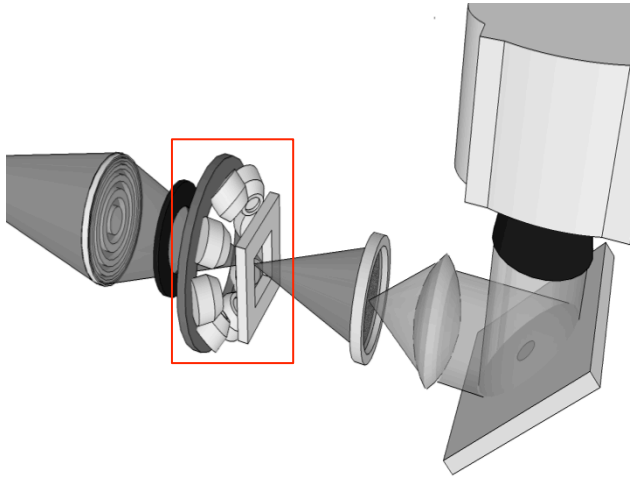

Detecting trace elements:

X-ray fluorescence: ~1000x better sensitivity than electrons for trace elemental mapping (ion concentrations etc.).

Low fluorescence yields for soft X-rays! !!

A. Gianoncelli, B. Kaulich, M. Kiskinova, R. Alberti, T. Klatka, A. Longoni, A. de Marco, A. Marcello, Simultaneous Soft X-ray Transmission and Emission Microscopy, Nucl. Instr. and Meth. A 608 (1), 195-198

Low-energy X-ray fluorescence:

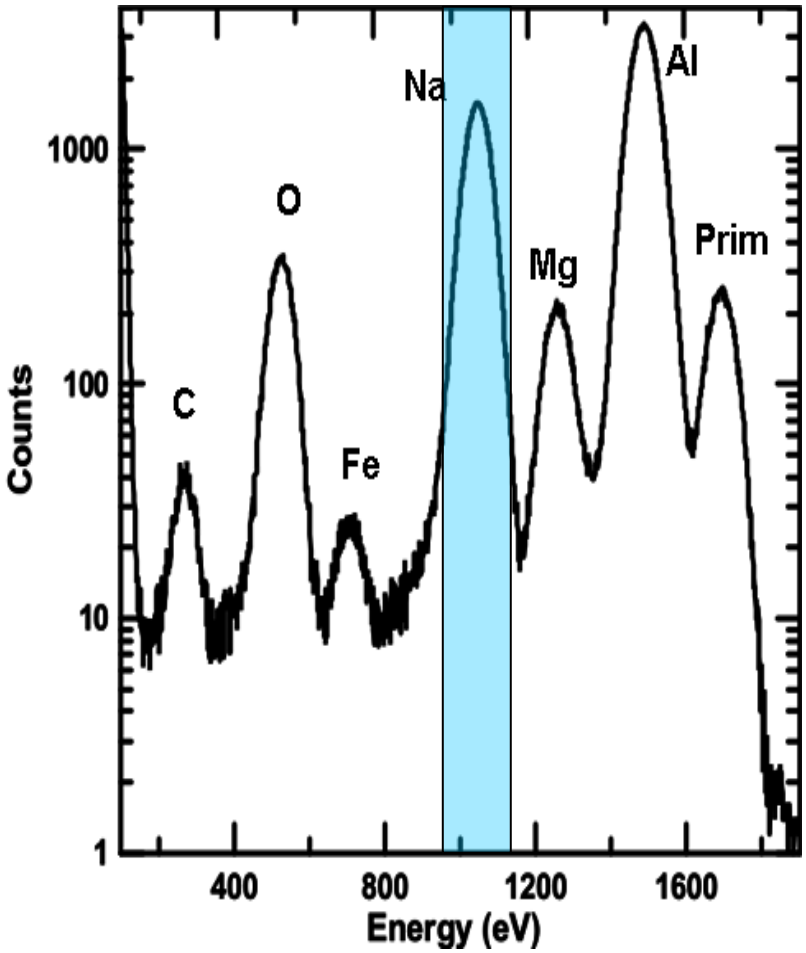

TwinMic LEXRF spectrum with unfocused beam of a test organic matrix on a metal shim

Dynamic range: up to 30 kcounts/s

Average FWHM energy resolution @ C- K edge: 69 eV

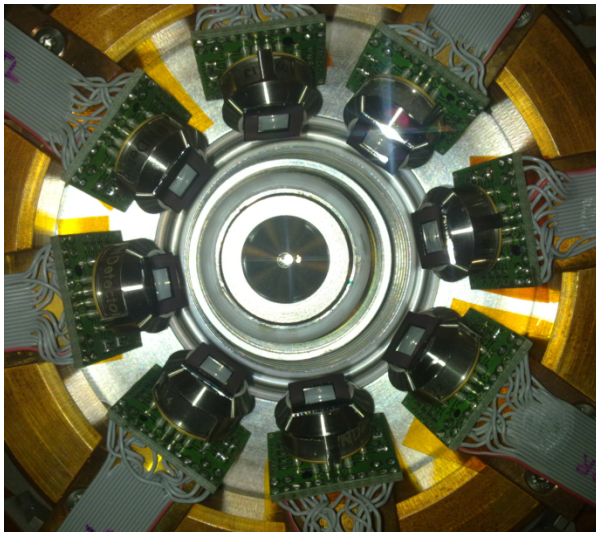

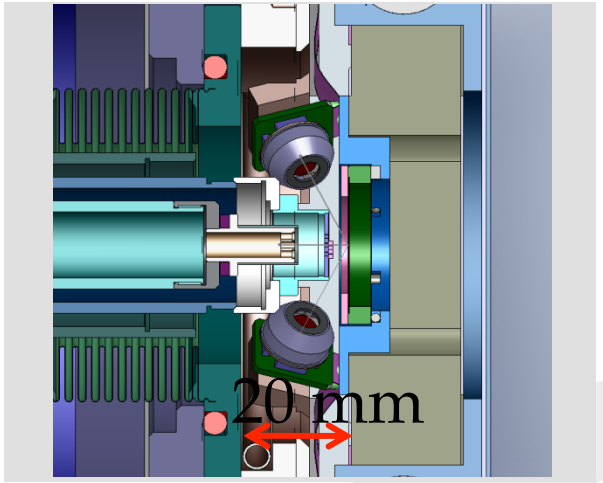

A. Gianoncelli, B. Kaulich, M. Kiskinova, R. Alberti, T. Klatka, A. Longoni, A. de Marco, A. Marcello, Simultaneous Soft X-ray Transmission and Emission Microscopy, Nucl. Instr. and Meth. A 608 (1), 195-198

Elettra
Sincrotrone
Trieste

LEXRF

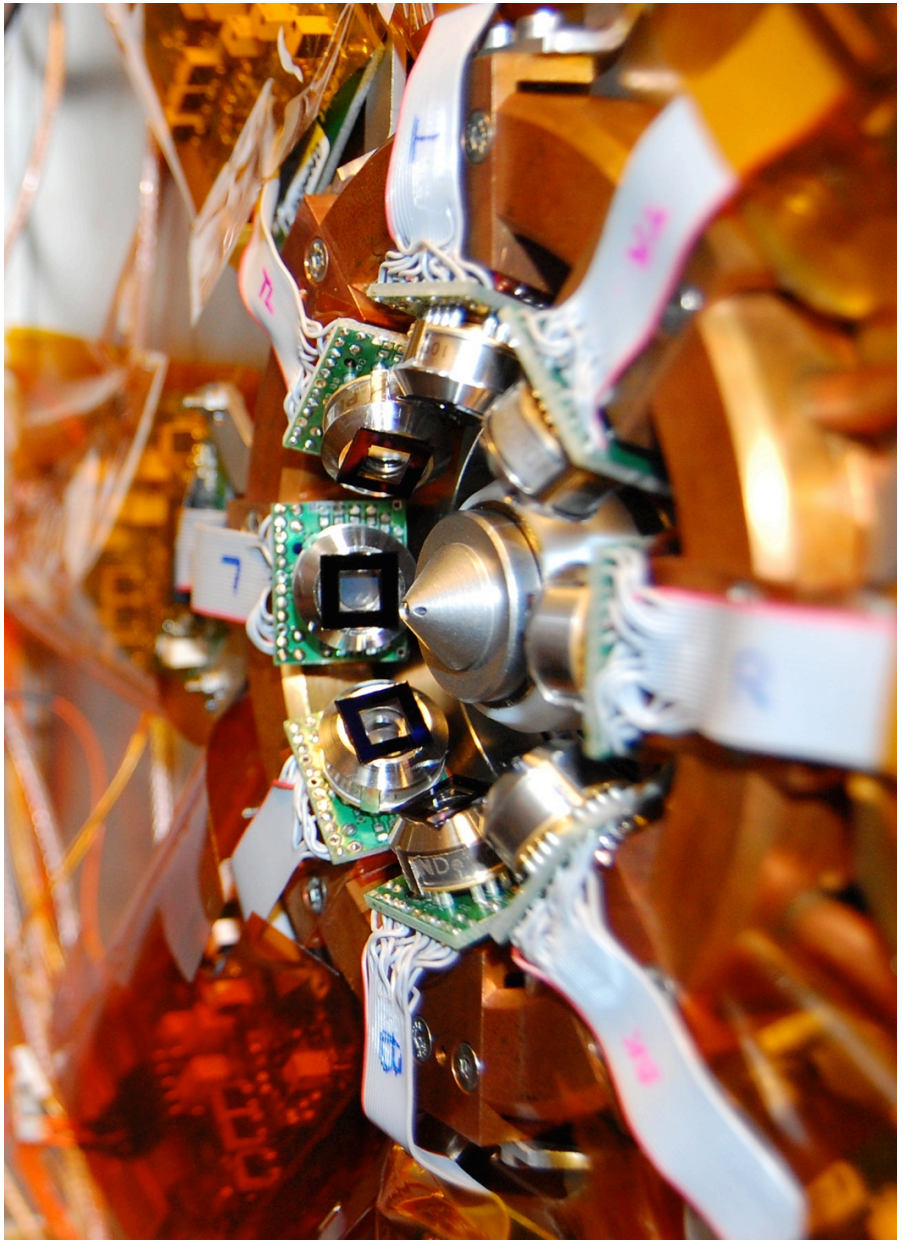

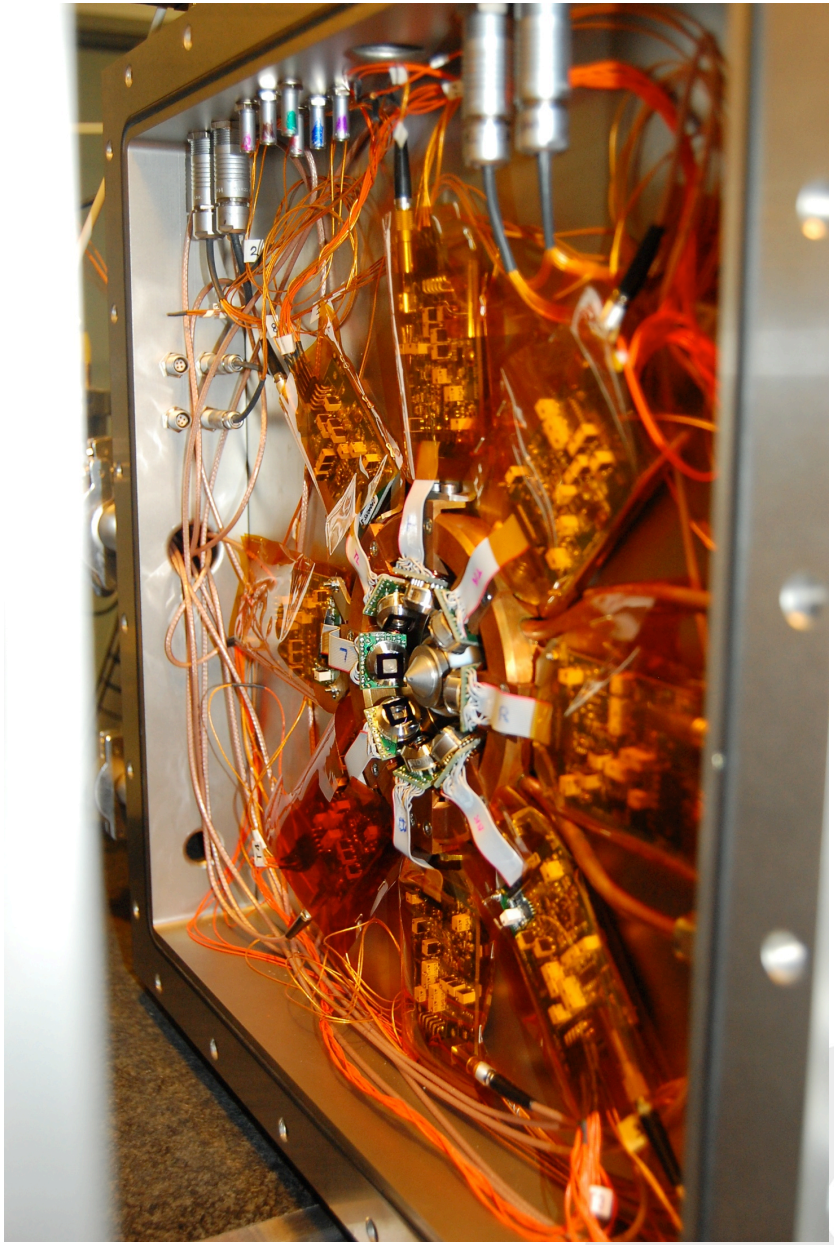

Elettra
Sincrotrone
Trieste

Aluminium toxicity

Soluble Al – "the most important growth-limiting factor for plants in most strongly acid soils and mine spoils" **Foy (1984)**

Acid soils occupy ~ 40 billion hectares (~ 30 %) of the world's ice free land area
von Uexküll and Mutert (1995)

In Australia alone, acid soils cost $1.5 billion p.a. in lost productivity

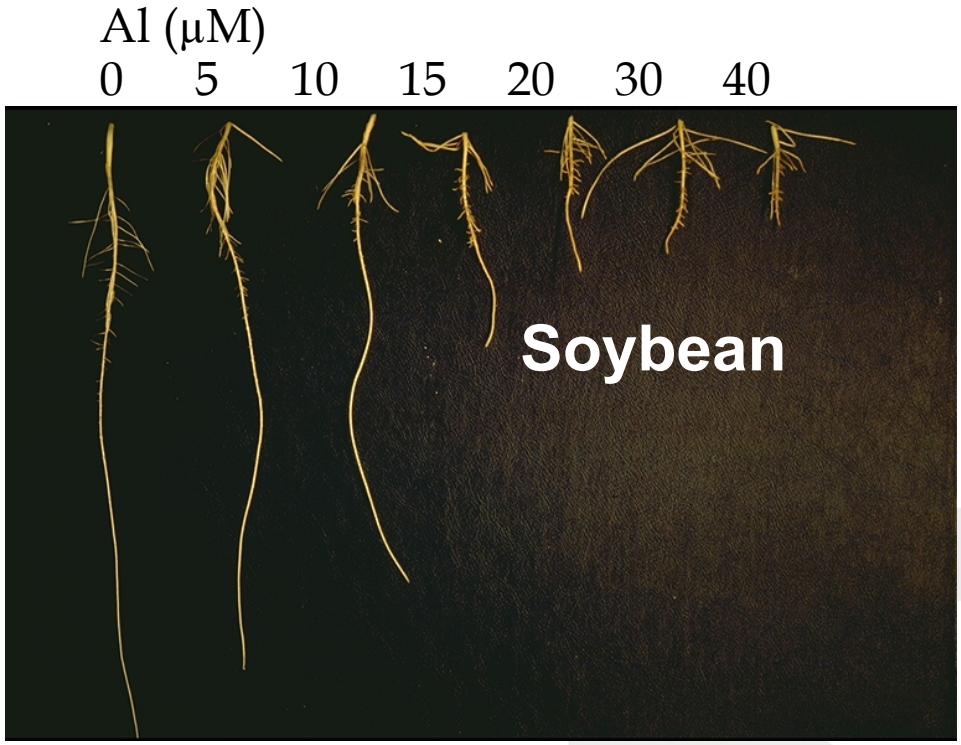

Elettra
Sincrotrone
Trieste

Aluminium toxicity

Soluble Al – "the most important growth-limiting factor for plants in most strongly acid soils and mine spoils" **Foy (1984)**

Although known since 1904 that Al is the primary factor causing a reduction in plant root growth in acid soils, the mechanism by which Al is toxic remains unclear

Recent research (2014) has shown that Al exerts its toxic effects very quickly, reducing root growth in ≤ 30 min. Therefore, a crucial step in elucidating how Al exerts its toxic effects is to examine where the Al is accumulating within the roots

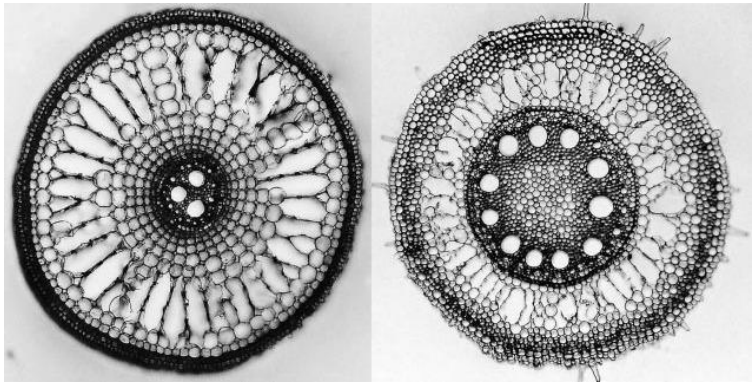

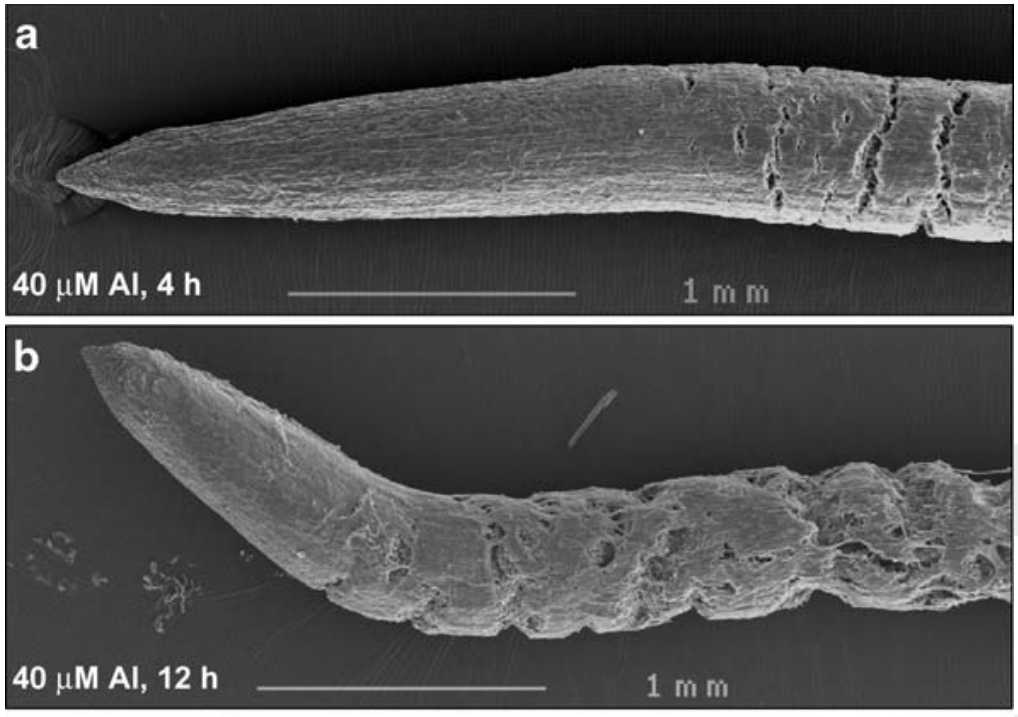

Elettra
Sincrotrone
Trieste

Aluminum toxicity

30 minutes, 6 mm, Sample 1

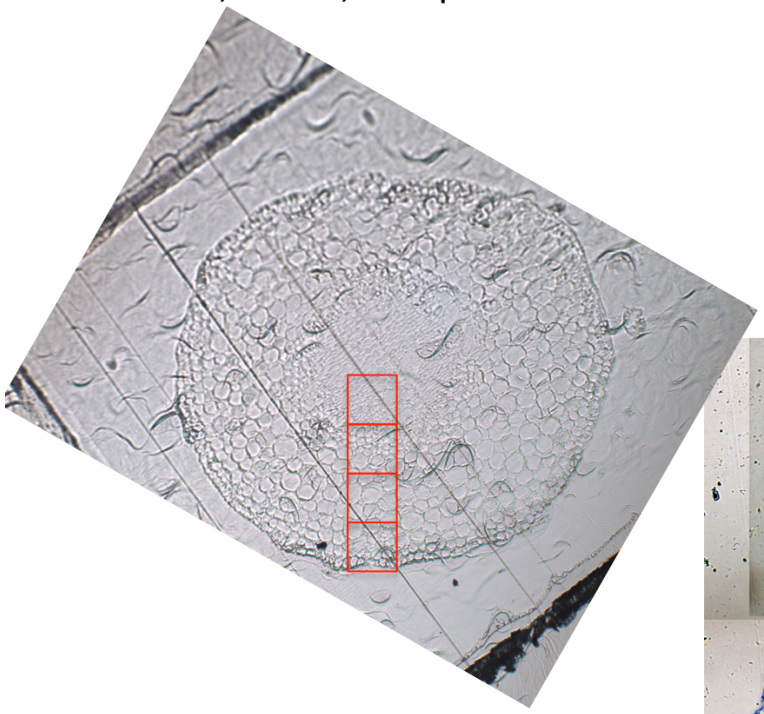

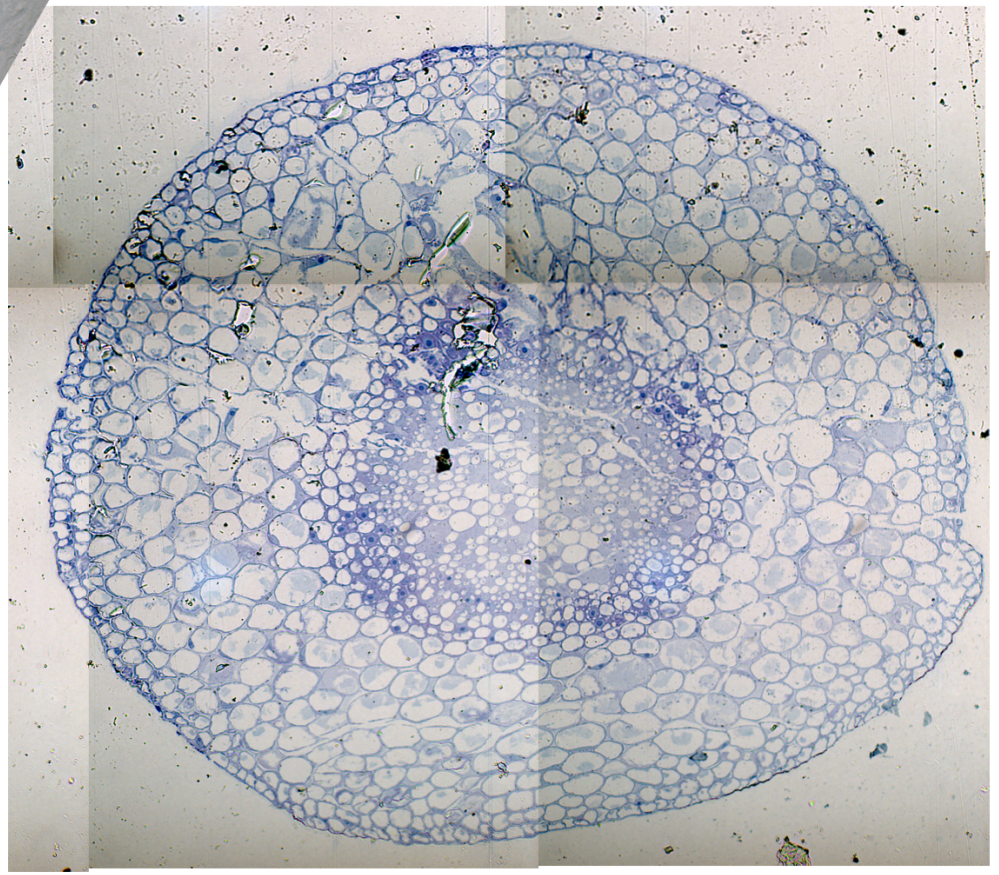

P. M. Kopittke, K. L. Moore , E. Lombi et al, "**Identification of the Primary Lesion of Toxic Aluminum in Plant Roots**" Plant Physiology, 2015, 167, 140

Elettra
Sincrotrone
Trieste

7 µm-thick transverse cross section of soybean roots

Exposed to 30 µM Al for 0.5 h.

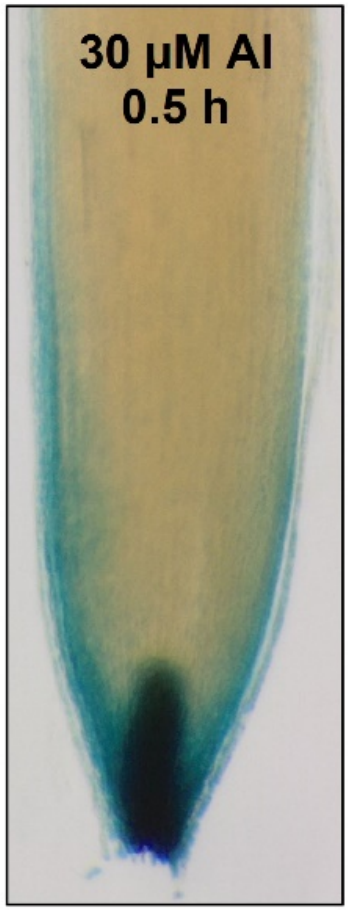

c) 6mm from apex

b) 2mm from Apex

a) 0.5 mm from Apex

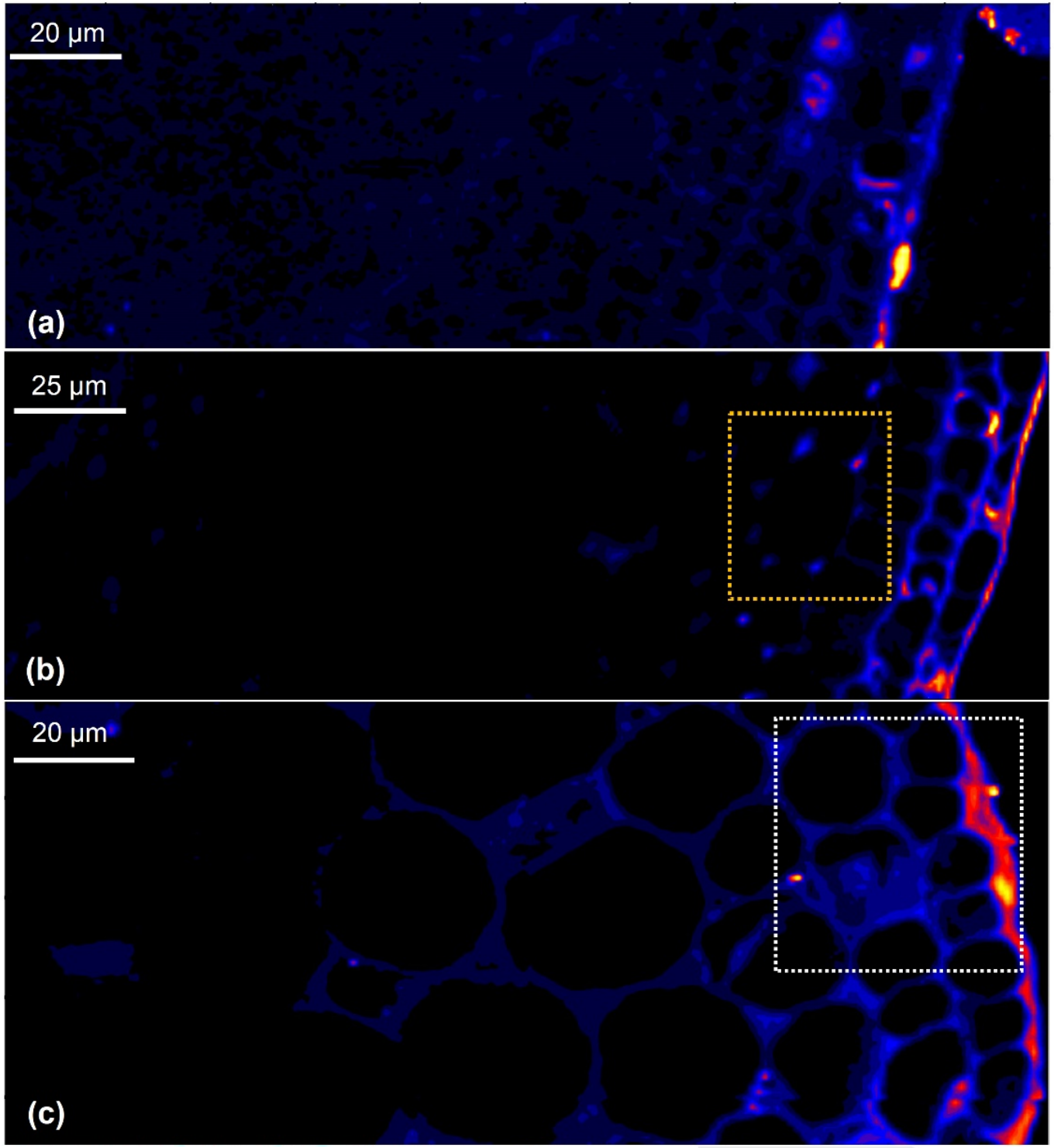

P. M. Kopittke, K. L. Moore , E. Lombi et al, "**Identification of the Primary Lesion of Toxic Aluminum in Plant Roots**" Plant Physiology, 2015, 167, 140

Elettra
Sincrotrone
Trieste

Soybean roots exposed to 30 µM Al for 24 h

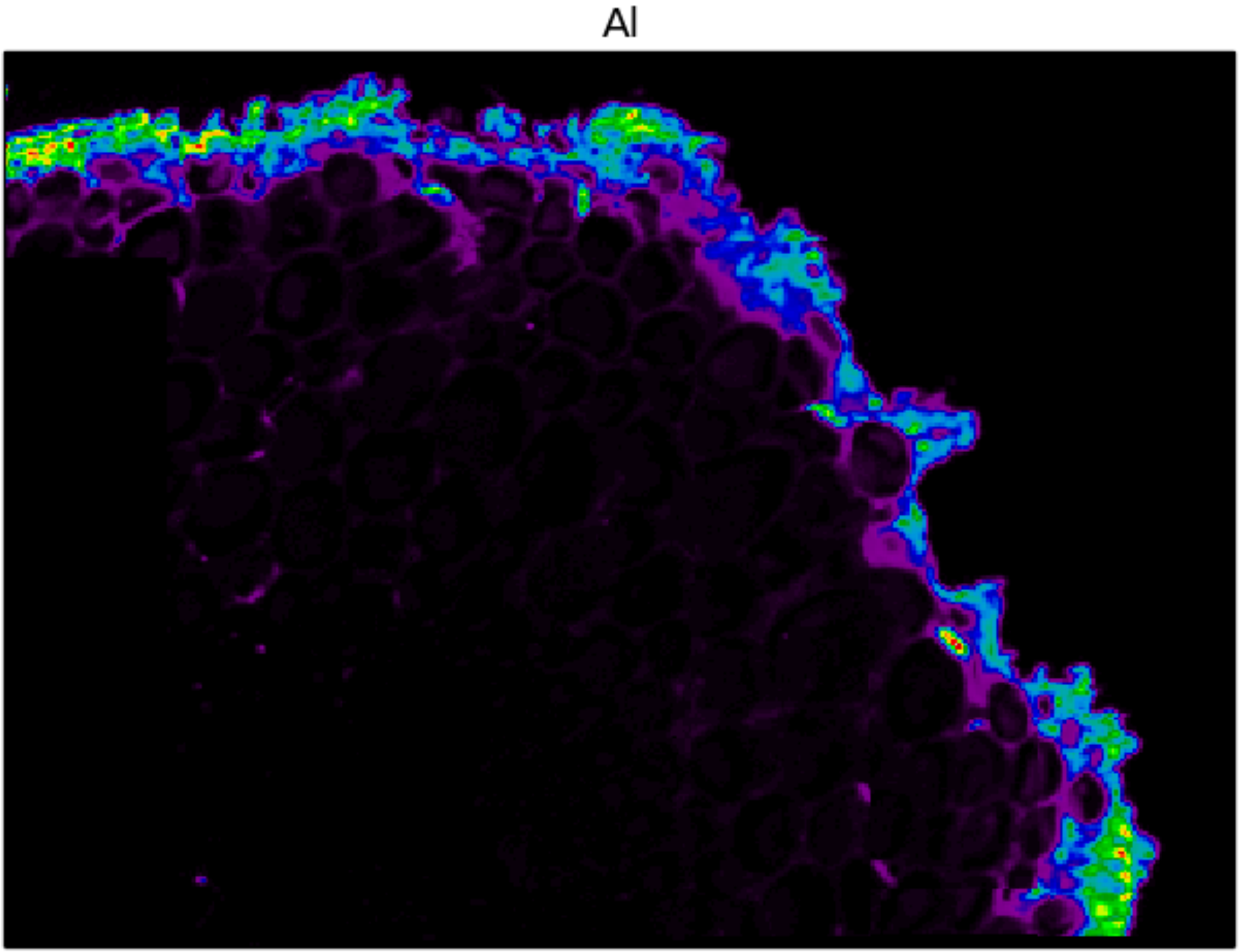

P. M. Kopittke, K. L. Moore , E. Lombi et al, "**Identification of the Primary Lesion of Toxic Aluminum in Plant Roots**" Plant Physiology, 2015, 167, 140

Elettra
Sincrotrone
Trieste

Soybean roots exposed to 30 µM Al for 0.5 h

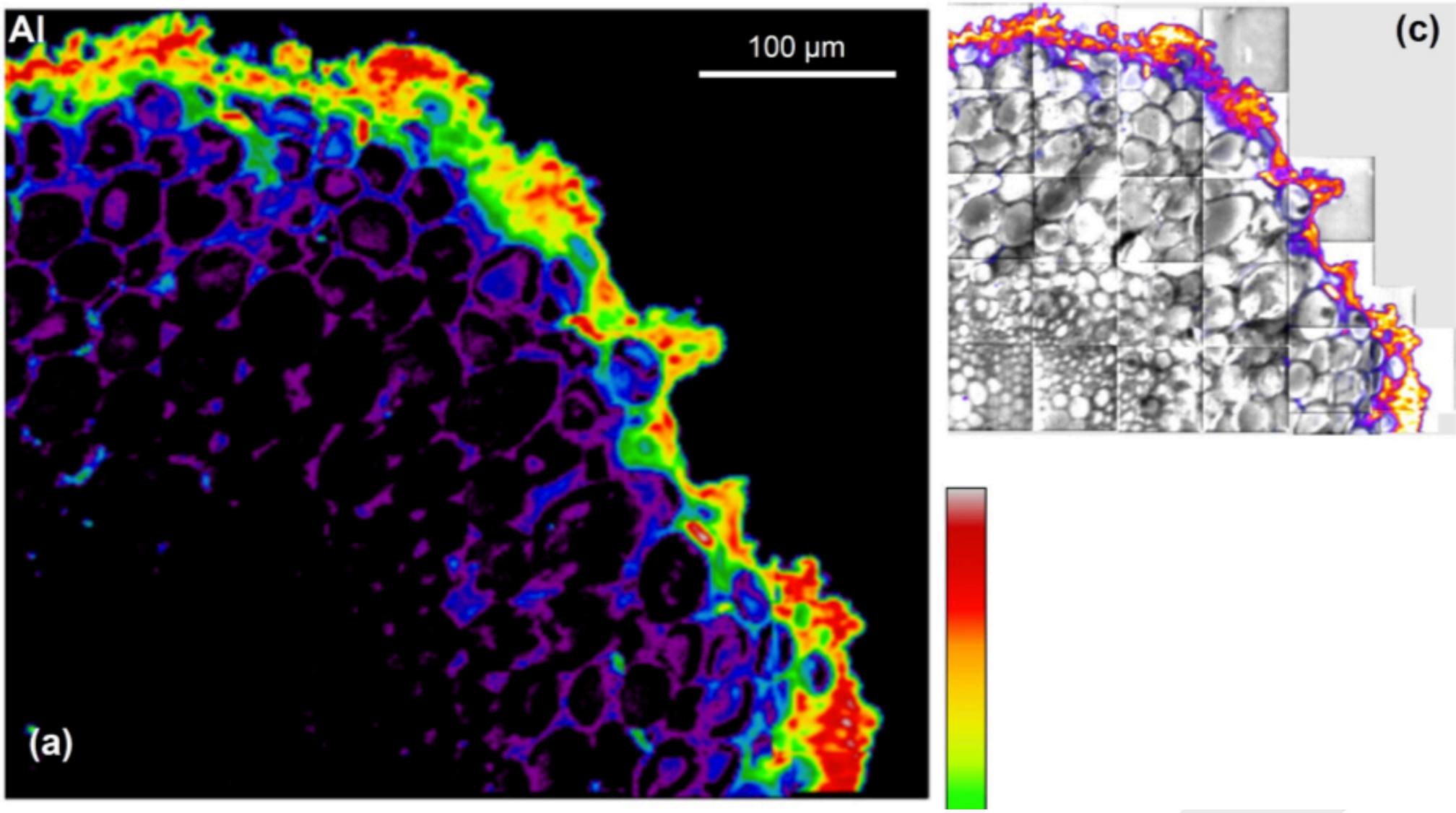

P.M. Kopittke et al "**Identification of the Primary Lesion of Toxic Aluminum in Plant Roots**" Plant Physiology 2015, 167, 140

Elettra
Sincrotrone
Trieste

Soybean roots exposed to 30 µM Al for 0.5 h

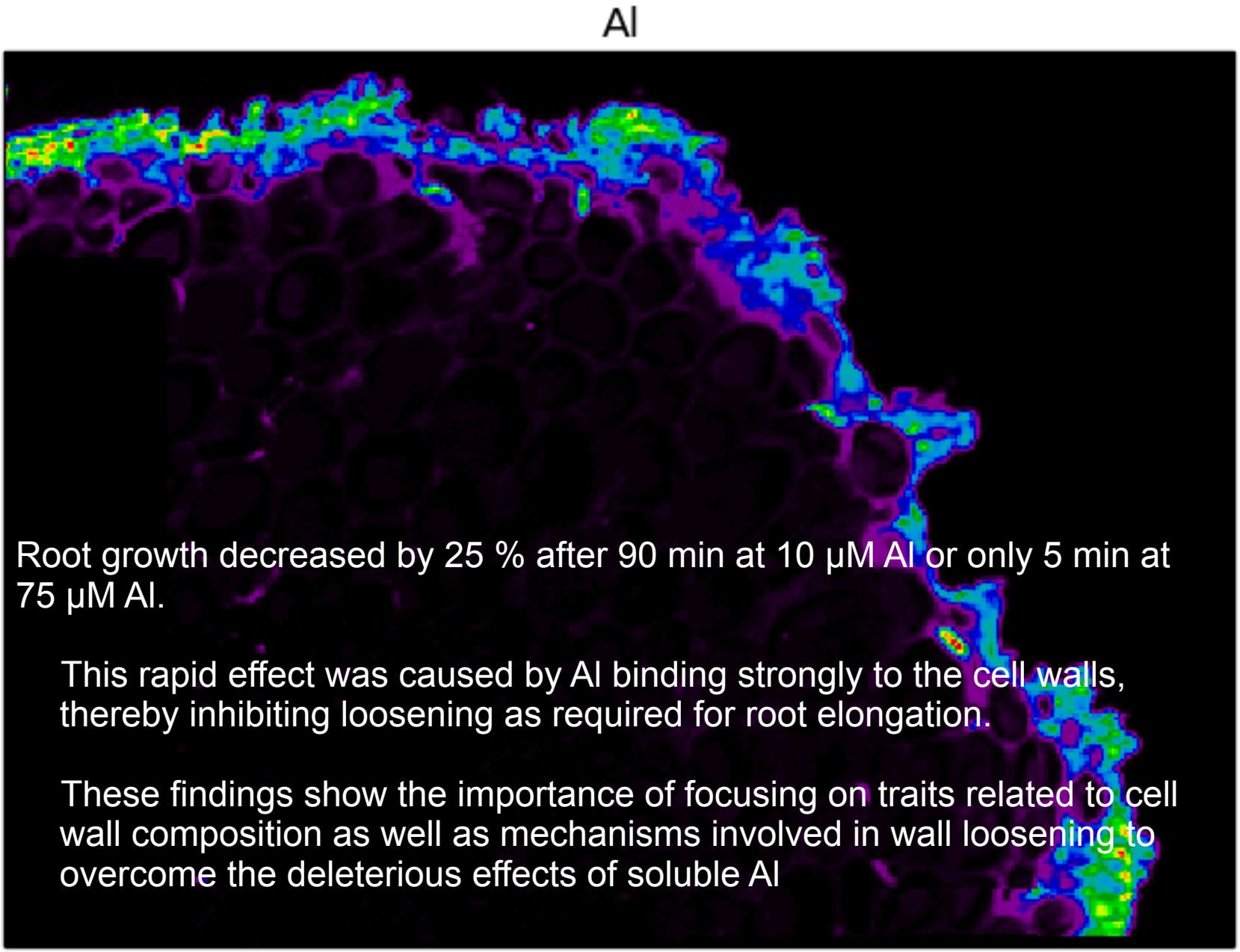

Root growth decreased by 25 % after 90 min at 10 µM Al or only 5 min at 75 µM Al.

This rapid effect was caused by Al binding strongly to the cell walls, thereby inhibiting loosening as required for root elongation.

These findings show the importance of focusing on traits related to cell wall composition as well as mechanisms involved in wall loosening to overcome the deleterious effects of soluble Al

P.M. Kopittke et al "**Identification of the Primary Lesion of Toxic Aluminum in Plant Roots**" Plant Physiology 2015, 167, 140

Elettra
Sincrotrone
Trieste

Al in wheat

- In wheat (Triticum aestivum), it is commonly assumed that Al is detoxified by the release of organic anions into the rhizosphere, but it is also possible that detoxification occurs within the apoplast and symplast of the root itself
- Rhizosphere = plant-root interface, not well definable in size or shape

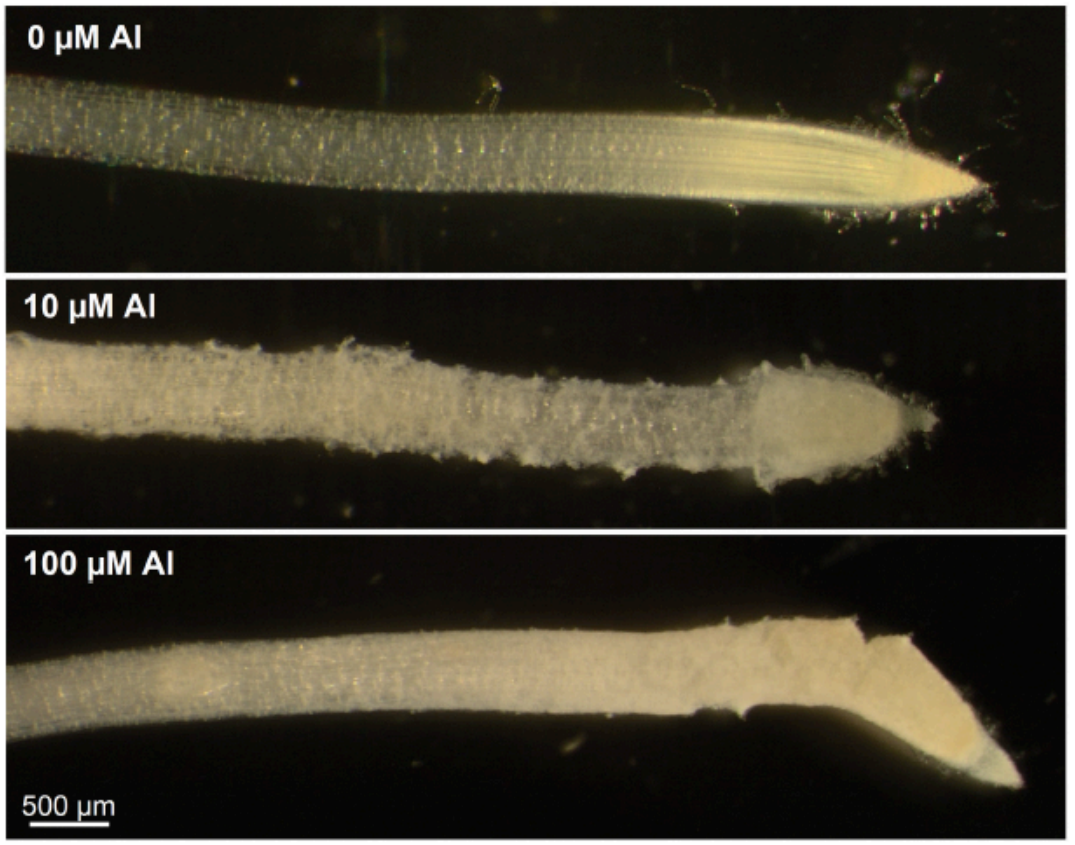

FIGURE 3 | Light micrographs showing roots of ES8 exposed to 0, 10, or 100 µM Al for 48 h. Note the tearing and rupturing evident in the outer tissues of roots exposed to 10 or 100 µM Al. The scale bar applies to all three images.

Kopittke et al. Frontiers in Plant Science 8, 1377 (2017)

Elettra
Sincrotrone
Trieste

XRF analyses @ TwinMic

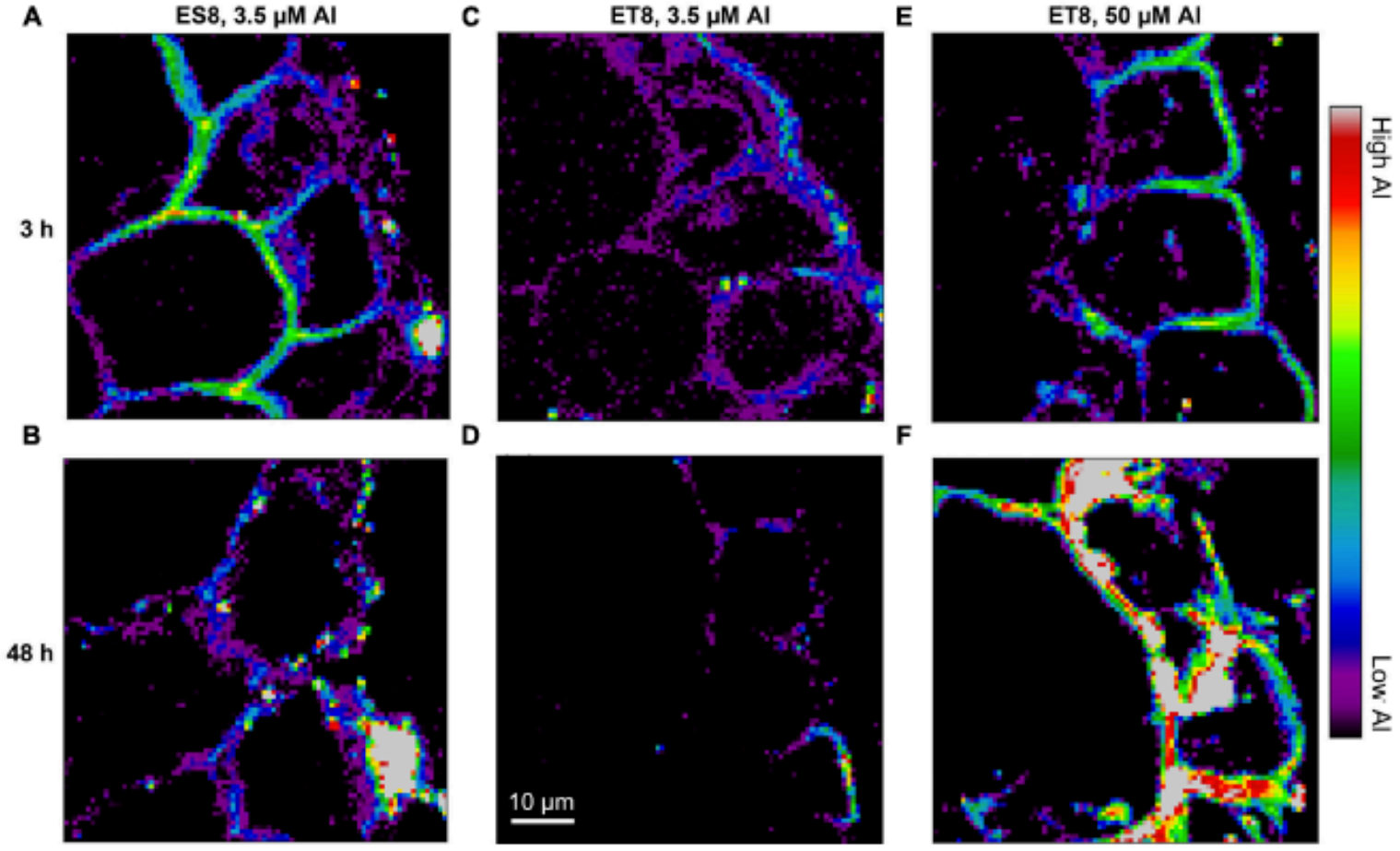

FIGURE 5 | The distribution of Al, examined using LEXRF, in 5-µm-thick transverse root sections taken 3 mm from the apex of ES8 and ET8 exposed to 3.5 or 50 µM Al for either 3 h **(A,C,E)** or 48 h **(B,D,F)**. In all cases, the rhizodermis (and exterior of the root) is on the right-hand side of the image, with only the rhizodermis and 1–2 layers of cortical cells shown. The signal intensity is presented as a color scale, with brighter colors corresponding to higher concentrations. All images were scaled to the same values, and hence intensities can be compared between images. The scale-bar in **(D)** applies to all images. See Supplementary Figure 1 for corresponding light micrographs.

Kopittke et al. Frontiers in Plant Science 8, 1377 (2017)

Elettra
Sincrotrone
Trieste

XANES on Al edge (@ CLS)

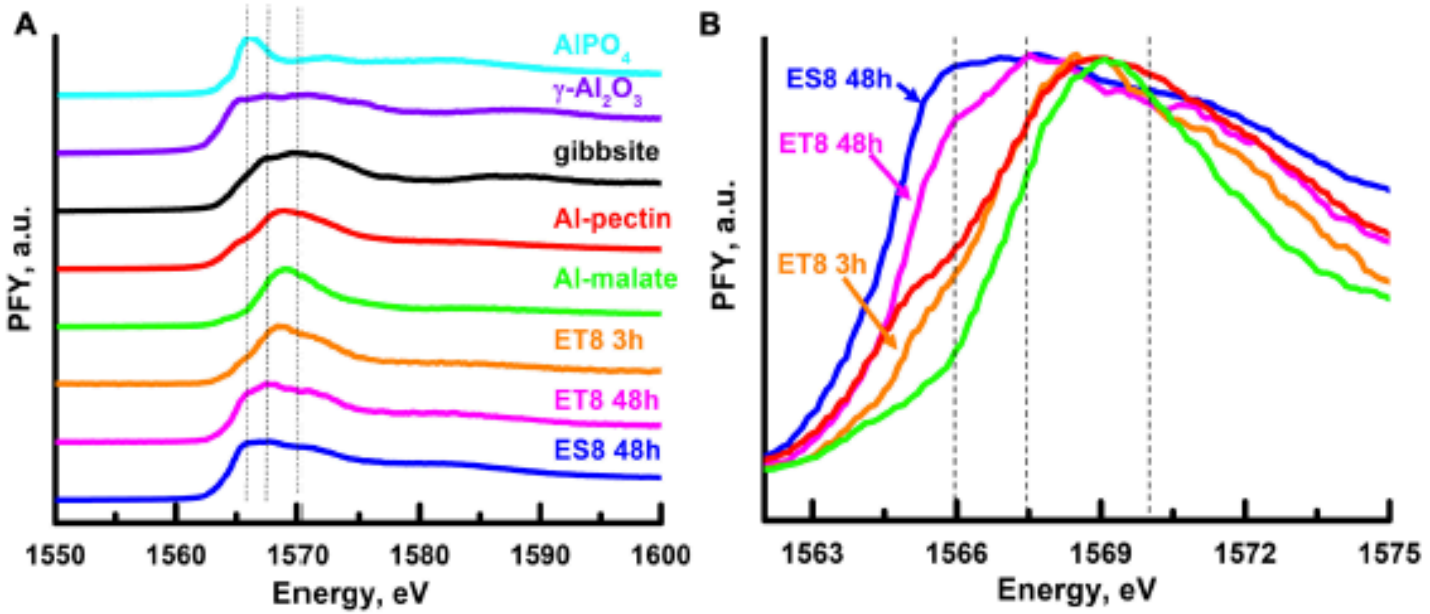

FIGURE 6 | *In situ* analyses of Al speciation using synchrotron-based X-ray absorption near edge structure (XANES). **(A)** Al K-edge XANES spectra of five standard compounds and for root tissues of the near-isogenic wheat lines where ET8 was exposed to 50 μM Al for 3 or 48 h and ES8 was exposed to 3.5 μM Al for 48 h. **(B)** Enlarged spectra (1,562–1,575 eV) for the three root tissues and two standards of interest, Al-malate and Al-pectin. The dotted lines are provided for reference, being 1,566 eV (corresponding to the strong single maximum of four-fold coordinated Al, such as for Al-phosphate), 1,567.7 eV (corresponding to the six-fold coordinated peak of gibbsite), and 1,570 eV (corresponding to the six-fold coordinated peak of γ-Al_2O_3).

- ET8 exposed for 3 h being a mixture of Al species, but mainly Al organic species including that of Al-malate and Al-pectin
- After exposure to Al for 48 h, much of the Al was four-fold coordinated (particularly for ES8, with ET8 still having a higher proportion of six-fold coordinated Al), although the exact form of this four-fold coordinated Al is not clear and further work is required.

Kopittke et al. Frontiers in Plant Science 8, 1377 (2017)

Elettra
Sincrotrone
Trieste

Conclusions

- When ES8 and ET8 were grown at 3.5 mM Al, roots of ES8 accumulated more Al than did those of ET8 (as is evident when comparing Figs 5A,B with Figs 5C,D).
- However, when grown at Al concentrations that resulted in the same reduction in RER (root elongation rate), root tissues of ET8 tended to accumulate more Al than did those of ES8
- The concentration of Al was highest in the rhizodermis in all six treatments, decreasing in the outer cortical tissues and even more so in the inner cortex.
- Furthermore, Al accumulated primarily in the cell wall in apical root tissues of both ES8 and ET8, with comparatively small amounts of Al found within the symplast. This indicates that Al complexed by malate within the root tissues of ET8 accumulated primarily within the apoplast of the rhizodermis and outer cortex.
- Roots, particularly for ES8, ruptured when exposed to high concentrations of Al – this having been observed previously in the roots of a wide range of plant species. These ruptures form initially in the elongation where Al was found to accumulate to high concentrations. This reaffirms the importance of Al accumulation in the cell walls, thereby decreasing root elongation by rapidly inhibiting the ability of the walls to loosen.
- Thus, it is apparent that the complexation of Al by malate in ET8, both in the rhizosphere and apoplast, reduces the strong binding of Al to the cell wall, and thereby reduces the damaging interactions of Al with the root cells.

Kopittke et al. Frontiers in Plant Science 8, 1377 (2017)

Food Science: Inside the wheat

Ivan Kreft, University Ljubljana

Functionality and toxicity of Zn in wheat and buckwhe analyzed on sub-cellular level

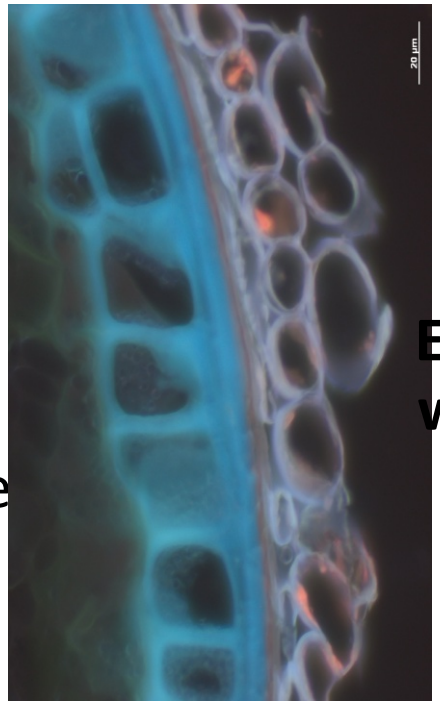

Structure of a wheat grain

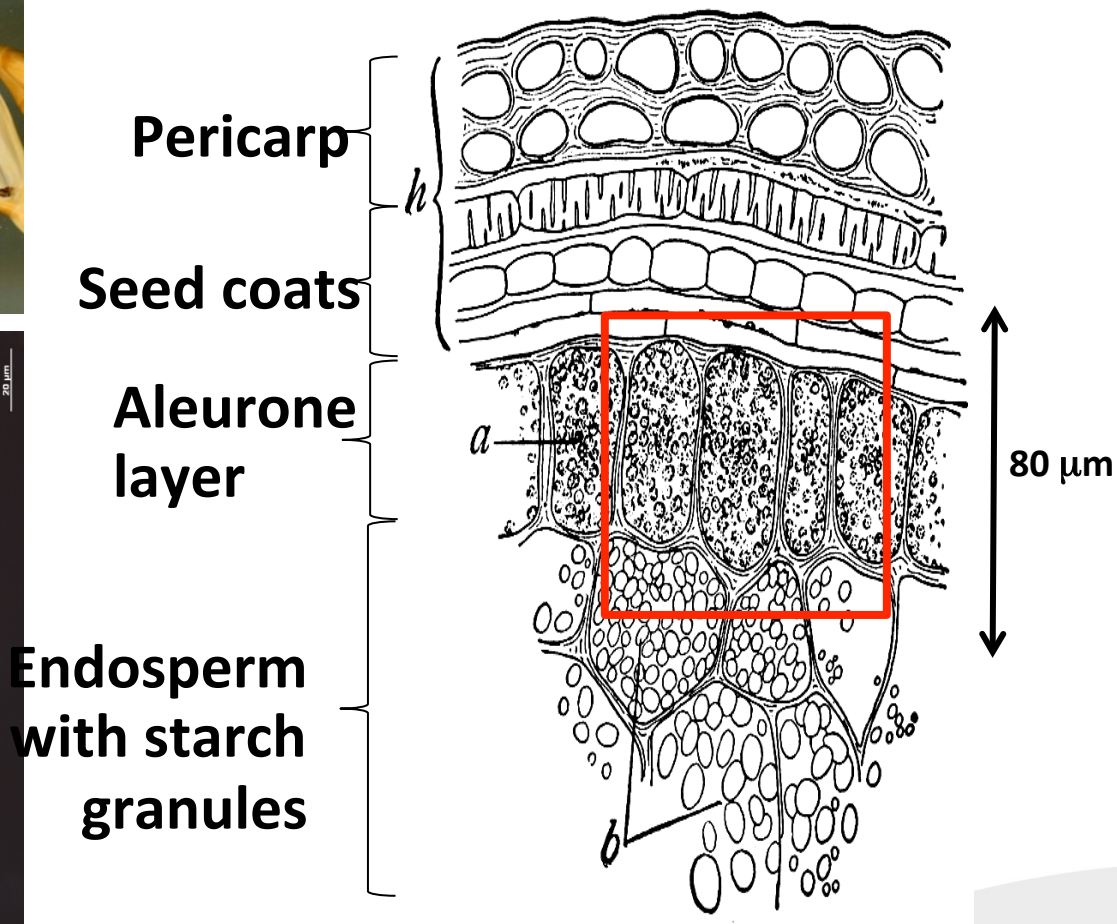

M. Regvar, D. Eichert, B. Kaulich, A. Gianoncelli, P. Pongrac, K. Vogel-Mikus, I. Kreft, New insights into globoids of protein storage vacuoles in wheat aleurone using synchrotron soft X-ray microscopy, Journal of Experimental Botany, Vol. 62, No. 11, 3929–3939, 2011.

Ivan Kreft,
Fac. of Biotechnology,
University Ljubljana

Functionality and toxicity of Zn in wheat and buckwheat analyzed on sub-cellular level

Healthy control wheat

E=1686 eV
80 x 80 mm^2
80 x 80 px
8 s dwell/ px
1 mm resolution
4 detectors

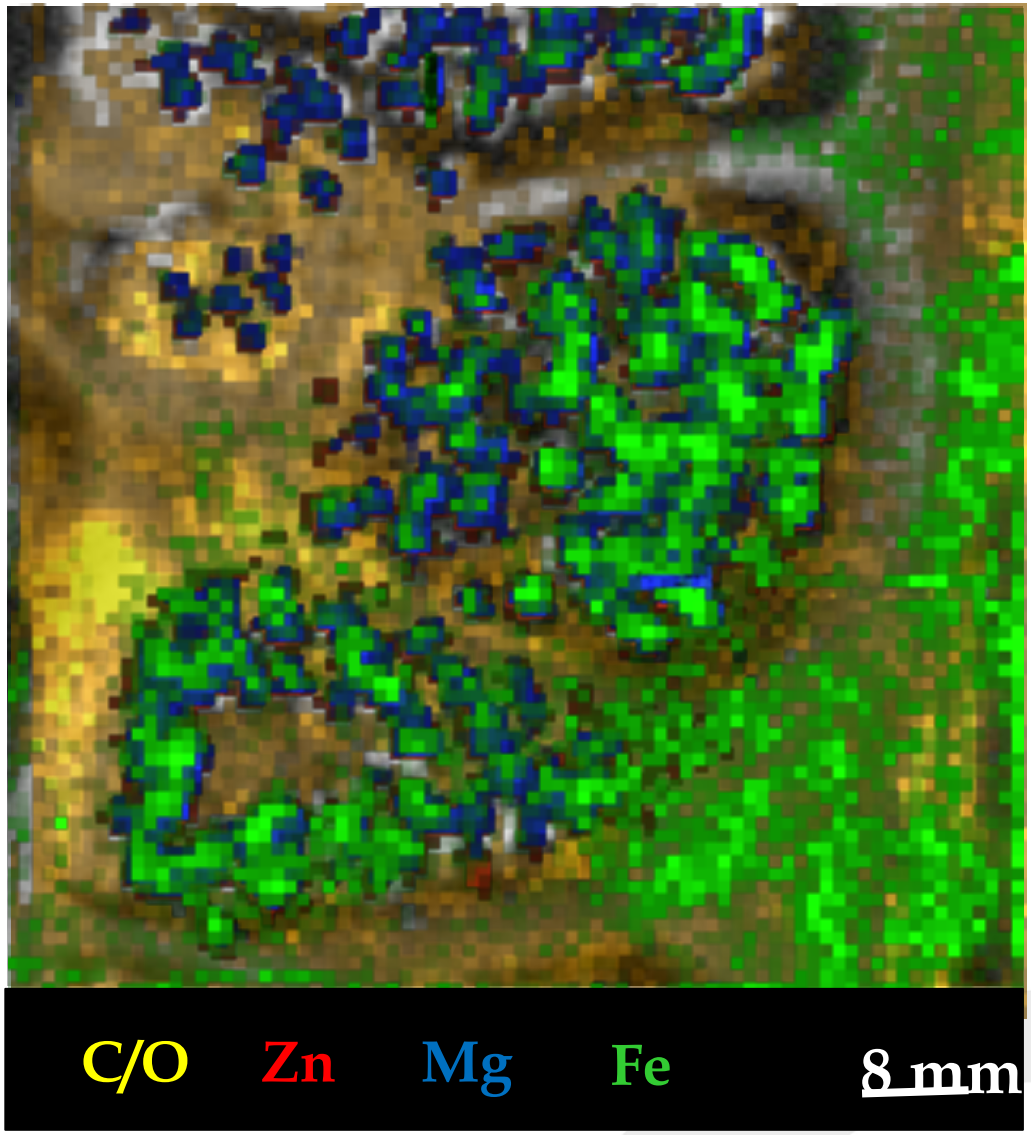

M. Regvar, D. Eichert, B. Kaulich, A. Gianoncelli, P. Pongrac, K. Vogel-Mikus, I. Kreft, New insights into globoids of protein storage vacuoles in wheat aleurone using synchrotron soft X-ray microscopy, Journal of Experimental Botany, Vol. 62, No. 11, 3929–3939, 2011.

Biogenetics and Food Science: Inside the wheat

Ivan Kreft,
Fac. of Biotechnology
University Ljubljana

Functionality and toxicity of Zn in wheat and buckwheat analyzed on sub-cellular level

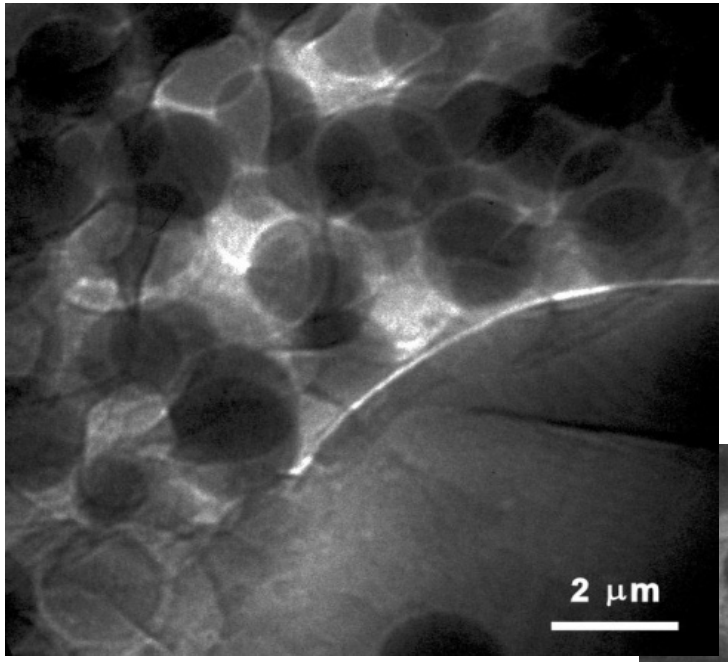

TXM images acquired with a double-frequency ZP (15nm outermost zone width from J. Vila-Comamala (PSI)

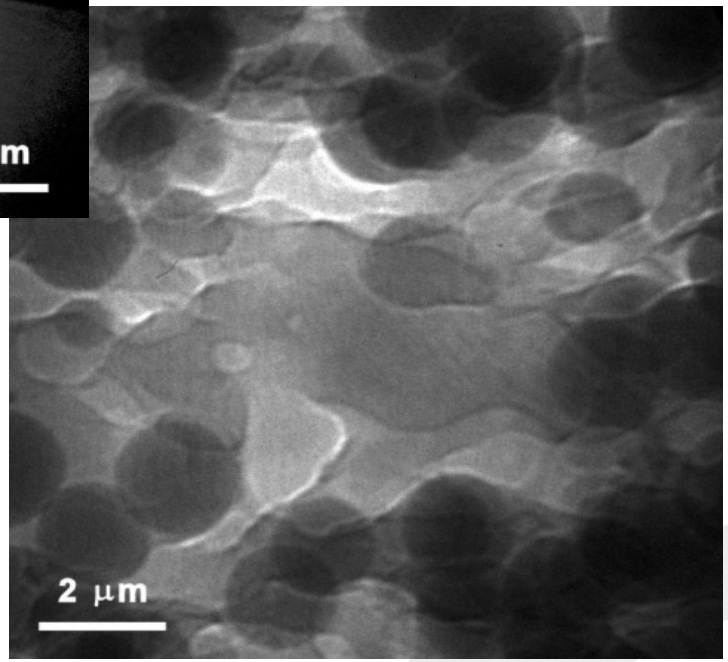

1s dwell, 740 eV photon energy

M. Regvar, D. Eichert, B. Kaulich, A. Gianoncelli, P. Pongrac, K. Vogel-Mikus, I. Kreft, New insights into globoids of protein storage vacuoles in wheat aleurone using synchrotron soft X-ray microscopy, Journal of Experimental Botany, Vol. 62, No. 11, 3929–3939, 2011.

Elettra
Sincrotrone
Trieste

Nanotoxicology

Cellular distribution and degradation of $CoFe_2O_4$ NPs in Balb/3T3 Fibroblast cells

Localization of engineered nanoparticles (ENPs) inside a cell and on the possible effects on the cell metabolic behaviour

G. Ceccone, P. Marmorato et al., EC Joint Research Center, Ispra, I

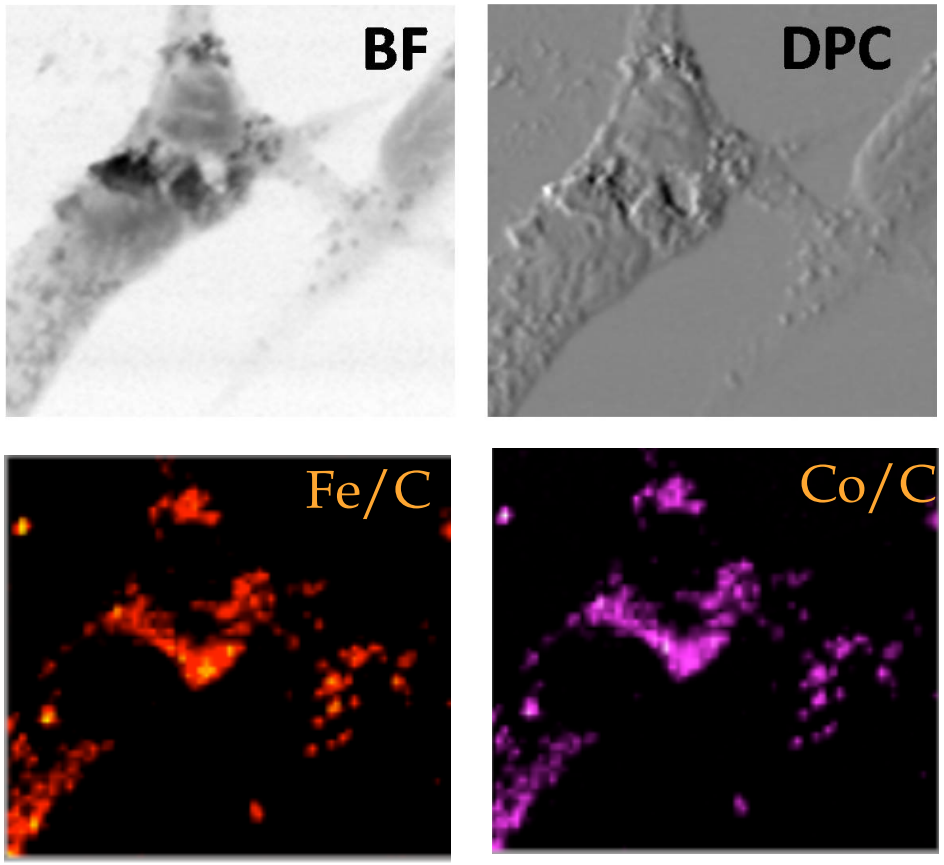

$CoFe_2O_4$ in mouse 3T3 fibroblast cells, E=2019 eV, 60um x 60 um

P. Marmorato, G. Ceccone, A. Gianoncelli, L. Pascolo, J. Ponti, F. Rossi, M. Salomé, B. Kaulich, and M. Kiskinova, *Cellular distribution and degradation of Cobalt Ferrite Nanoparticles in Balb/3T3 Fibroblasts*, Toxicology Letters, 2011, 207 - 2, 128-136.

Elettra
Sincrotrone
Trieste

Balb/3T3 exposed to 1000mM

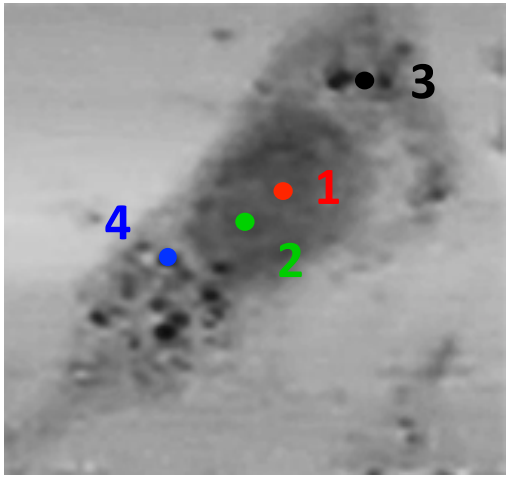

Fe/Co~0.8

Fe/Co~1.5

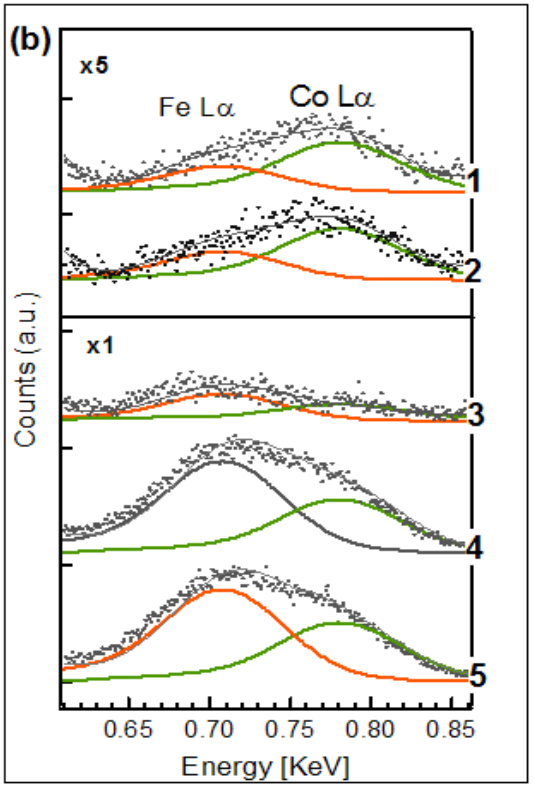

Similar behaviour (but less evident) in the nuclear region for 500µM concentration

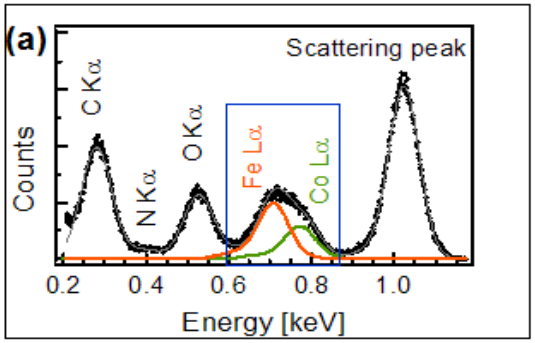

P. Marmorato, G. Ceccone, A. Gianoncelli, L. Pascolo, J. Ponti, F. Rossi, M. Salomé, B. Kaulich, and M. Kiskinova, *Cellular distribution and degradation of Cobalt Ferrite Nanoparticles in Balb/3T3 Fibroblasts*, Toxicology Letters, 2011, 207 - 2, 128-136.

Elettra
Sincrotrone
Trieste

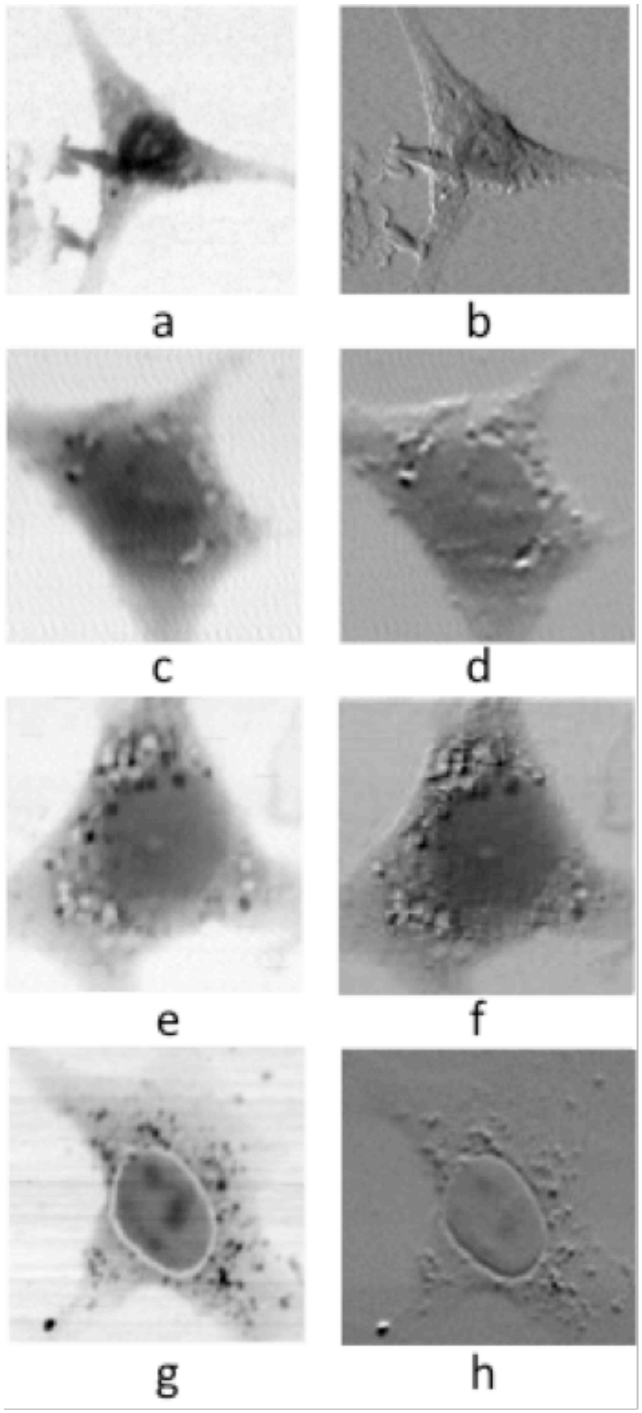

Control

40 μM

250 μM

500 μM

High-resolution scanning transmission soft X-ray microscopy for rapid probing of nanoparticle distribution and sufferance features in exposed cells Kourousias G, Pascolo L, Marmorato P, Ponti J, Ceccone G, Kiskinova M, Gianoncelli A *X-Ray Spectrometry (2015)*

Elettra
Sincrotrone
Trieste

Fibroblast cells exposed to $CoFe_2O_4$ NPs

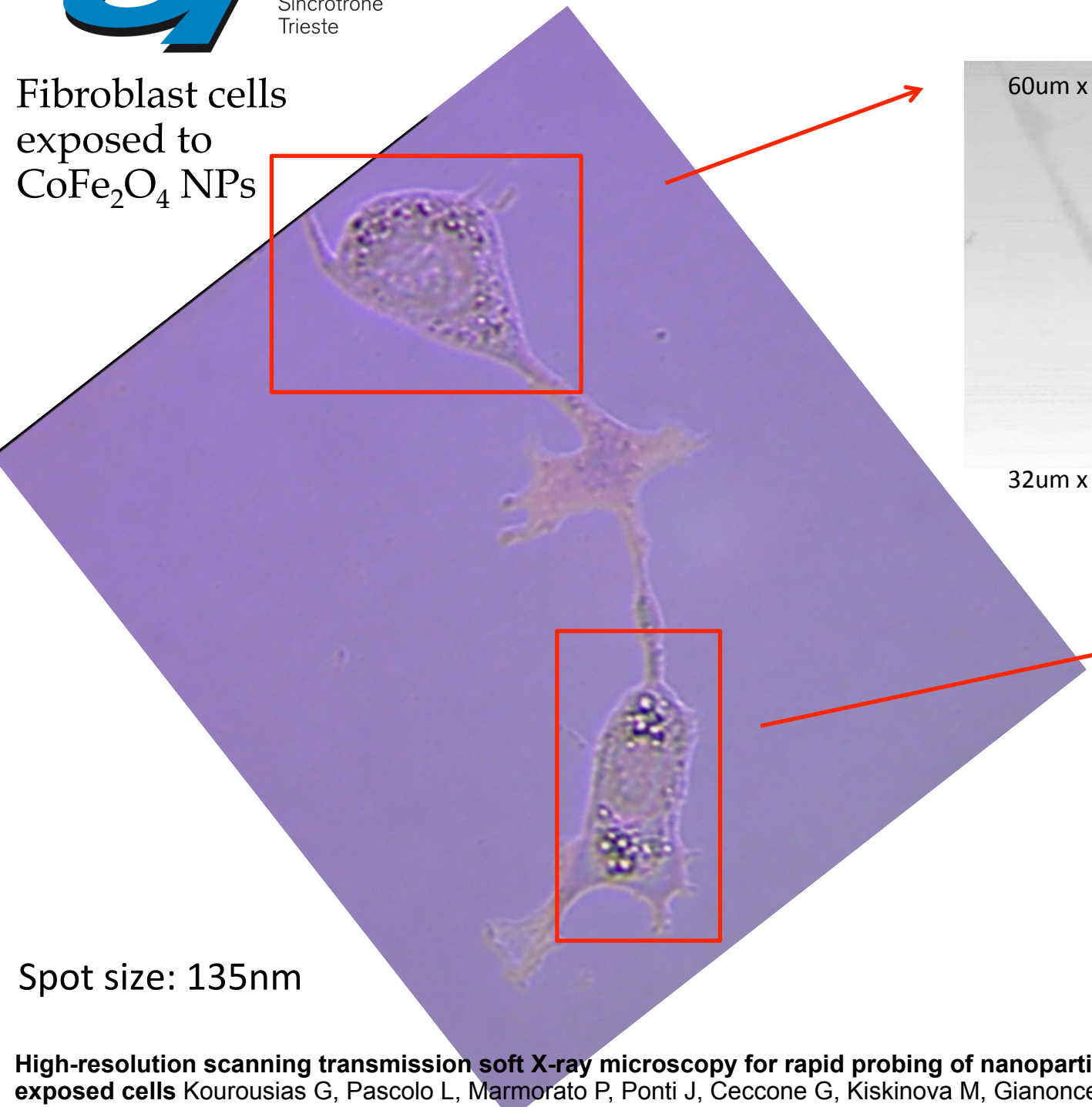

60um x 40um, 480x320 pixels, 20ms dt, 900eV

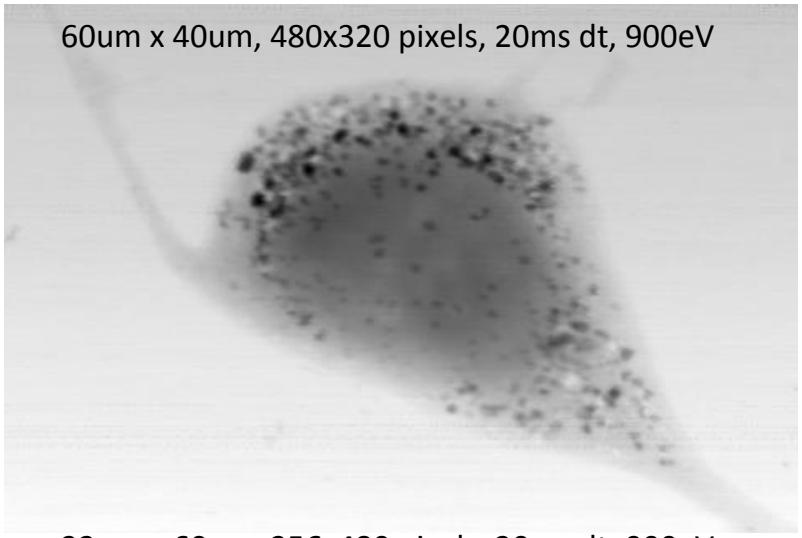

32um x 60um, 256x480 pixels, 20ms dt, 900eV

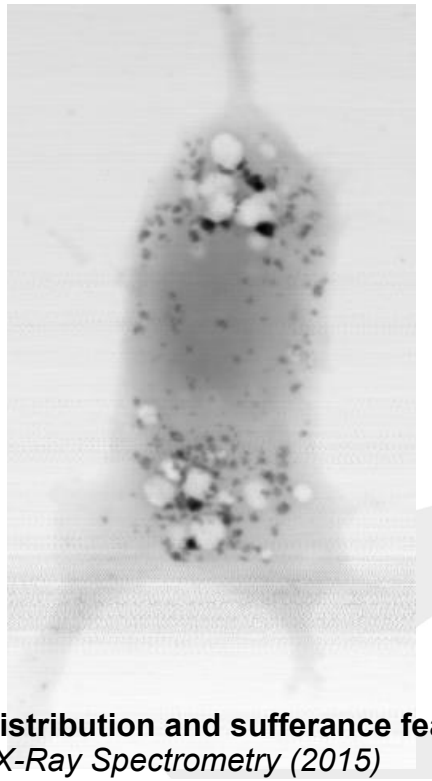

Spot size: 135nm

High-resolution scanning transmission soft X-ray microscopy for rapid probing of nanoparticle distribution and sufferance features in exposed cells Kourousias G, Pascolo L, Marmorato P, Ponti J, Ceccone G, Kiskinova M, Gianoncelli A *X-Ray Spectrometry (2015)*

Elettra
Sincrotrone
Trieste

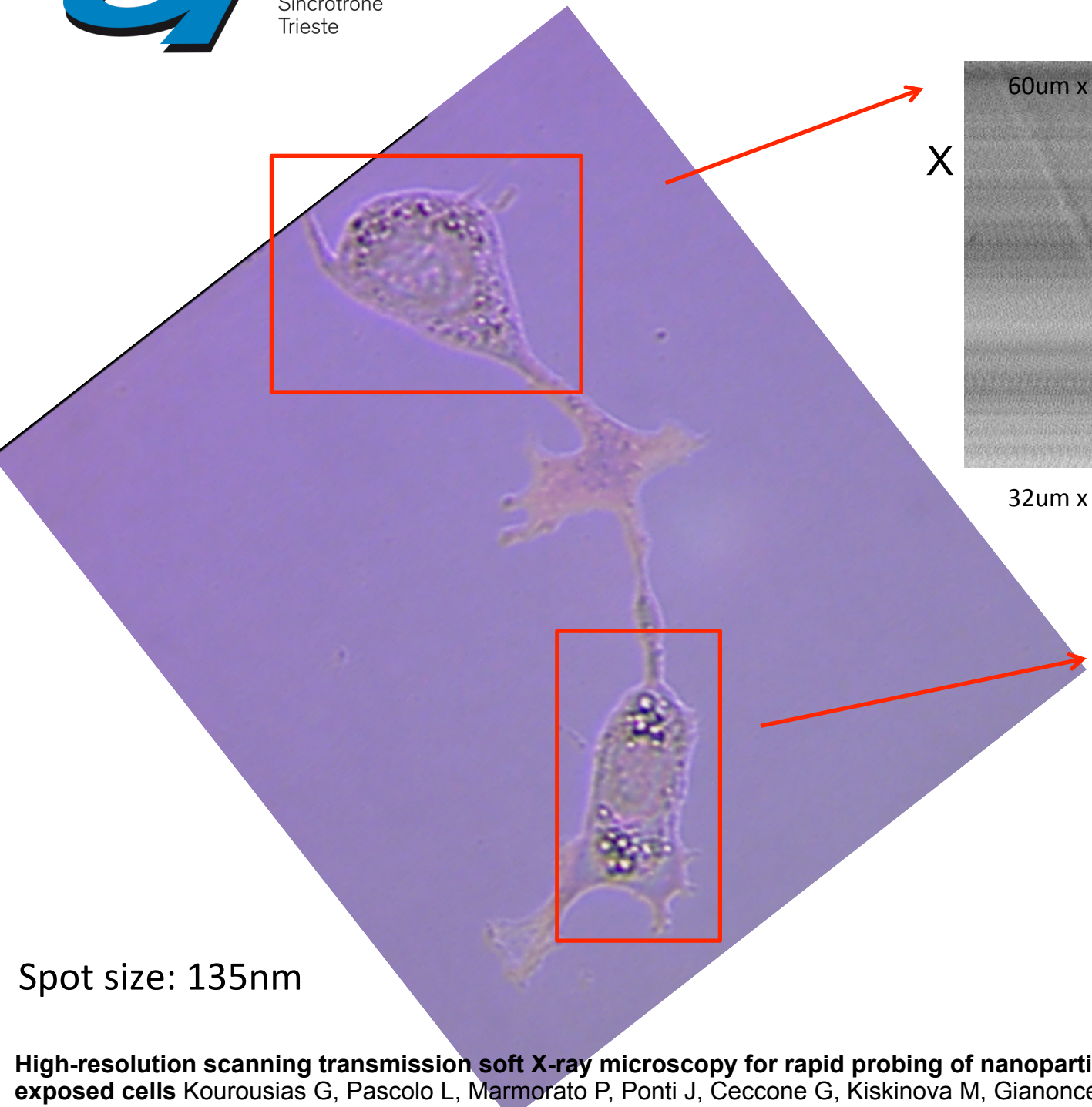

X

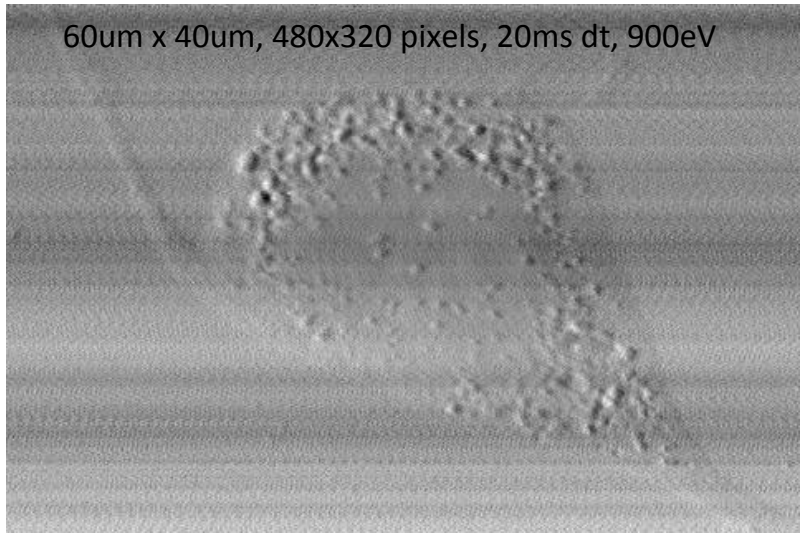

32um x 60um, 256x480 pixels, 20ms dt, 900eV

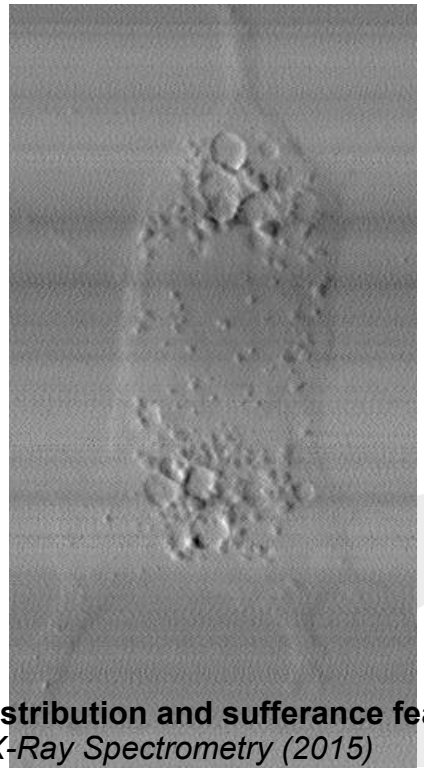

X

Spot size: 135nm

High-resolution scanning transmission soft X-ray microscopy for rapid probing of nanoparticle distribution and sufferance features in exposed cells Kourousias G, Pascolo L, Marmorato P, Ponti J, Ceccone G, Kiskinova M, Gianoncelli A *X-Ray Spectrometry (2015)*

Elettra
Sincrotrone
Trieste

Red oil specifically stains lipids

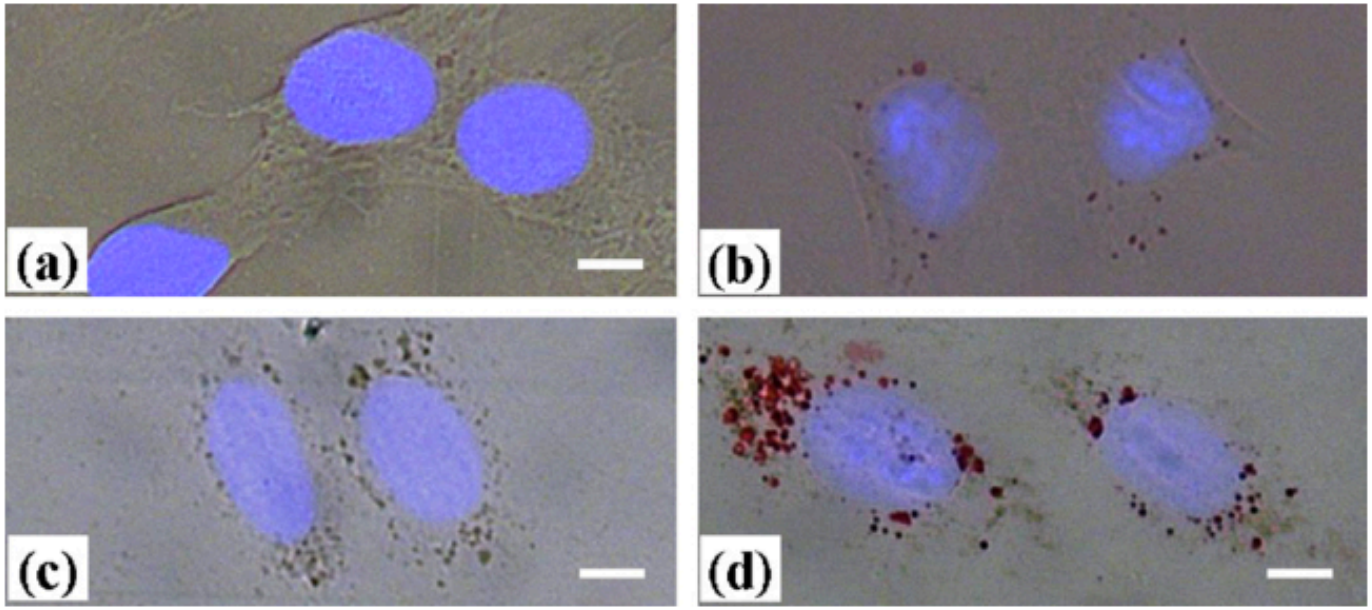

Fig. 6. Optical images of Balb/3T3 control cells (a and b) and incubated for 24 h with 500 μM $CoFe_2O_4$ NPs suspension (c and d). Red spots represent lipids stained by Red Oil O solution (b and d) whilst nuclei are stained in blue by Hoechst. Bar = 10 μm. (For interpretation of the references to color in this figure legend, the reader is referred to the web version of the article.)

P. Marmorato, G. Ceccone, A. Gianoncelli, L. Pascolo, J. Ponti, F. Rossi, M. Salomé, B. Kaulich, and M. Kiskinova, *Cellular distribution and degradation of Cobalt Ferrite Nanoparticles in Balb/3T3 Fibroblasts*, Toxicology Letters, 2011, 207 - 2, 128-136.

Nanotoxicology: $CoFe_2O_4$ ENPs

Control

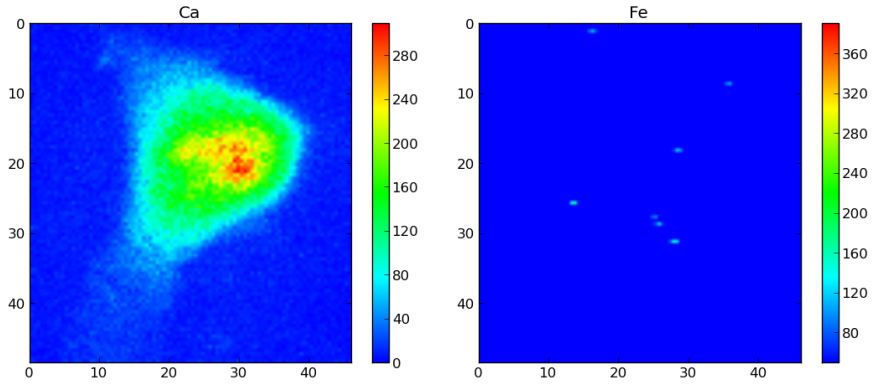

Exposed to 500μM

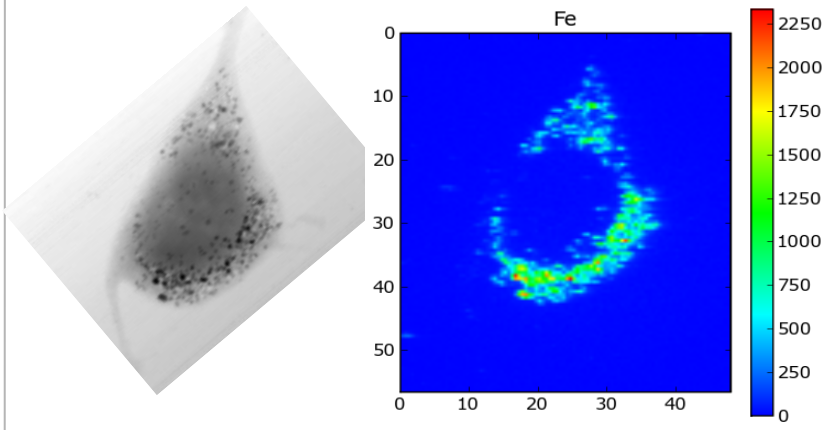

Exposed to 40μM

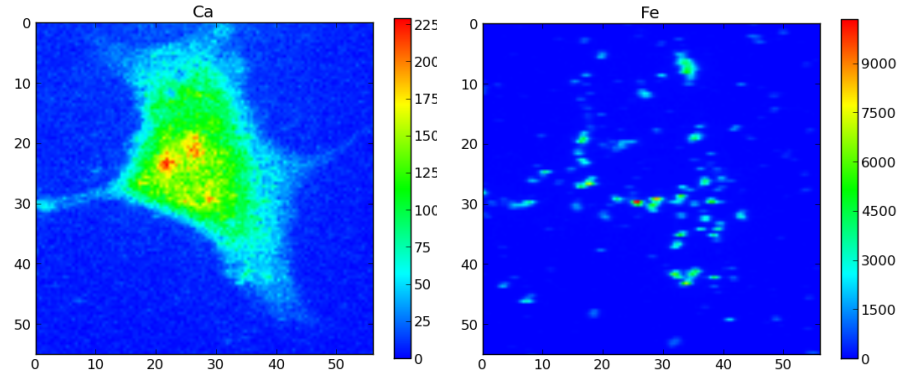

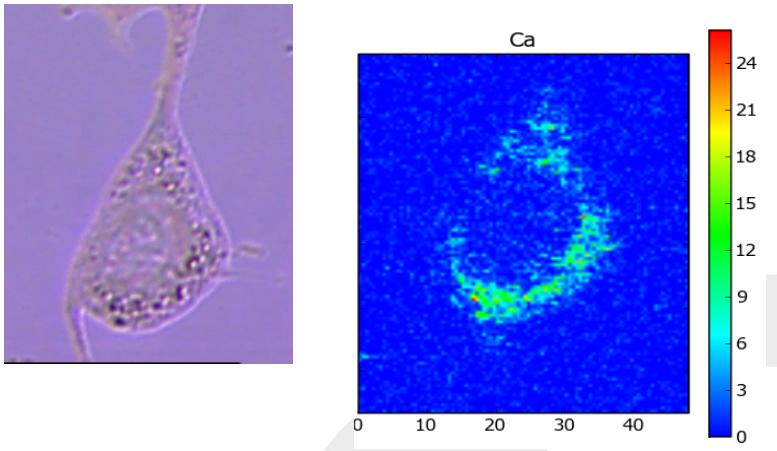

P. Marmorato, G. Ceccone, A. Gianoncelli, L. Pascolo, J. Ponti, F. Rossi, M. Salomé, B. Kaulich, and M. Kiskinova, Cellular distribution and degradation of Cobalt Ferrite Nanoparticles in Balb/3T3 Fibroblasts, in press in Toxicology Letters

Elettra
Sincrotrone
Trieste

Exposure to Asbestos

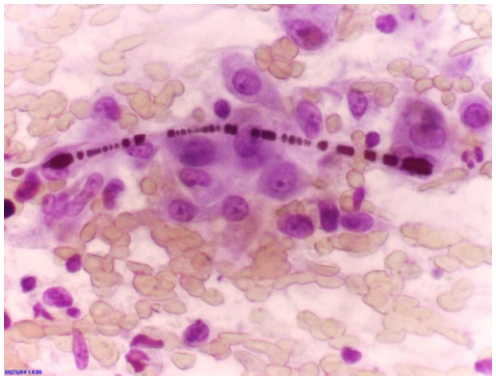

L. Pascolo, M. Melato, Burlo Hospital, Trieste, Italy

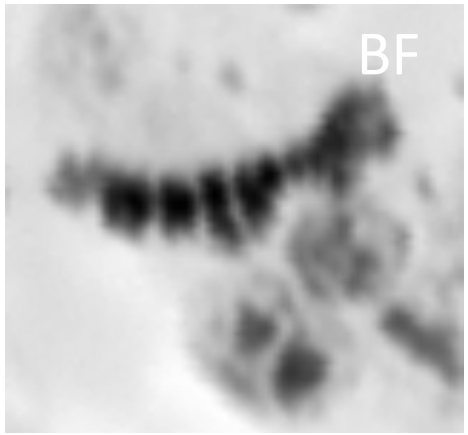

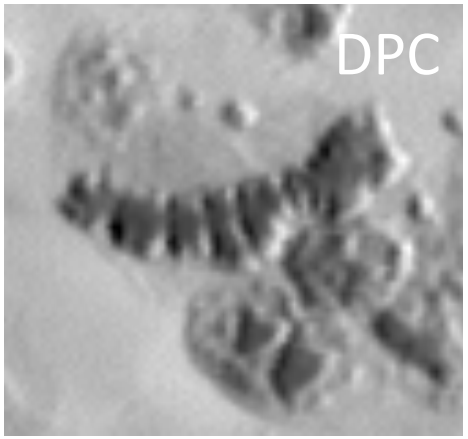

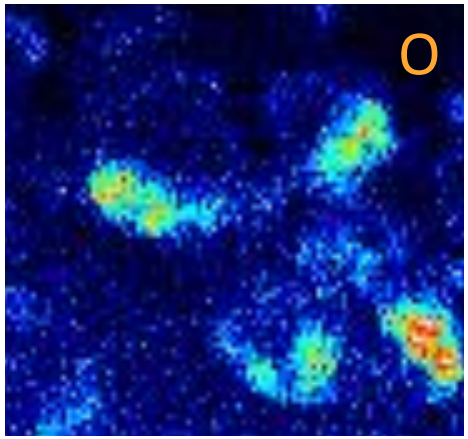

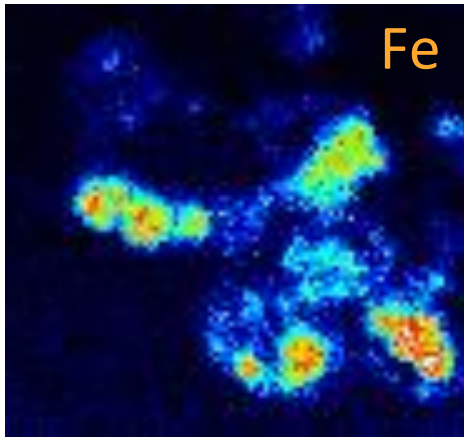

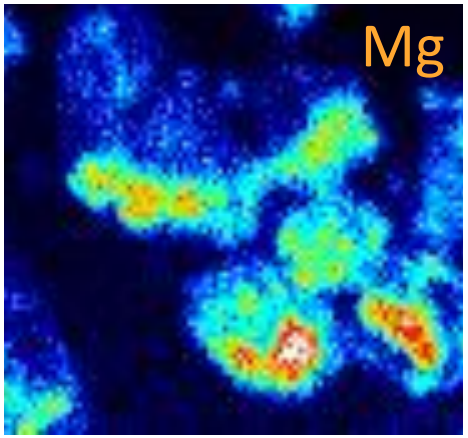

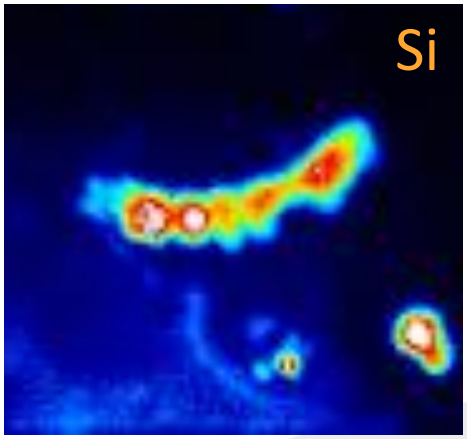

Mesothelioma and differentiation of lung tissue due to asbestos;
the role of Mg

E=2019 eV, 50mm x 50 mm, 100 x 100 pixels, 15s/pixel LEXRF, 4 SDDs

L. Pascolo, A. Gianoncelli, et al. Particle and Fibre Toxicology 2011, 8:7.
L. Pascolo, A. Gianoncelli, et al. Scientific Reports 2013, 3.

Elettra
Sincrotrone
Trieste

Tissue with a phagocytated asbestos fibre.

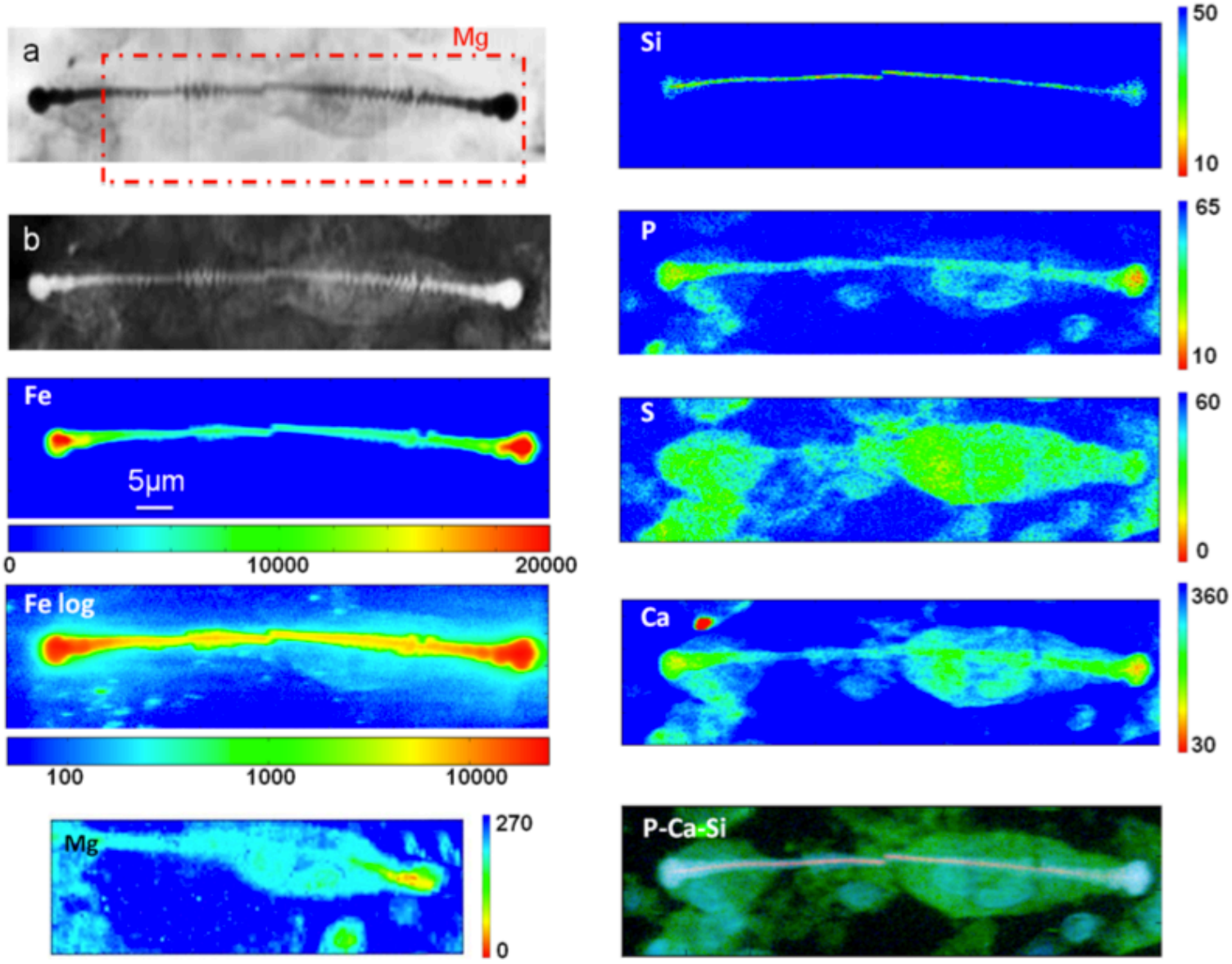

L. Pascolo, A. Gianoncelli, et al. Particle and Fibre Toxicology 2011, 8:7.
L. Pascolo, A. Gianoncelli, et al. Scientific Reports 2013, 3.

Elettra
Sincrotrone
Trieste

Fe K-edge XANES measured in selected ~ 1 mm^2 spots of an asbestos body

- Most of the Fe detected around asbestos fibres (coating and ferruginous bodies) is compatible with the presence of ferritin and the Fe3+ oxidation state of iron.
- The most novel and intriguing result was the detection of significant percentages of haematite in the asbestos bodies that we suppose is the results of ferritin transformation occurring during the long residence time in the asbestos bodies in the lung tissues.

Figure 6

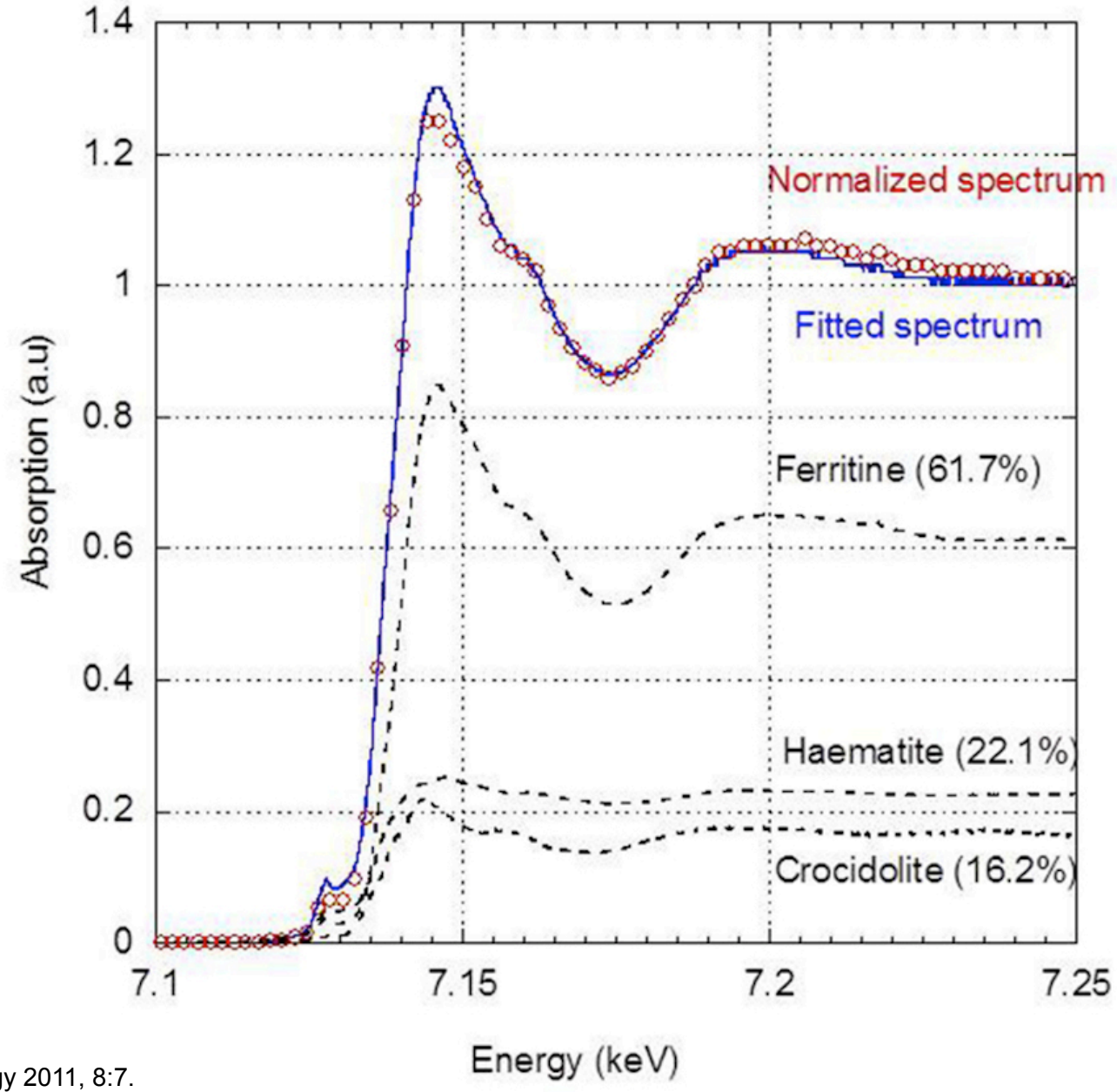

L. Pascolo, A. Gianoncelli, et al. Particle and Fibre Toxicology 2011, 8:7.
L. Pascolo, A. Gianoncelli, et al. Scientific Reports 2013, 3.

Elettra Sincrotrone Trieste

First real Clinical case at TwinMic

SCIENTIFIC REPORTS

OPEN

SUBJECT AREAS:
PATHOGENESIS
BIOPHYSICS
CHEMICAL MODIFICATION

Received
19 May 2014

Accepted
9 September 2014

Published
7 October 2014

Calcium micro-depositions in jugular truncular venous malformations revealed by Synchrotron-based XRF imaging

Lorella Pascolo[1], Alessandra Gianoncelli[2], Clara Rizzardi[3], Veronica Tisato[4], Murielle Salomé[5], Carla Calligaro[6], Fabrizio Salvi[7], David Paterson[8] & Paolo Zamboni[9]

[1]Institute for Maternal and Child Health, IRCCS Burlo Garofolo, Trieste, Italy, [2]Elettra-Sincrotrone Trieste, Area Science Park, Basovizza, Trieste, Italy, [3]Department of Pathology and Forensic Medicine, University of Trieste, Trieste, Italy, [4]Department of Morphology, Surgery and Experimental Medicine and LTTA Centre, University of Ferrara, Ferrara, Italy, [5]European Synchrotron Radiation Facility, Grenoble Cedex 9, France, [6]Servizio Diagnostica Veterinaria, University of Udine, Udine, Italy, [7]IRCCS Neurological Sciences, Centro il Be.Ne, Ospedale Bellaria, Bologna, Italy, [8]Australian Synchrotron, Clayton, Victoria, Australia, [9]Vascular Diseases Center, University of Ferrara, Cona (Ferrara), Italy.

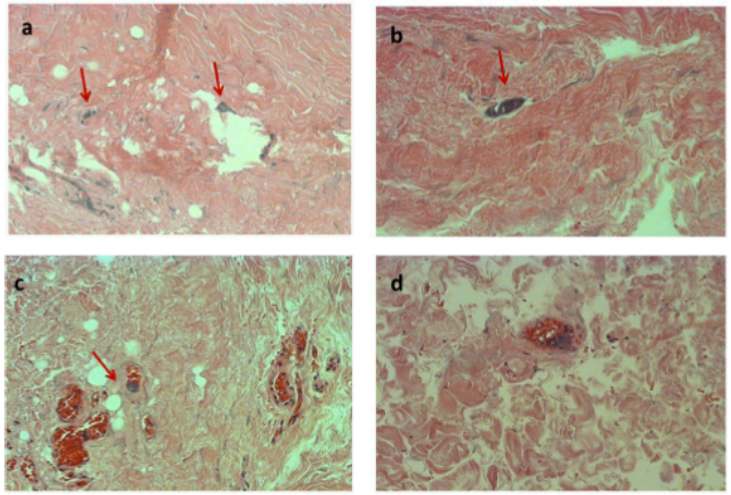

Figure 1 | Optical microscopy images of anomalies in MS jugular vein tissues. Images a and b show suggested micro-calcifications (arrows). A scratch in the tissue is evident in a, while b, c and d show the singular appearance of same microvessel. The arrow in c indicates the presence of basophilic-calcified material inside a capillary. The same is revealed in panel d. All images are at 40 × magnification.

Started at TwinMic
Then extended to 2 other synchrotron facilities to get complementary information:

- ESRF (ID21)
- Australian Synchrotron (XFM)

Rapid XRF imaging at XFM beamline (Australian Synchrotron)

Elettra Sincrotrone Trieste

Rapid XRF analyses on large tissue areas at 12.74 keV showed an increased Ca presence in the pathological samples, mainly localized in tunica adventitia microvessels.

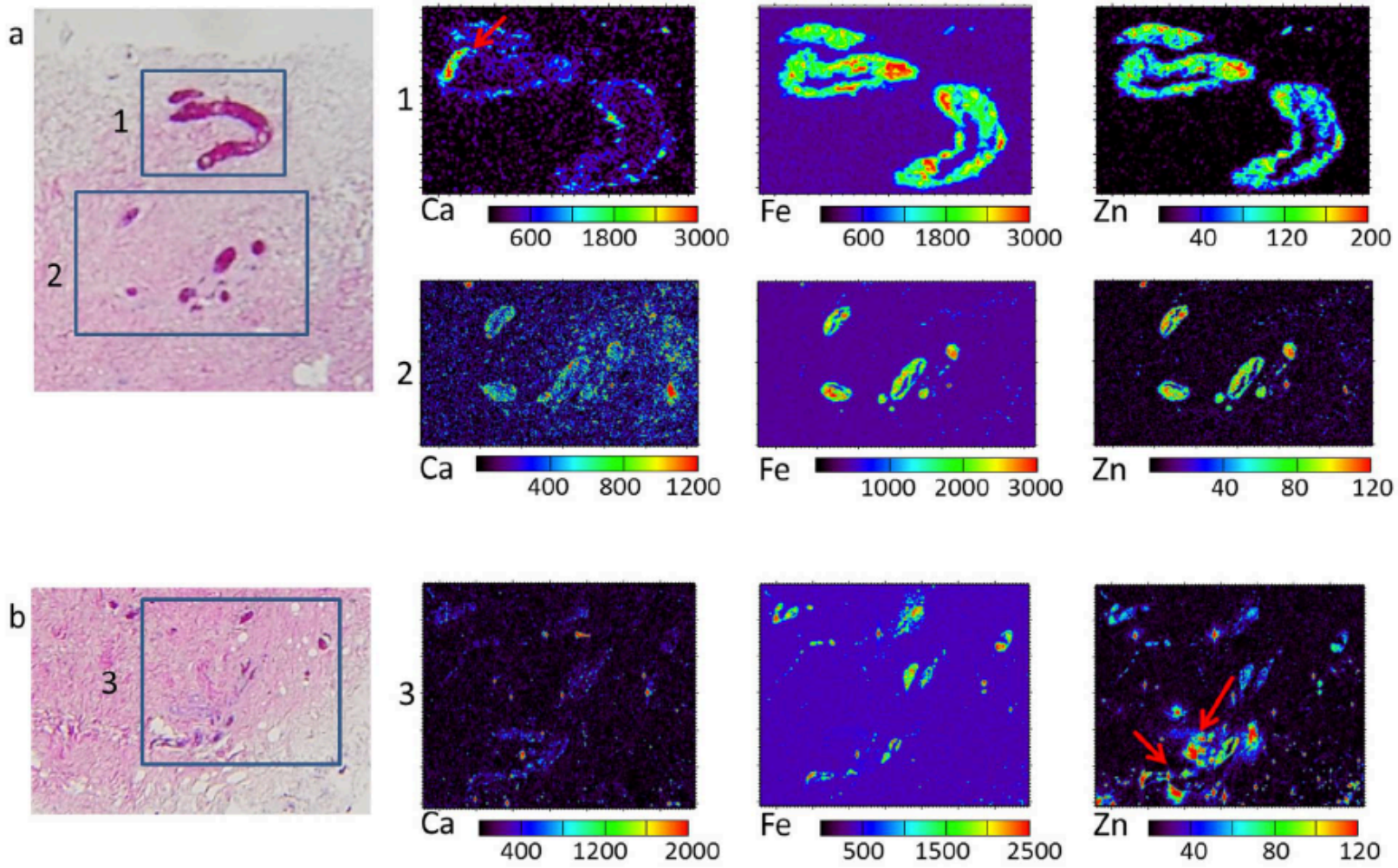

Figure 2 | XRF elemental maps at 12.74 keV in MS2 tissue jugular sections. Three consecutive tissue sections of MS2 sample are used: two unstained for XRF analyses and one HH stained for tissue structure recognition. a) and b): light microscopy images, the boxes indicate the selected regions for XRF analyses in the unstained sections. The corresponding elemental maps of Ca, Fe and Zn of regions 1, 2 and 3 acquired at the XFM beamline at 12.74 keV with 2 μm spatial resolution on the corresponding unstained tissue slices are shown in rows 1, 2 and 3 respectively. Red arrow in Ca map (1) indicates a calcification further analyzed at 4.12 keV. Arrows in Zn map indicate potential contaminants and tissue debris. The concentrations reported on the scale bars are in ppm. Region 1: 250 μm × 170 μm; Region 2: 600 μm × 400 μm; Region 3: 700 μm × 600 μm.

Investigations at lower energy demonstrated that the high Ca level corresponded to micro-calcifications, also containing P & Mg.

www.nature.com/scientificreports

ID21, ESRF

TwinMic, Elettra

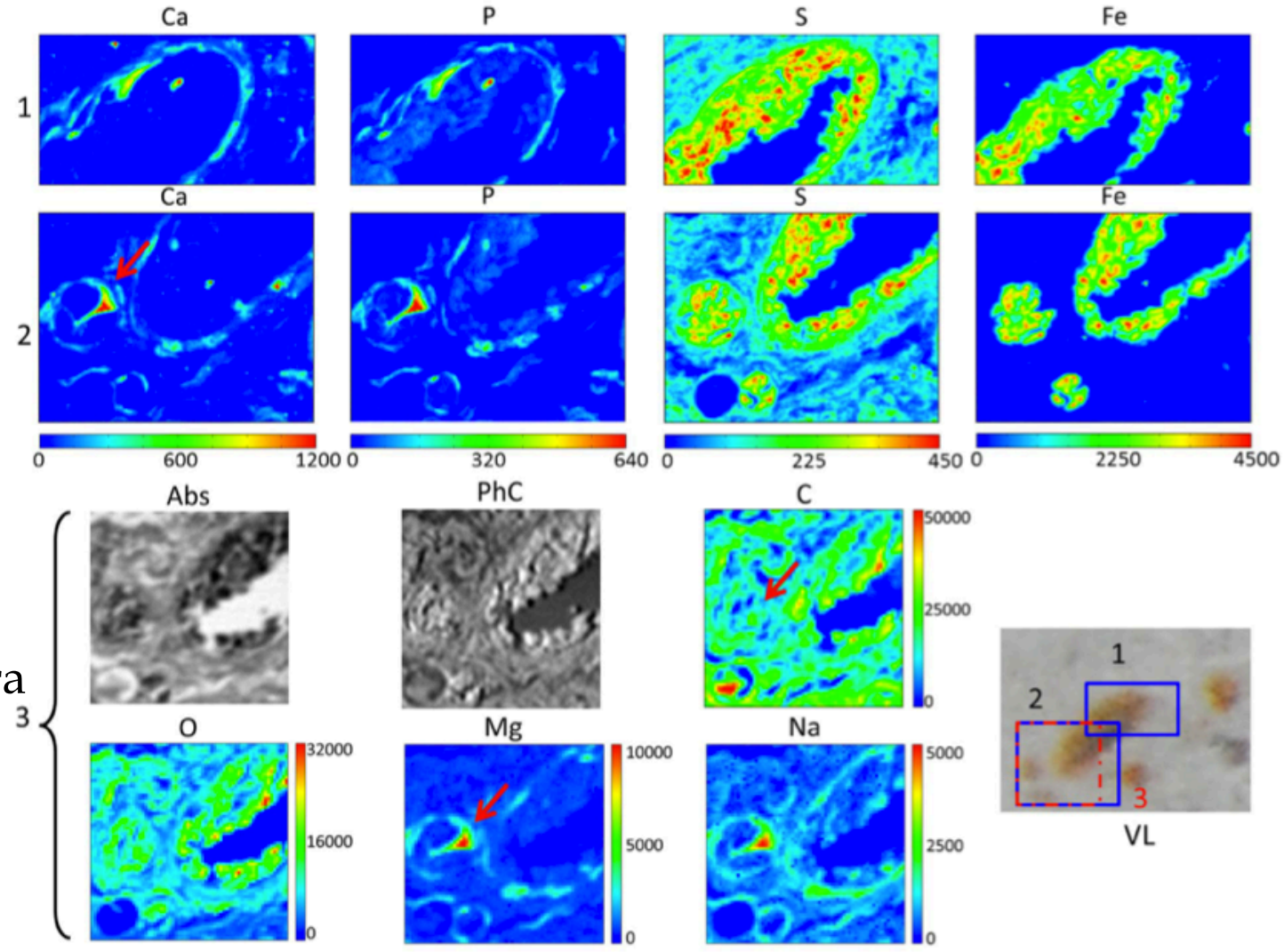

Figure 3 | XRF analyses of microvessels in a MS2 jugular tissue section. Row 1: elemental maps of Ca, P, S and Fe acquired on regions 1 (100 μm × 54.5 μm) at 7.2 keV (ID21 beamline) with 0.5 μm spatial resolution and 300 ms/pixel acquisition time; Row 2: elemental maps of Ca, P, S and Fe acquired on region 2 (100 μm × 76 μm) at 7.2 keV (ID21 beamline) with 0.5 μm spatial resolution and 300 ms/pixel acquisition time; Row 3: Absorption (Abs) and phase contrast images (PhC) with the corresponding elemental maps of C, O, Mg and Na collected on region 3 (80 μm × 80 μm) at 1.5 keV (Twinmic beamline) with 0.5 μm spatial resolution and 10 s/pixel acquisition time. The analysed regions are indicated in the corresponding visible light image (VL) of the MS2 tissue section. The red arrow indicates a region analysed at 4.12 keV too.

Elettra
Sincrotrone
Trieste

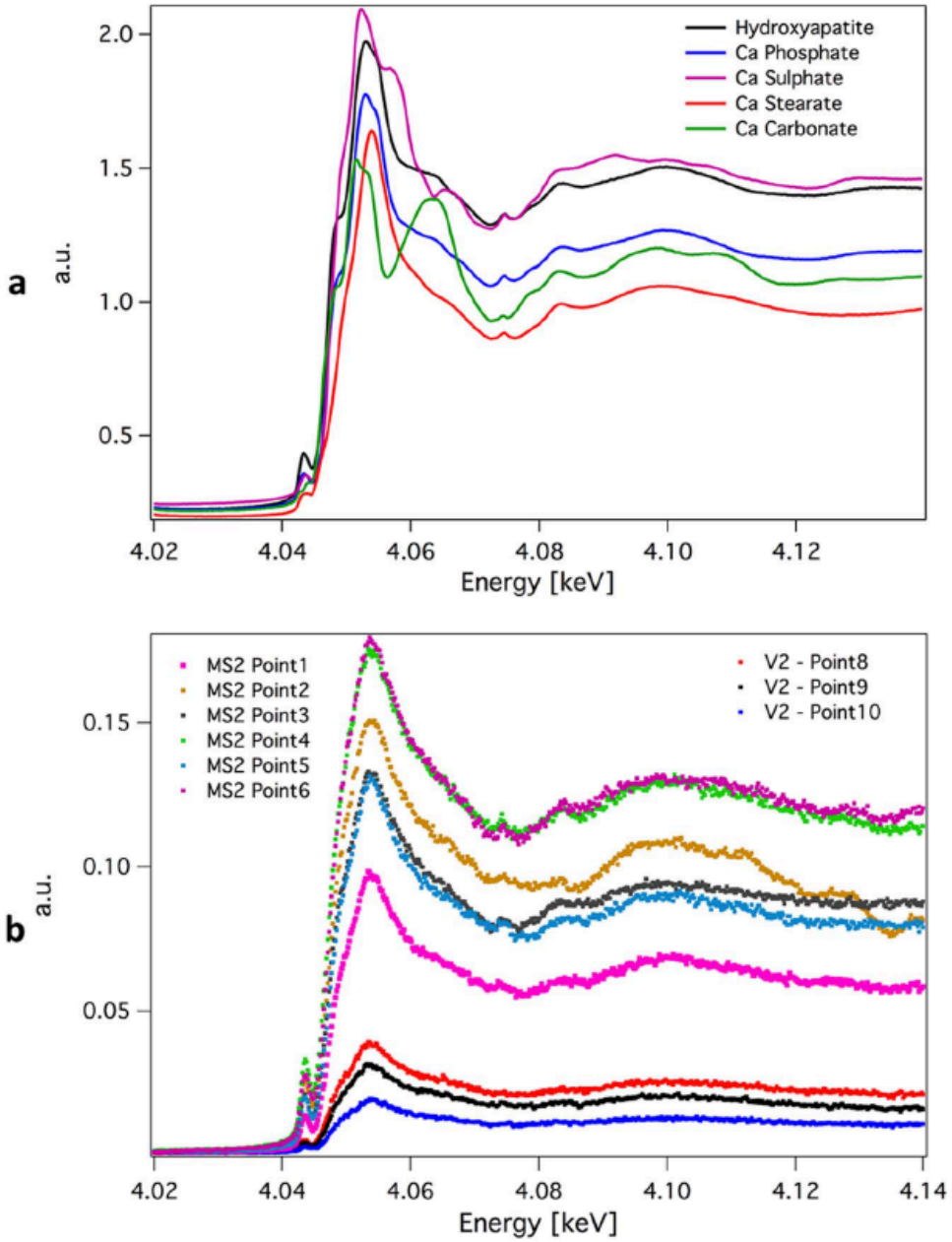

In control tissues, the major contributions in the XANES spectra seem to come from organic Ca salts.

On the contrary, in the diseased subject tissues the XANES results are in line with a substantial presence of hydroxyapatite (and other inorganic calcium salts) in clear connection with the vasa venorum.

Elettra
Sincrotrone
Trieste

Thank you!

Elettra
Sincrotrone
Trieste

www.elettra.eu